NASA CONTRACTOR REPORT

NASA CR-1325

EXPERIMENTS AND A MODEL FOR PILOT DYNAMICS WITH VISUAL AND MOTION INPUTS

by Robert L. Stapleford, Richard A. Peters, and Fred R. Alex

Prepared by
SYSTEMS TECHNOLOGY, INC.
Hawthorne, Calif.
for Ames Research Center

NATIONAL AERONAUTICS AND SPACE ADMINISTRATION • WASHINGTON, D. C. • MAY 1969

EXPERIMENTS AND A MODEL FOR PILOT DYNAMICS WITH VISUAL AND MOTION INPUTS

By Robert L. Stapleford, Richard A. Peters,
and Fred R. Alex

Issued by Originator as Technical Report No. 168-2

Prepared under Contract No. NAS 2-3650 by
SYSTEMS TECHNOLOGY, INC.
Hawthorne, Calif.

for Ames Research Center

NATIONAL AERONAUTICS AND SPACE ADMINISTRATION

For sale by the Clearinghouse for Federal Scientific and Technical Information
Springfield, Virginia 22151 – CFSTI price $3.00

FOREWORD

The research reported here was sponsored by the Man/Machine Integration Branch, Biotechnology Division, Ames Research Center, National Aeronautics and Space Administration. It was conducted by Systems Technology, Inc., Hawthorne, California, under Contract No. NAS2-3650 with NASA support for the experiments. The NASA Project Monitor was John D. Stewart. The contractor's Technical Director was Duane T. McRuer and the Project Engineer was Robert L. Stapleford.

The authors would like to express their gratitude to the NASA personnel for their excellent cooperation throughout the experiments. Special thanks are due to John D. Stewart and the pilots who acted as subjects—George E. Baltes, George E. Cooper, Ronald M. Gerdes, and Milton L. Jines.

ABSTRACT

This report describes the results of a simulator program to investigate the effects of motion cues on a manual-control tracking task. The experimental variables were controlled-element dynamics, linear motion characteristics, and angular motion characteristics. The data obtained include: pilot describing functions, both overall (combined visual and motion feedbacks) and separate (independent visual and motion pathways); remnant characteristics; and tracking performance. These data are also compared with previous experimental results.

From the previous and present data, a multimodality pilot model for both visual and motion feedbacks is derived. The dynamics of the two (angular and linear) motion feedback paths and the integration of visual and motion feedbacks are discussed. The overall effects of motion on the crossover model are found to be the lower pilot effective time delays and higher crossover frequencies. The changes are roughly 0.15 sec and 1 rad/sec. These effects are primarily due to an angular rate feedback via the semicircular canals. The lead provided by this vestibular path allows the pilot to reduce his lead in the visual path and increase his low frequency gain. The relative magnitudes of the visual and vestibular feedbacks depend on the controlled element dynamics (whether or not pilot low frequency lead equalization is required).

The implications of the experimental data and the multimodality pilot model on the design requirements for moving-base simulators are also reviewed. While the effects of motion cues on manual tracking, failure detection, and realism must be considered, the only definitive requirements are those relating to tracking. Translational motion cues appear to be generally less important than rotational ones, although linear motions can be significant in special situations. A conservative estimate for the requirements on angular cues seems to be good fidelity over the frequency range of 0.5-10 rad/sec. A procedure for establishing tracking requirements for a specific problem is outlined.

CONTENTS

FIGURES

TABLES

SYMBOLS

a	Inverse time constant of controlled element lag
a_y	Lateral acceleration as sensed by accelerometer
$a_{y_{sub}}$	Pilot's subjective lateral acceleration
b	Lateral acceleration component due to roll rate
c	Stick deflection
c_i	Pilot output (stick deflection, c) components at input frequencies
d	Disturbance input
e	Roll angle error
e_i	Error, e, components at input frequencies
e_n	Error, e, components at noninput frequencies
g	Acceleration due to gravity
i	Command input
j	$\sqrt{-1}$
K	Transfer function gain
K_c	Controlled element gain
ℓ_s	Height of pilot's head above the simulator roll axis of rotation
ℓ_z	Height of pilot's head above the simulated vehicle c.g.
n_c	Pilot remnant injected at pilot's output
n_e	Pilot remnant injected at pilot's input
p_y	Inverse time constant in lateral position washout
p_φ	Inverse time constant in roll washout
s	Laplace operator, $s = \sigma + j\omega$
t	Time
T	Time constant

T	Run length
y_i	Lateral position command to simulator
y_s	Lateral position of simulator cab
Y_c	Controlled element transfer function
Y_m	Pilot describing function for motion feedback (includes simulator dynamics, washouts, and equalization)
Y_p	Overall pilot describing function; includes visual and motion feedbacks
Y_v	Pilot describing function for visual feedback
Y_y	Transfer function of lateral position washout and equalization circuit
Y_φ	Transfer function of roll washout circuit
α	Angular acceleration
Δ''	$1 + Y_c(Y_v + Y_m)$
ζ	Damping ratio of second-order mode; particularized by subscript
$\rho^2_{a_c}$	Relative correlated (pilot) output, $\rho^2_{a_c} = \overline{c_i^2}/\overline{c^2}$
$\rho^2_{a_e}$	Relative correlated error, $\rho^2_{a_e} = \overline{e_i^2}/\overline{e^2}$
σ	Real part of s
σ_x	Root mean square (rms) value of x
τ	Transport lag
φ	Roll angle, $\varphi = \varphi_m + d$
φ_i	Roll angle command to simulator
φ_m	Controlled element output
φ_s	Roll angle of simulator cab
$\dot{\varphi}_{sub}$	Pilot's subjective roll rate
Φ_{xx}	Power spectral density of x
ω	Angular rate

ω	Imaginary part of s
ω	Undamped natural frequency of second-order mode; particularized by subscript
ω_{co}	Crossover frequency
ω_T	Angular rate threshold

SECTION I

INTRODUCTION

A. BACKGROUND

Motion cues can have an important effect on manual control of aerospace vehicles. Consequently, designers and researchers working in the field of manual control are faced with several analytical and simulation problems. Analytical pilot models have been developed and have proven invaluable aids to flight control system design and general handling qualities research; however, these models have either considered only visual inputs to the pilot or have combined the visual and motion cue effects into an equivalent model for visual inputs alone.

The lack of a pilot model which specifically includes the separable effects of motion cues may place certain restrictions on the applicability of analytical results. The possible effects of motion cues also raise several questions on the design of simulation programs, including:

- When is it necessary to go to the cost and complexity of using a moving-base simulator or a variable-stability airplane?
- If a moving-base simulator or variable-stability airplane is necessary, which motion quantities must be duplicated and with what fidelity?
- If all the motion quantities are not exactly duplicated, how does one extrapolate the results to that of flight of the actual vehicle?

The primary objective of the research reported here was to extend the existing pilot models to include the separable effects of motion cues. This would eliminate the analytical restrictions noted above and the model could also be used to provide some answers to the questions on simulation design.

The first phase of this program included a thorough review of the literature on:

- Psychological and physiological data relating to human perception of motion
- The effects of motion cues on performance for manual control tracking tasks
- The effects of motion on pilot describing function measurements

The literature on the first item was extensive and the results of the review are documented in Ref. 1. A moderate amount of performance data was available, but useful describing function data were very limited, Refs. 2 and 3. (Section IV presents a more detailed discussion of the describing function data which existed at the time of the literature survey and Ref. 4, which was published shortly before the completion of this project.)

Based on the material obtained in the literature survey, a preliminary multimodality pilot model for visual and motion inputs was formulated. Of necessity, some features of this preliminary model had an extremely limited data base. Therefore, a validation experiment was planned and executed. The experimental results generally supported the preliminary model, but did allow some refinements to be made.

Because of the similarity between the preliminary and revised models, the preliminary one is not discussed here. Instead, the body of the report presents:

- The results of the validation experiment
- The correlation of these results with previous data
- The current, revised Multimodality Pilot Model

B. OUTLINE OF THE REPORT

The experimental conditions and data reduction procedures which were used are described in Section II. Additional details on the data reduction procedure used for some of the test conditions are given in the Appendix.

The experimental results are discussed in Section III. This discussion is divided into three parts. The first, and most extensive, part considers the basic effects of motion on a number of quantities, including:

- Pilot describing functions
- Crossover frequency and phase margin
- Pilot remnant
- Tracking performance

The second and third parts treat the effects of changes in the linear motion cues and in the angular motion washout.

The correlation of the present results with previous data is discussed in Section IV.

Section V describes the proposed pilot model for visual and motion feedbacks. Also included in this section is a discussion of the implications of the data and model on the requirements for moving-base simulation.

Section VI is a summary.

SECTION II

EXPERIMENTAL CONDITIONS AND MEASUREMENT PROCEDURES

A. PHYSICAL LAYOUT AND EQUIPMENT

The overall goals of the experimental program were to validate and refine the preliminary Multimodality Pilot Model. The formulation of the test conditions to achieve these goals was guided by the following desiderata:

- The piloting task should be attitude control because attitude control, as either a command or inner loop, is essential in flying an airplane.
- The task should be single axis to avoid the complications of multi-axis interactions and to simplify the correlation of the results with previous data.
- The visual feedback should be attitude alone (no path information) to avoid the confounding effects of additional feedbacks on the data interpretation.
- The linear acceleration motion cues should be variable to investigate the relative roles of the angular and linear cues.
- The task as presented to the pilot should be as realistic a flight situation as possible.

Guided by the above, a roll control task with variable lateral acceleration cues was selected.

The general task presented to the subjects was to roll stabilize a high performance VTOL which was hovering in gusty air. They were instructed to keep the roll deviations as small as possible and were given no information on their lateral position (simulator was hooded and the only display was roll angle. The experiments were conducted on the NASA Ames Six Degree of Freedom Simulator, Fig. 1, using the roll and lateral translation modes of the simulator. In response to visual and motion cues, the pilot manipulated a sidestick controller.

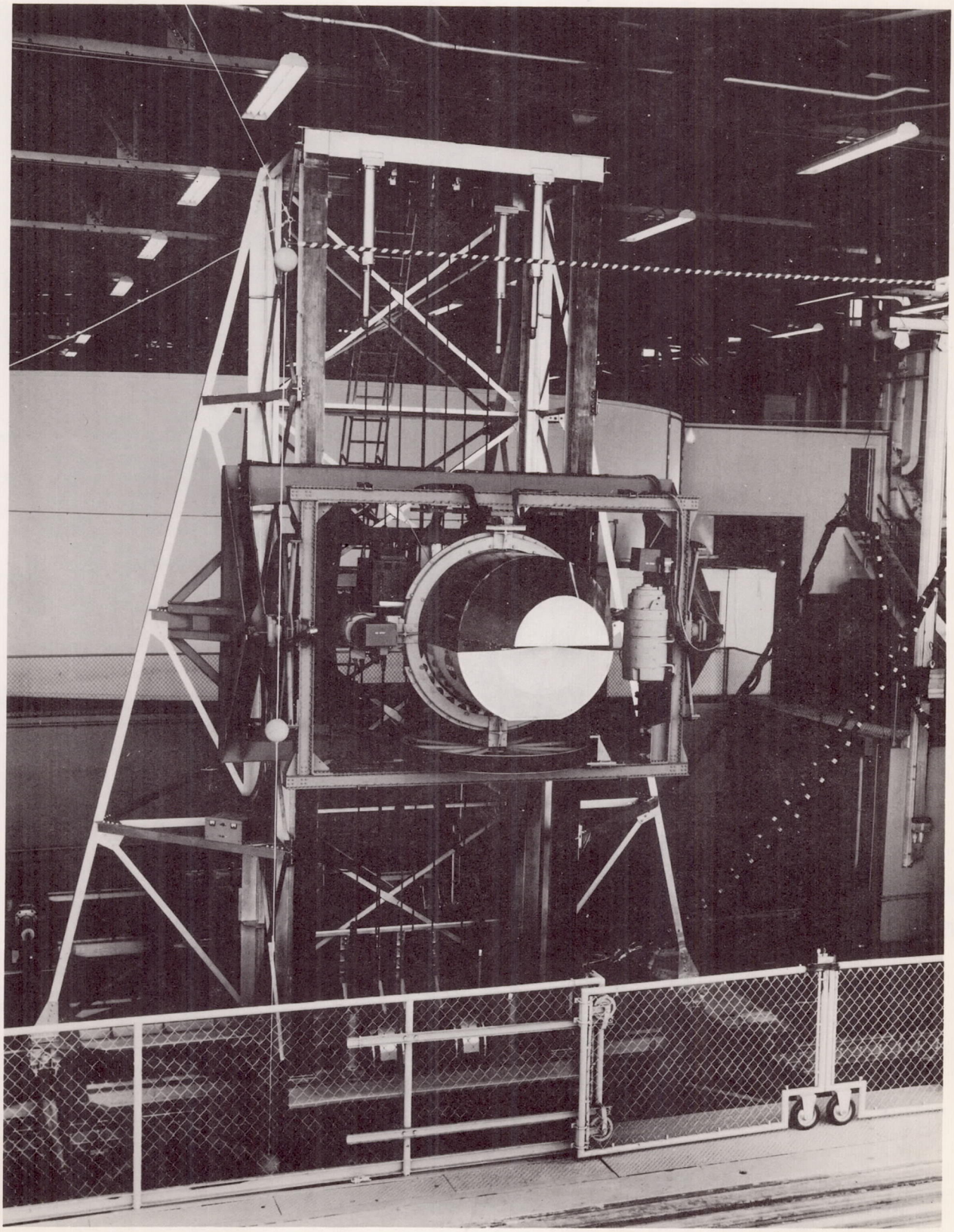

A-39901

Figure 1. Six-Degrees-of-Freedom Simulator

Stick position was fed to an analog computer which was used to simulate a variety of controlled element dynamics, derive the input signals to the display and the simulator, and provide a performance measure (see Fig. 2). The following paragraphs describe the various elements in the overall simulation.

The controller was a low inertia, spring-restrained sidestick with ±15 deg of travel. It had a breakout torque of approximately 1.5 in.-lb and a gradient of approximately 0.32 in.-lb/deg.

The controlled element dynamics were always of the form

$$Y_c = \frac{K_c}{s(s+a)} \tag{1}$$

where a was 0, 1, or 10 sec^{-1}. Each subject was allowed to select the gain, K_c, he preferred for each value of a. The values selected by the three subjects are given in Table I.

TABLE I

PILOT-SELECTED GAINS

a (sec^{-1})	SUBJECT			
	GB	GC	RG	MJ
0	6.5	5	5	7.5
1	2.5	4	5	10
10	65	15	25	75

Gain, K_c, in units of sec^{-2}

For all test conditions, a disturbance input, d, was added to the controlled element output. This input is equivalent to the hands-off gust response of the simulated vehicle. The input was composed of 10 sine waves and had a rms value of 4.3 deg. The frequencies of the 10 component waves are listed in Table II. The amplitudes of the 4

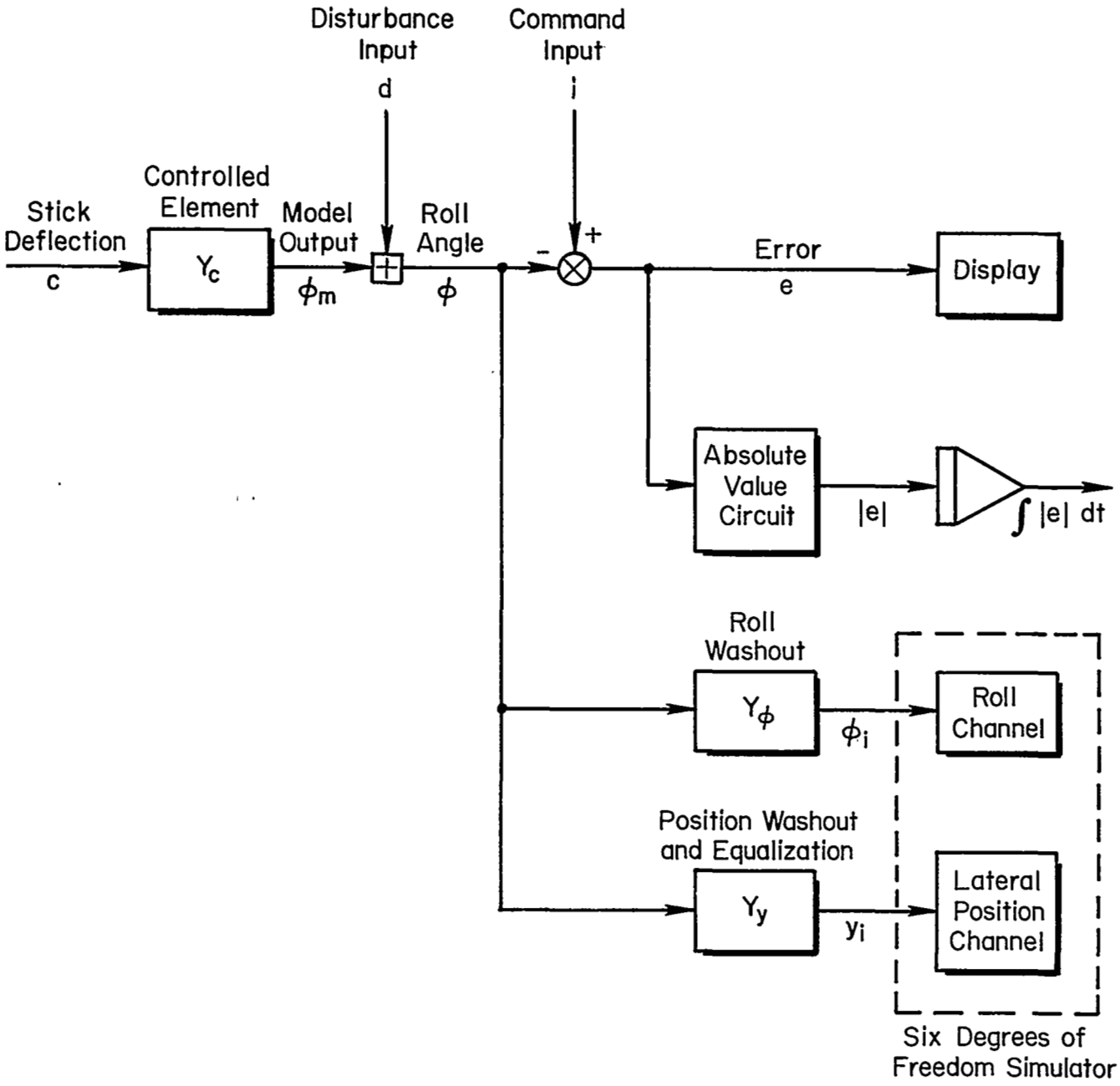

Figure 2. Simulation Schematic

TABLE II

DISTURBANCE INPUT COMPONENTS

NO. OF CYCLES IN 4 MIN	FREQUENCY (RAD/SEC)	RELATIVE AMPLITUDE
4	0.10472	1
7	0.18326	1
13	0.34034	1
19	0.49742	1
31	0.81158	1
55	1.4399	1
95	2.4871	0.1
155	4.0579	0.1
262	6.8592	0.1
443	11.598	0.1

highest frequency components were 1/10 those of the low frequency components.

For some of the tests a command input, i, was also used, see Fig. 2. The basic difference between the command and disturbance inputs is that the disturbance input feeds directly into both the display and the moving-base simulator; whereas, the command feeds only into the display. Thus, d tends to disturb the vehicle and the pilot attempts to cancel its effects and keep the vehicle level; while i is a roll command which the pilot attempts to follow. The command input was used so that the pilot's visual and motion feedbacks could be separated. This subject is discussed in detail in Section II.C.

The command input was also composed of 10 sine waves, see Table III. The rms value was either 1/4 or 1/2 that of the disturbance input.

The roll angle error, e, was displayed to the pilot on a 5 in. attitude indicator (8-ball). Without the command input, the ball approximated the true horizon, i.e., the ball was nearly inertially stabilized and the cab rotated around it. The integral of the absolute

TABLE III

COMMAND INPUT COMPONENTS

NO. OF CYCLES IN 4 MIN	FREQUENCY (RAD/SEC)	RELATIVE AMPLITUDE
5	0.13090	1
9	0.23562	1
16	0.41888	1
26	0.68068	1
42	1.0996	1
71	1.8588	0.1
120	3.1416	0.1
202	5.2884	0.1
340	8.9012	0.1
574	15.027	0.1

value of the error was also computed to provide an on-line check on pilot performance.

A washout,

$$Y_\varphi = \frac{s}{s + p_\varphi} \tag{2}$$

was used between the roll angle, φ, and the input to the roll channel of the Six-Degrees-of-Freedom Simulator (see Fig. 2). The inverse time constant, p_φ, was an experimental parameter and values of 0.5, 1, and 2 sec^{-1} were tested.

The equalization between φ and the lateral position channel was used to simulate different pilot head positions relative to the vehicle c.g. Most hovering VTOL's have very low side force characteristics, so that the linear acceleration sensed by the pilot is primarily due to the angular acceleration and his distance from the c.g. Thus, the sensed acceleration at the pilot's head would be

$$a_y = \ell_z s^2 \varphi_s \tag{3}$$

where ℓ_z = height of pilot's head above the simulated vehicle c.g.

Now in a simulator the sensed acceleration would be

$$a_y = s^2(y_s + \ell_s \varphi_s) - g\varphi_s \tag{4}$$

where y_s = lateral position of the simulator cab

ℓ_s = height of pilot's head above the simulator roll axis of rotation (approximately 1.5 ft in these tests)

Combining these two expressions gives the desired transfer function between simulator roll angle and position.

$$\frac{y_s}{\varphi_s} = \frac{(\ell_z - \ell_s)s^2 + g}{s^2} \tag{5}$$

The double integration is undesirable because of the very large position changes required for any low frequency roll motions. Any bias in the mean roll angle would be especially bad as it would quickly produce excessive translations. This problem was avoided by adding a second-order washout, $(s/s + p_y)^2$, in the position loop. Thus, the net transfer function between the roll angle and the input to the lateral position channel of the simulator was

$$\frac{y_i}{\varphi} = Y_y = \frac{(\ell_z - \ell_s)s^2 + bs + g}{(s + p_y)^2} \tag{6}$$

For the vast majority of the test conditions b was set to zero but a few runs were made with a nonzero value to see if a $\dot{\varphi}$ component of lateral acceleration would produce any significant effects. The simulated head position was either on the c.g. ($\ell_z = 0$) or 3.5 ft

above the c.g. ($\ell_z = 3.5$ ft). The washout inverse time constant was also varied and was set at 0.5, 1, or 2 sec^{-1}.

Let us now review the pertinent characteristics of the Six-Degrees-of-Freedom Simulator. The roll channel limits of the simulator were as follows:

Roll angle	±35 deg
Roll rate	±75 deg/sec
Roll acceleration	±580 deg/sec^2

The lateral position limits were:

Position	±9 ft
Velocity	±8 ft/sec
Acceleration	±9.2 ft/sec^2

As part of the data reduction, the simulator describing functions were computed for some of the test runs. It was found that over the range of input frequencies the roll dynamics could be closely approximated by

$$\frac{\varphi_s}{\varphi_i} \doteq \frac{e^{-\tau s}}{Ts + 1} \tag{7}$$

where φ_s = actual roll angle of simulator cab
φ_i = commanded roll angle
$\tau = 0.04$ sec
$T = 1/12$ sec

The measured describing functions for lateral position showed considerable run-to-run variability for frequencies greater than 3 rad/sec, which suggests that the acceleration limits were being reached. A rough approximation to the position dynamics is given by

$$\frac{y_s}{y_i} \doteq \frac{\omega_s^2}{s^2 + 2\zeta_s\omega_s s + \omega_s^2} \tag{8}$$

where y_s = actual lateral position of simulator cab

y_i = commanded lateral position

$\zeta_s = 0.7$

$\omega_s = 5$ rad/sec

Four subjects were used in these experiments; their pertinent backgrounds are summarized in Table IV. Describing function analyses were performed only on subjects GB, RG, and MJ. They were each allowed several practice runs on the various configurations and data runs were made only after their performance, as measured by $\int|e|dt$, had stabilized. The data runs were approximately 4.5 min long, of which 4 min was used in the data analysis.

TABLE IV

SUBJECT BACKGROUNDS

GB: Retired Air Force pilot; approximately 7,000 hr in multi-engine aircraft

GC: Head of Flight Operations Branch at NASA Ames Research Center; approximately 5,000 hr total with 60 percent in single-engine aircraft (mainly fighters); helicopter rating

RG: NASA Research Pilot; approximately 4,200 hr total, mostly in single-engine fighters, 500 hr in helicopters and VTOL aircraft

MJ: Airline pilot; formerly military pilot; approximately 1,200 hr in jet fighters and 20 hr in multi-engine aircraft

Subject GC was used to provide subjective evaluations of the different configurations because of his much more extensive flight and simulator experience. His evaluations are discussed later.

B. EXPERIMENTAL PLAN

The experimental configurations were divided into three groups. The Priority 1 configurations were selected to provide basic information on the effects of:

- Controlled element dynamics
- Pilot's head location
- Roll and lateral position washouts.

The 21 Priority 1 configurations are indicated in Table V. All four subjects flew the Priority 1 configurations.

TABLE V

PRIORITY 1 CONFIGURATIONS

CONTROLLED ELEMENT a (sec^{-1})	HEAD POSITION ℓ_z (ft)	ROLL WASHOUT p_φ (sec^{-1})	LATERAL POSITION WASHOUT p_y (sec^{-1})	SECOND INPUT rms i/rms d	LATERAL ACCELERATION COMPONENT DUE TO ROLL RATE b (ft/sec)
0, 1, 10	Fixed Base			0	—
0, 1, 10	0, 3.5	0.5	0.5	0	0
0, 10	0	1, 2	0.5	0	0
0, 10	0, 3.5	0.5	1, 2	0	0

The Priority 2 and 3 configurations were primarily selected to evaluate the two-input method of directly separating the visual and motion feedbacks. Also included in Priority 2 were nonzero values of the lateral acceleration component due to roll rate, b. The 10 Priority 2 configurations are listed in Table VI. Two subjects flew those configurations. The 12 Priority 3 configurations, listed in Table VII, were flown by one subject.

C. DATA REDUCTION PROCEDURES

The data was originally recorded in analog form on a 14-channel FM magnetic tape recorder. The data was subsequently sampled at 20 samples/sec and converted to a digital format. The digital data was then analyzed on a large scale digital computer using the BOMM program (Ref. 5). The

TABLE VI

PRIORITY 2 CONFIGURATIONS

CONTROLLED ELEMENT [a] (sec^{-1})	HEAD POSITION ℓ_z (ft)	ROLL WASHOUT p_φ (sec^{-1})	LATERAL POSITION WASHOUT p_y (sec^{-1})	SECOND INPUT rms i/rms d	LATERAL ACCELERATION COMPONENT DUE TO ROLL RATE [b] (ft/sec)
0, 10	0, 3.5	0.5	0.5	0.25, 0.50	0
0, 10	0	0.5	0.5	0	1.5*

*For some runs, 10 ft/sec was used instead of 1.5 ft/sec

TABLE VII

PRIORITY 3 CONFIGURATIONS

CONTROLLED ELEMENT [a] (sec^{-1})	HEAD POSITION ℓ_z (ft)	ROLL WASHOUT p_φ (sec^{-1})	LATERAL POSITION WASHOUT p_y (sec^{-1})	SECOND INPUT rms i/rms d	LATERAL ACCELERATION COMPONENT DUE TO ROLL RATE [b] (ft/sec)
0, 10	0, 3.5	0.5	1	0.25, 0.50	0
0, 10	0	1	0.5	0.25, 0.50	0

actual calculations used to compute pilot describing function with one or two inputs and pilot remnant are discussed below.

For the one input (disturbance) runs only an overall pilot describing function can be measured. This describing function, Y_p, contains the combined effects of pilot visual and motion feedbacks. The effective loop structure is therefore reduced to the single loop form of Fig. 3.

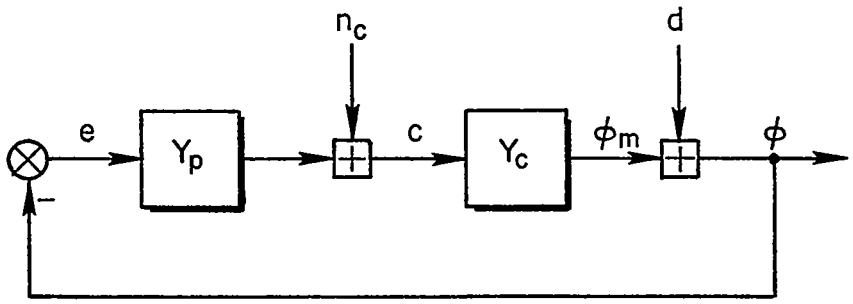

Figure 3. Effective Loop Structure for One-Input Runs

The digital computer evaluated the Fourier transforms of e, c, and φ_m at each of the 10 input frequencies* and computed the following ratios

$$\left[\frac{F(c)}{F(e)}\right] \doteq Y_p \tag{9}$$

$$\left[\frac{F(\varphi_m)}{F(e)}\right] \doteq Y_p Y_c \tag{10}$$

The above approximations are quite accurate if the remnant is small. Data from two runs made with an analog pilot with no remnant simulation were analyzed. The average absolute values of the errors in the measured describing function were 0.18 dB and 1.8 deg. The maximum errors were 0.38 dB and 6.2 deg. Thus, in the absence of remnant, the measurement technique is quite accurate.

When remnant is present, errors in the measured describing functions are introduced because the Fourier coefficients actually contain some remnant power. The magnitude of the errors was investigated by computing the Fourier coefficients for the minimum frequency separation of 1/run length (1/240 Hz). Since the coefficients at noninput frequencies represent remnant effects, the measurements are accurate as

*Frequencies of the 10 components of d.

long as the magnitudes at input frequencies are much greater than at noninput frequencies; i.e., the coefficient is primarily due to the input rather than the remnant. Review of this data for several runs showed that the remnant effects on e at low frequencies were the most limiting factor. It was concluded that the describing function data for frequencies less than roughly 0.5 rad/sec were not reliable because of excessive remnant effects.

As noted earlier, some runs were also made with both command and disturbance inputs. For these runs the effective loop structure is shown in Fig. 4. Here Y_v is the pilot describing function for visual feedback and Y_m is the describing function for motion feedback. It

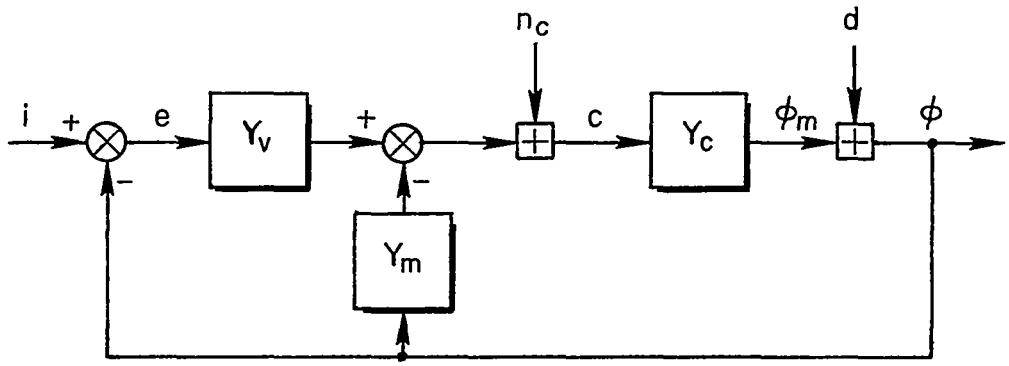

Figure 4. Effective Loop Structure for Two-Input Runs

must be noted that Y_m actually represents the sum of two separate motion feedback channels — one angular and one linear. Furthermore all simulator dynamics, washouts, and equalizations are included in Y_m. Without the command input, the loop structure of Fig. 4 reduces to that of Fig. 3 with

$$Y_p = Y_v + Y_m \tag{11}$$

The reason for adding the second input was to attempt to separate the visual and motion feedbacks. Measurement of the two describing functions, Y_v and Y_m, requires two uncorrelated inputs which are inserted at different points in the system. However, there is a problem in using a command input. A large command input will destroy the correlation

between the pilot's visual display and his sensed motions. When the two feedbacks disagree he may tend to place a different relative weighting on the two types of inputs, e.g., ignore the motion cues and use only a visual feedback.* This problem can be minimized by using a command input which is very small relative to the disturbance input.

With a small enough command input, the pilot will not be consciously aware of the visual/motion discrepancies and will operate as if there were only the disturbance input. On the other hand, if the input is too small, we have signal/noise problems. One of the objectives of this program was to determine if a command input could be found which was both small enough not to affect the piloting technique and large enough to provide reasonable data. Accordingly, two command input levels were tested — rms values of 1/4 and 1/2 that of the disturbance input. The effects of the command input were analyzed by comparing the effective visual describing function, Y_p, data for one and two inputs. An example comparison is shown in Fig. 5. As can be seen, the effects were insignificant. Since the signal levels were also large enough to provide good measurements, the original objective was achieved.

The data reduction procedure for two inputs are considerably more difficult than for the one. As detailed in the appendix, the calculation of the Y_v and Y_m describing functions requires solving two simultaneous equations. One equation involves the ratios of various Fourier transforms measured at d input frequencies, the other at i input frequencies. Because the measurements for each input cannot have any common frequencies,† the measured ratios must be interpolated to provide numerical values for both equations at common frequencies. Because of the complicated data reduction procedure only 31 two-input runs were analyzed. With one exception, these consisted of two replications for two subjects

*A more detailed discussion of this subject is contained in Section V.C.

†The two inputs must be uncorrelated and, since both are the sum of sine waves, this means they cannot have any common frequencies.

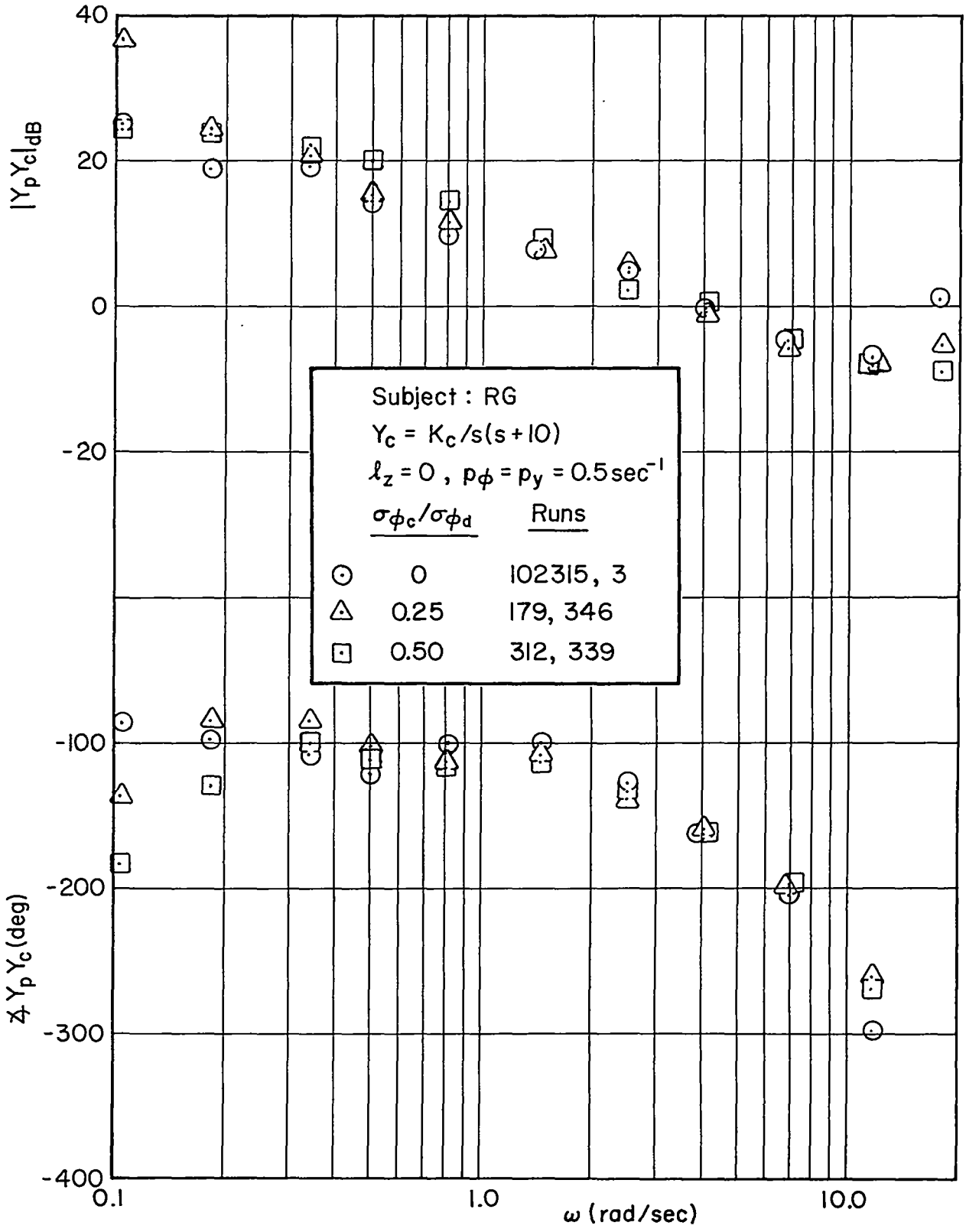

Figure 5. Comparison of One-Input and Two-Input Data

(GB and RG), with two values of ℓ_z (0 and 3.5 ft), two levels of the command input, and two controlled elements [$Y_c = K_c/s(s + 10)$ and $Y_c = K_c/s^2$].

The first step in the reduction of the remnant data was to compute the power spectra of e and c. For frequencies greater than 5 rad/sec, the classic approach used was to compute the autocorrelation function and then the Fourier transform. This technique was not satisfactory at the lower frequencies because input and remnant effects could not be separated. To get data between input frequencies would require using a small frequency resolution which means large measurement variability.

To get the low frequency data, the Fourier coefficients of e and c were computed for the minimum frequency separation (1/run length = 1/240 Hz) up to 6 rad/sec. After discarding the values at input frequencies, the data was averaged over ten adjacent frequency points. When multiplied by a suitable constant this gave the e and c spectra due to remnant alone. Had the Fast Fourier Transform Algorithm been available in the BOMM program, this technique would have been used for all frequencies. However, without this algorithm it was more inexpensive to use the combination of techniques. The results from the two methods overlapped in the frequency range 5 – 6 rad/sec and the two different sets agreed very well in this overlap region.

By averaging over 10 frequencies, the low frequency spectra data have 20 degrees of freedom and a normalized standard error* of 0.32, Ref. 6. The higher frequency data have 80 degrees of freedom (120 lags with 4800 samples) and a normalized standard error of 0.16.

Until this point we have been discussing closed-loop remnant, i.e., the remnant component of e or c. A more significant quantity is the equivalent open-loop remnant referred to the pilot's input or output. The power spectra of the c closed-loop remnant and the spectra of the

*Normalized standard error is the rms error in the spectral measurement divided by the true value.

open-loop remnant injected at the pilot's output are related by (see Fig. 3)

$$\Phi_{cc} = \frac{\Phi_{n_c n_c}}{|1 + Y_p Y_c|^2} \tag{12}$$

Over the frequency for which Y_p data is available, Eq. 12 can be used to determine the open-loop spectra, $\Phi_{n_c n_c}$, from the measured closed-loop spectra, Φ_{cc}.

This completes the description of the experimental conditions and measurement procedures. The next section presents the experimental results.

SECTION III

EXPERIMENTAL DATA

A. GENERAL DISCUSSION

The subsequent presentation of the experimental results has been organized into three parts as follows:

- **Part 1**, basic motion effects, differences between fixed-base and a nominal moving-base configuration
- **Part 2**, effects of changes in linear motion cues with angular cues held constant
- **Part 3**, effects of changes in roll washout

The specific parameter variations which are considered in each part are indicated in Table VIII.

TABLE VIII

ORGANIZATION OF DATA PRESENTATION

	CONTROLLED ELEMENT Y_c	HEAD POSITION ℓ_z	ROLL WASHOUT p_φ (sec^{-1})	LATERAL POSITION WASHOUT p_y (sec^{-1})	SECOND INPUT rms i/rms d	LATERAL ACCELERATION COMPONENT DUE TO ROLL RATE b
Part 1	Var*	Fixed Base			0	—
		0	0.5	0.5	Var	0
Part 2	Var	Var	0.5	Var	Var	Var
Part 3	Var	0	Var	0.5	0	0

*Var indicates a parameter variation

Throughout the discussion, frequent reference is made to the vestibular system feedbacks of angular and linear motion cues. While there are several motion-sensing mechanisms in the human body, the vestibular system is

generally accepted as the primary one in a normal subject. Therefore, we refer to various effects as being due to vestibular feedback, but the data, per se, are really independent of this assumption. It is in the interpretation of the data that the particular motion-sensing mechanism becomes significant. It will be shown that the data presented here are compatible with the physiological data on the dynamics of the vestibular system, at least the semicircular canals.

While the dynamics of the vestibular organs, the semicircular canals and the utricles, are treated in some detail in Section V, a brief preview is given here to assist the reader in interpreting the data presented. The semicircular canals are essentially angular accelerometers. However, in the frequency range of most concern in tracking tasks they respond like rate sensors (e.g., rate gyros) with a 0.1 sec lag. Likewise, the utricles can be considered as linear accelerometers with a first-order lag at 1.5 rad/sec.

To further prepare the reader for the subsequent discussions of the data, the several metrics to be used are defined below:

Y_p	Pilot equivalent visual describing function; $Y_p = Y_v + Y_m$
Y_v	Pilot visual describing function
Y_m	Motion feedback describing function; includes linear and angular feedbacks, washouts, and simulator dynamics, see Fig. 4
ω_{co}	Crossover frequency; $\lvert Y_p Y_c(j\omega_{co}) \rvert = 1$
	Phase margin; 180 deg + $\measuredangle\, Y_p Y_c(j\omega_{co})$
$\rho^2_{a_e}$	Relative correlated error;* $\rho^2_{a_e} = \overline{e_i^2}/\overline{e^2}$, where $\overline{e_i^2}$ is the mean-square value of e components at input frequencies and $\overline{e^2}$ is the mean-square value of e
$\rho^2_{a_c}$	Relative correlated output;* $\rho^2_{a_c} = \overline{c_i^2}/\overline{c^2}$, where $\overline{c_i^2}$ is the mean-square value of c components at input frequencies and $\overline{c^2}$ is the mean-square value of c

*These performance measures are given only for the one input data runs.

Φ_{xx}	Power spectral density of x
$\overline{e^2}/\overline{d^2}$	Normalized mean-squared error*
$\overline{e_i^2}/\overline{d^2}$	Normalized mean-squared error at input frequencies*
$\overline{e_n^2}/\overline{d^2}$	Normalized mean-squared error at noninput frequencies;* $\overline{e_n^2}/\overline{d^2} = \overline{e^2}/\overline{d^2} - \overline{e_i^2}/\overline{d^2} = (\overline{e^2}/\overline{d^2})(1-\rho_{a_e}^2)$
$\overline{\lvert e \rvert}$	Mean absolute error;* $\overline{\lvert e \rvert} = 1/T \int_0^T \lvert e \rvert dt$

Not all of the above metrics will be considered in each of the three subsequent discussions. The reduction of the two-input data for Y_v and Y_m and the power spectral density computations were rather expensive and were done for only a few runs.

B. MOTION EFFECTS

To demonstrate the basic effects of the motion cues we will compare fixed-base results with the moving-base data for $\ell_z = 0$ and minimum washouts ($p_\varphi = p_y = 0.5$ sec^{-1}).

1. Describing Function Data

Motion effects on the pilot equivalent visual describing function are shown in Figs. 6–8. Examination of these data shows:

- The simple crossover model form of Ref. 7 with all its ramifications on pilot dynamic performance, adjustment rules, etc., holds for these data.
- A reduction in pilot phase lag when motion cues are added, especially for the three highest frequencies. The phase change is roughly equivalent to a time delay reduction of 0.1–0.2 sec.
- With less phase lag, the pilot can and does increase his mid-frequency gain and crossover frequency.

*These performance measures are given only for the one input data runs.

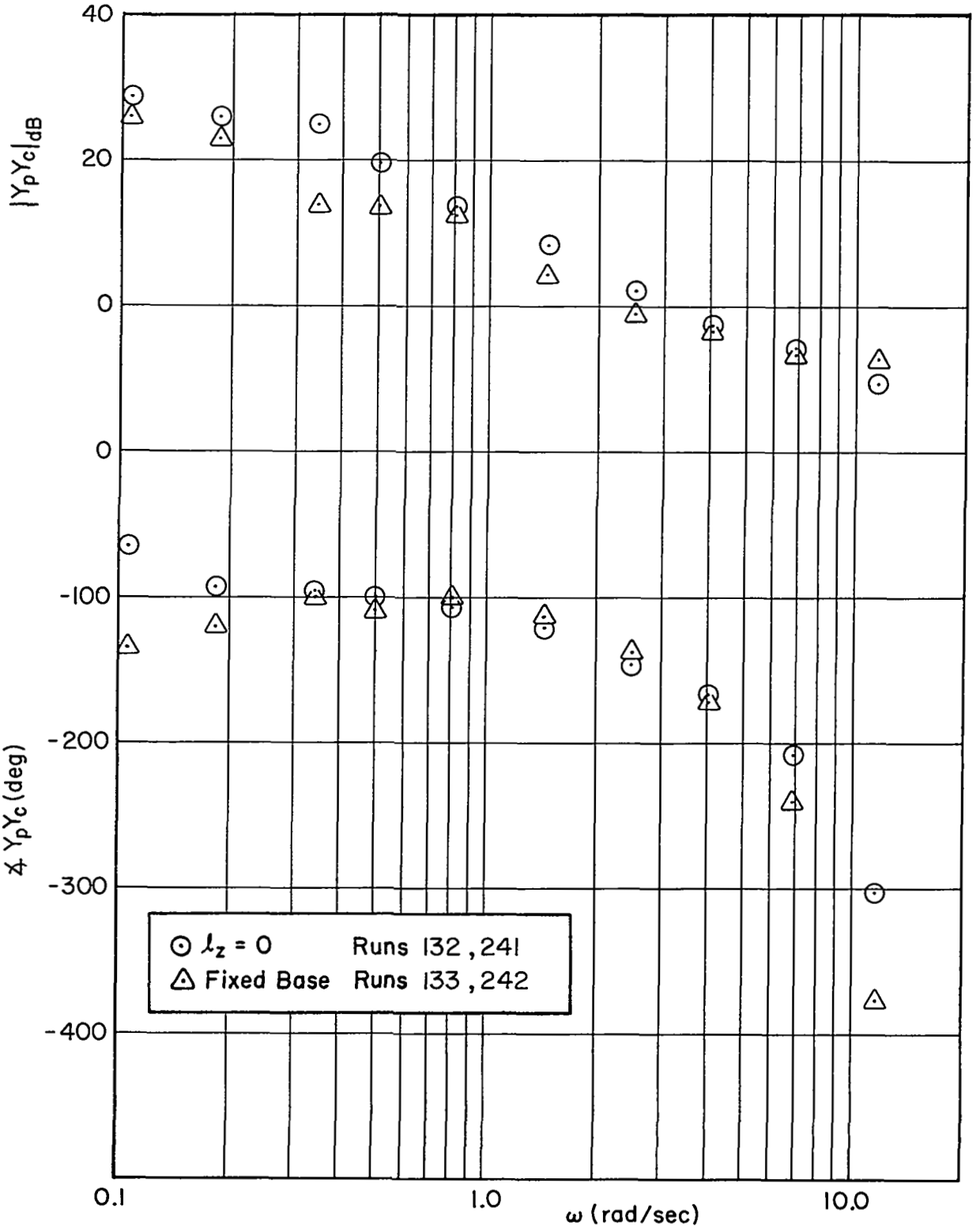

Figure 6. Motion Effects for $Y_c = K_c/s(s + 10)$

a. Subject: GB

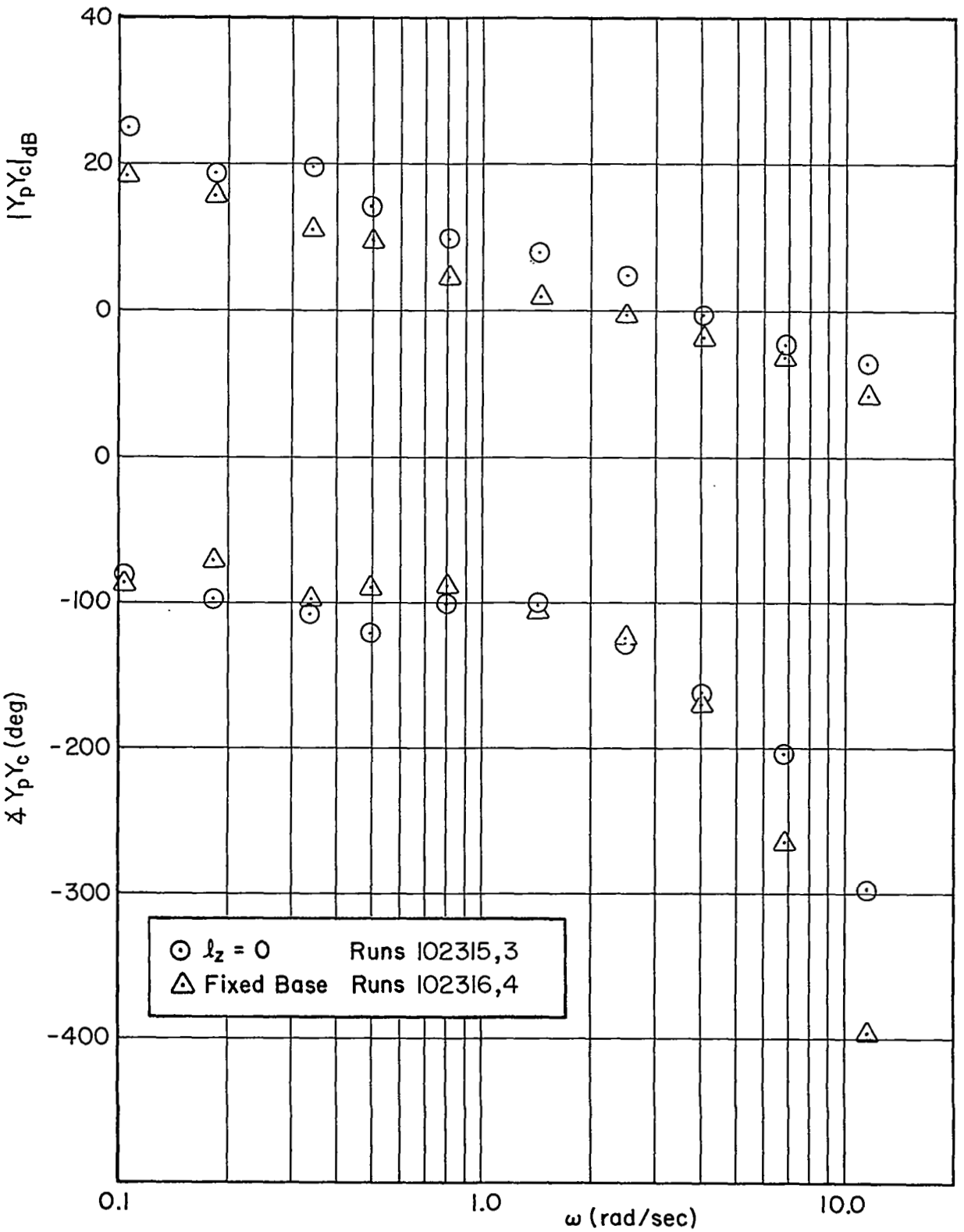

Figure 6 (Continued)

b. Subject: RG

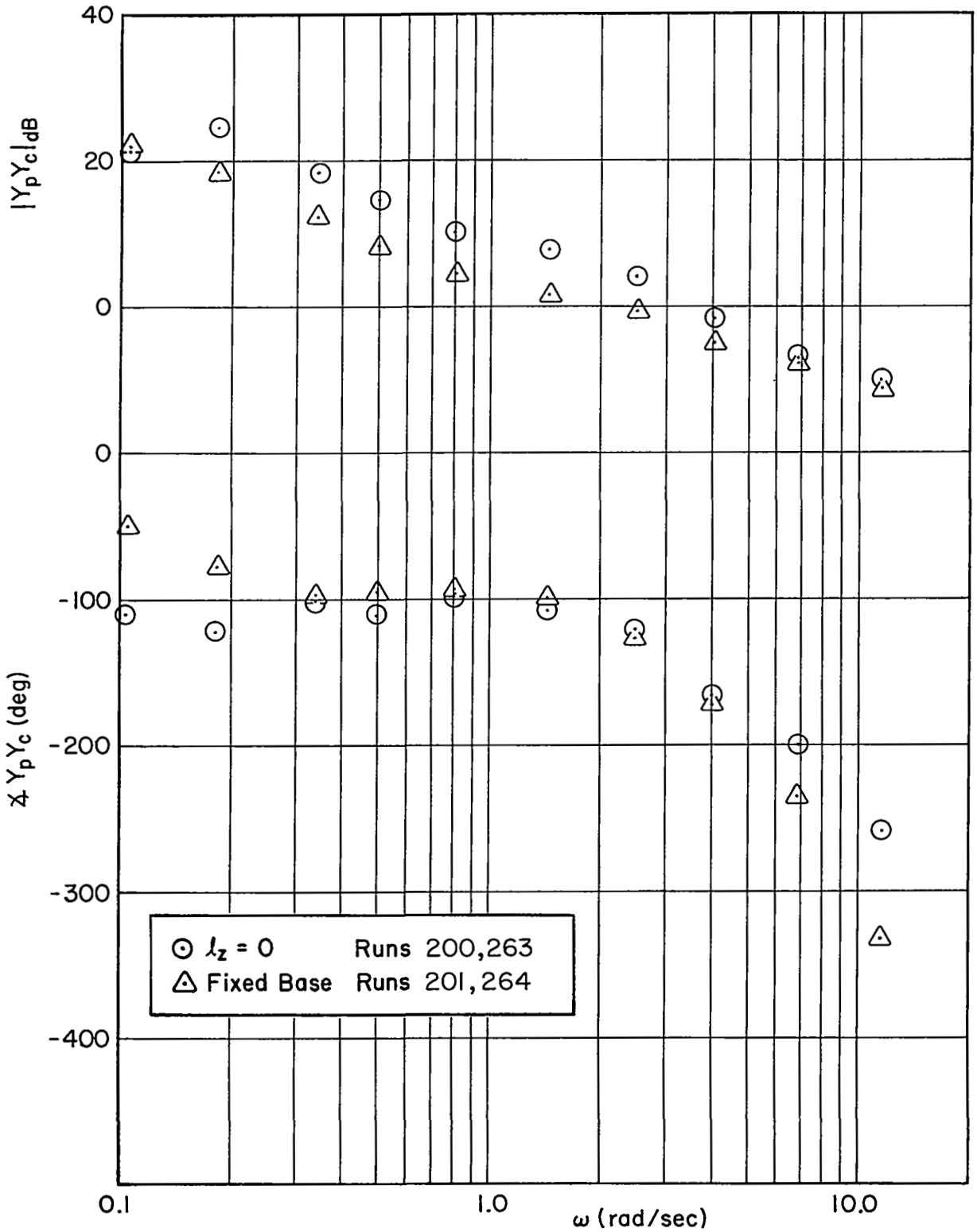

Figure 6 (Concluded)

c. Subject: MJ

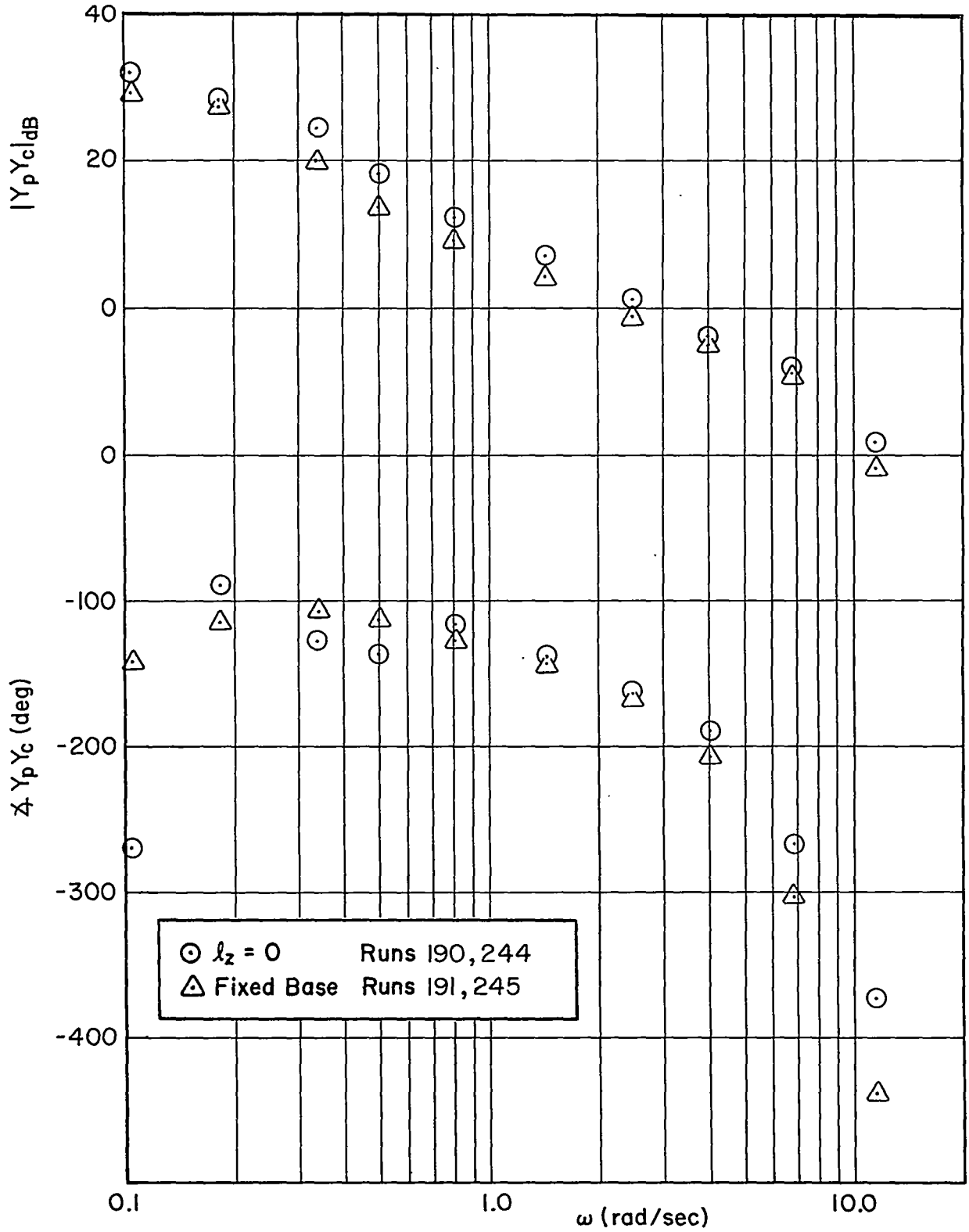

Figure 7. Motion Effects for $Y_c = K_c/s(s+1)$

a. Subject: GB

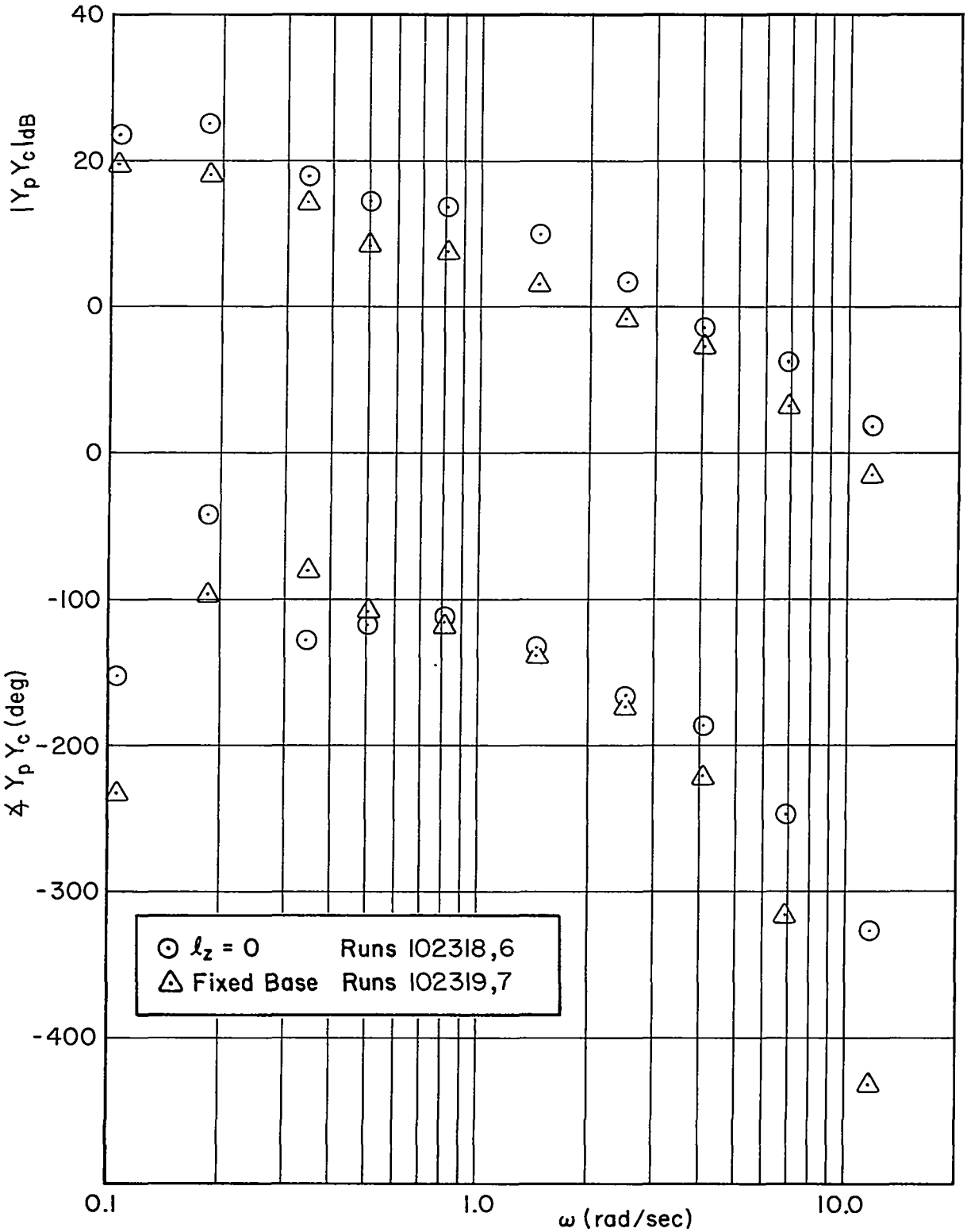

Figure 7 (Continued)

b. Subject: RG

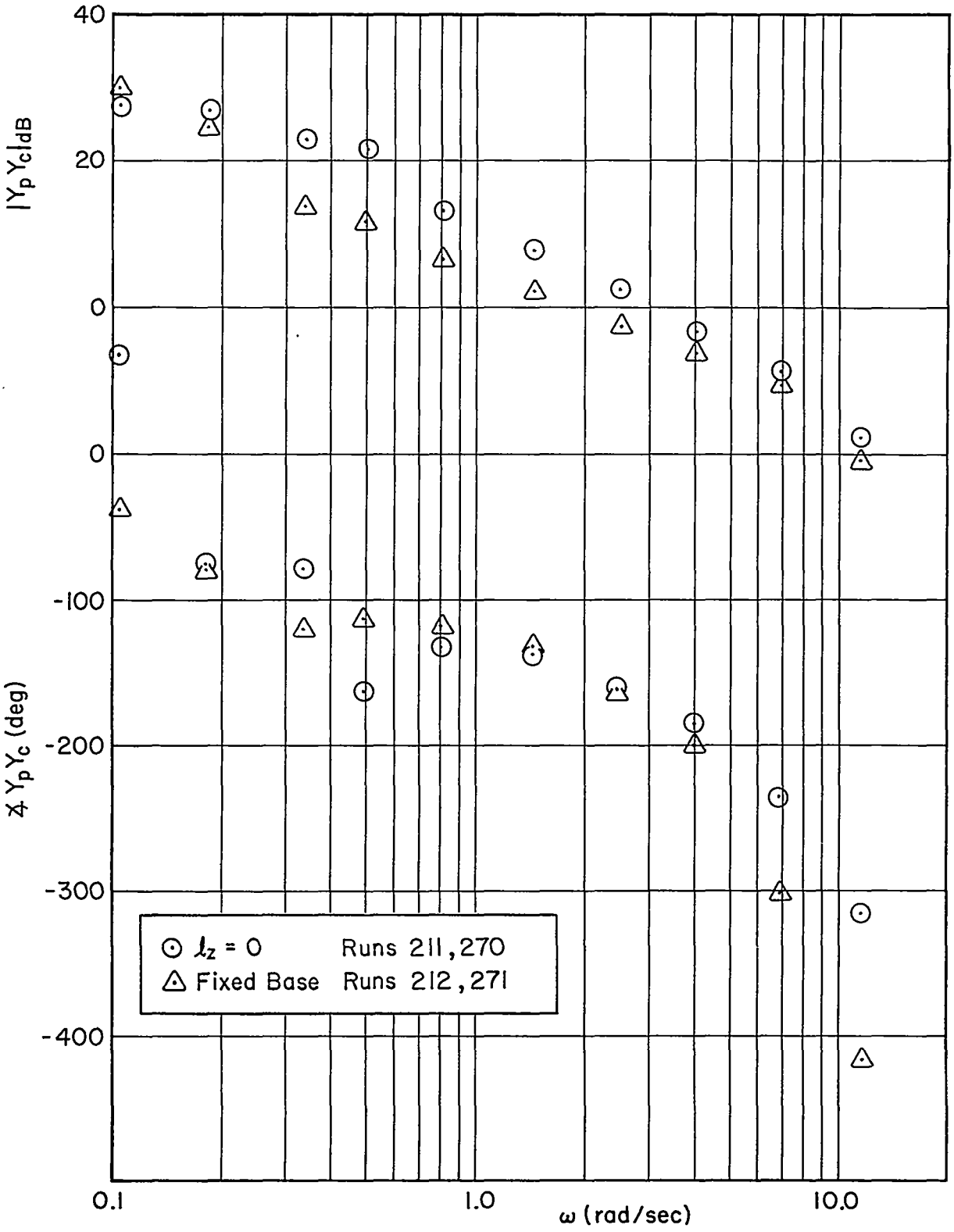

Figure 7 (Concluded)

c. Subject: MJ

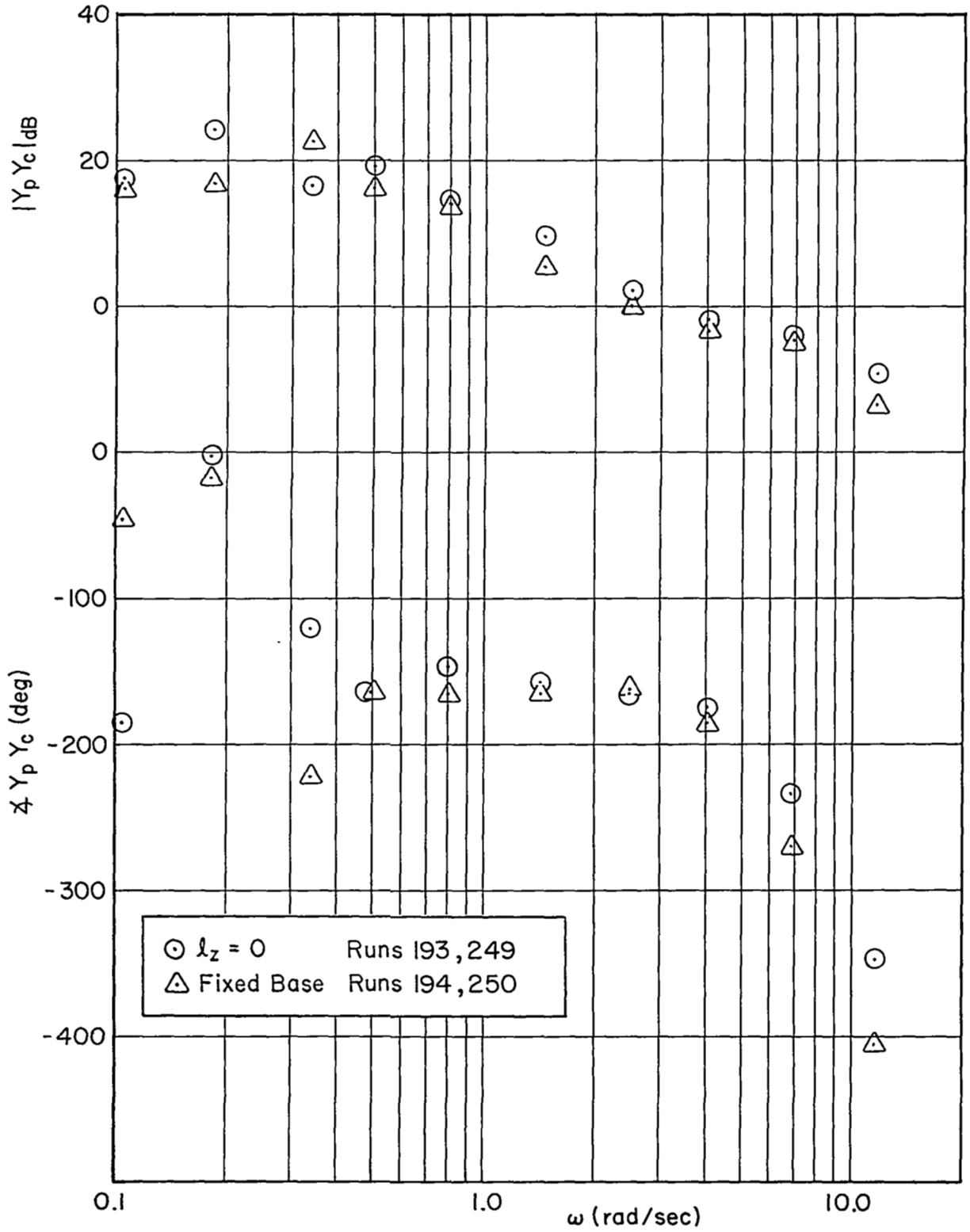

Figure 8. Motion Effects for $Y_c = K_c/s^2$

a. Subject: GB

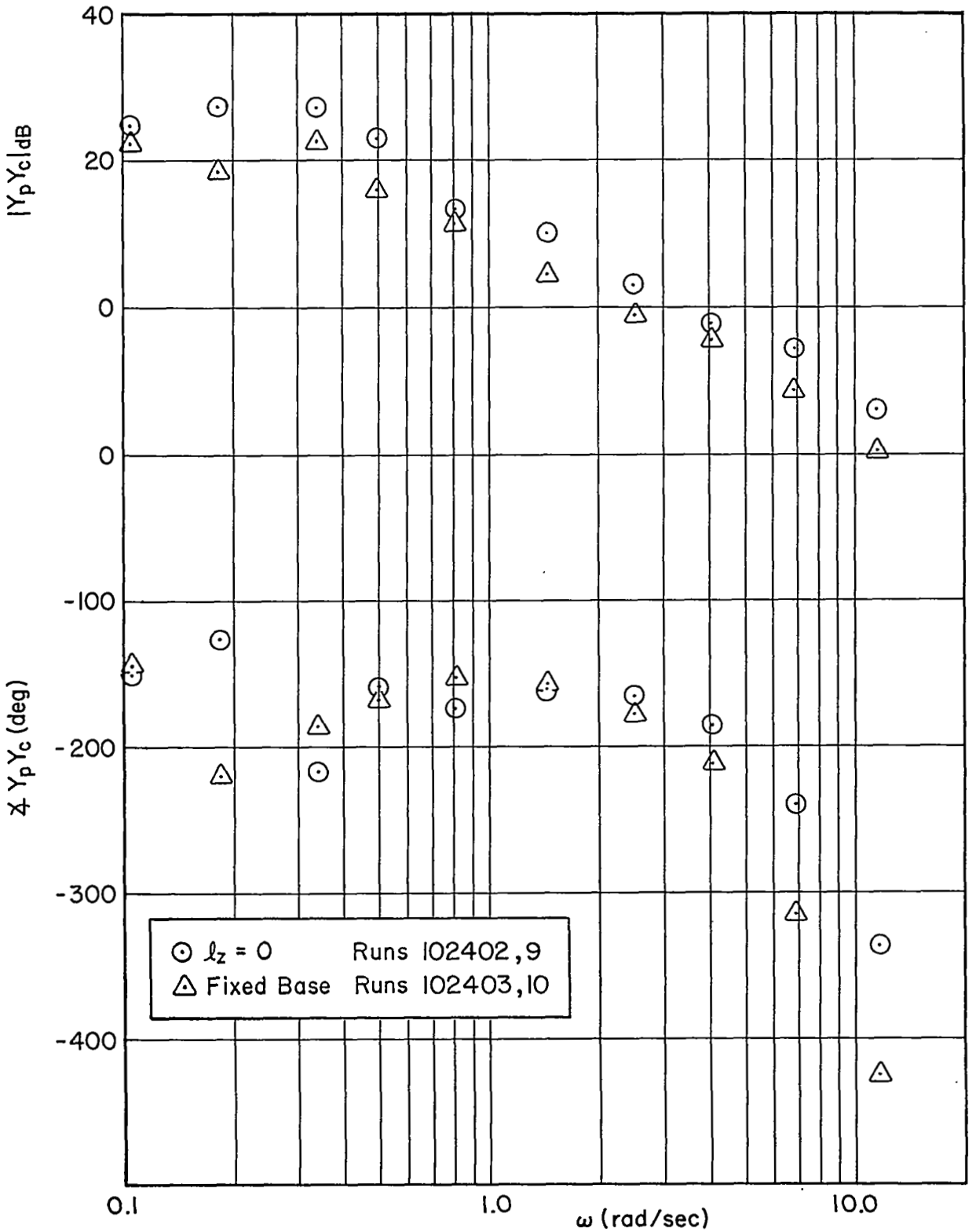

Figure 8 (Continued)

b. Subject: RG

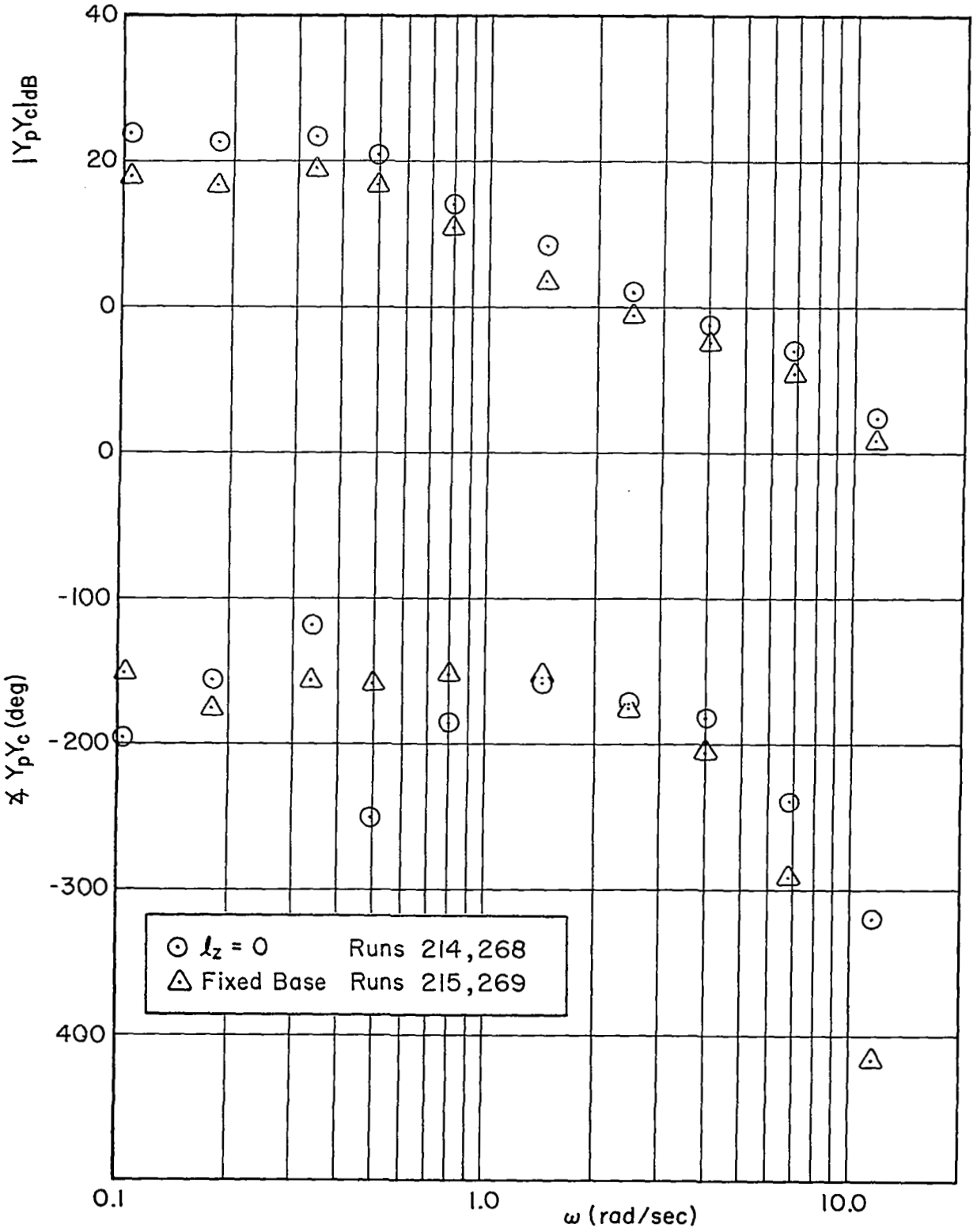

Figure 8 (Concluded)

a. Subject: MJ

- The motion effects are somewhat different for the various subjects. In particular, the changes are somewhat less for Subject GB than the other two. This may be due to his background which is primarily in multi-engine aircraft with their slower responses and smaller motion cues.

Crossover frequencies and phase margins were estimated from Figs. 6-8. The results are summarized in Fig. 9.* We see that with motion cues the crossover frequency is increased 0.5-1.5 rad/sec. The changes are less for $Y_c = K_c/s^2$ and less for Subject GB for all controlled elements. The phase margin data show large reduction (20-40 deg) with motion for $K_c/s(s+10)$, slight reductions (10-25 deg) for $K_c/s(s+1)$, and no change for K_c/s^2. Significant phase margin reductions were not possible for K_c/s^2 as the fixed-base values were already low (5-15 deg).

The above discussed only the overall effects of motion without any details on the mechanism by which the pilot utilizes the motion cues. The two-input data allows us to separate the visual and motion feedbacks for the $\ell_z = 0$ cases. These data were obtained for Subjects GB and RG and controlled elements $K_c/s(s+10)$ and K_c/s^2. The faired curves which result from the data reduction procedure detailed in the Appendix are shown in Figs. 10 and 11. Also shown in these figures are the Y_p data for the fixed-base runs. Since the fixed-base Y_p is a visual feedback, comparison of those data and the Y_v data shows how the pilot adjusts his visual feedback when motion cues are added.

From Figs. 10 and 11, we see that when motion cues are present, the visual feedback gain at low frequency is increased and less lead is used in the visual path, i.e., the low frequency phase lags are greater. To the extent that the semicircular canals act as rate gyros, this result might be expected. With the lead information supplied by the motion cues, the pilot does not need to supply as much visual lead as he does fixed base. He can also increase his gain and achieve a higher crossover frequency because his effective time delay is reduced.

*Phase margins were estimated to nearest 5 deg.

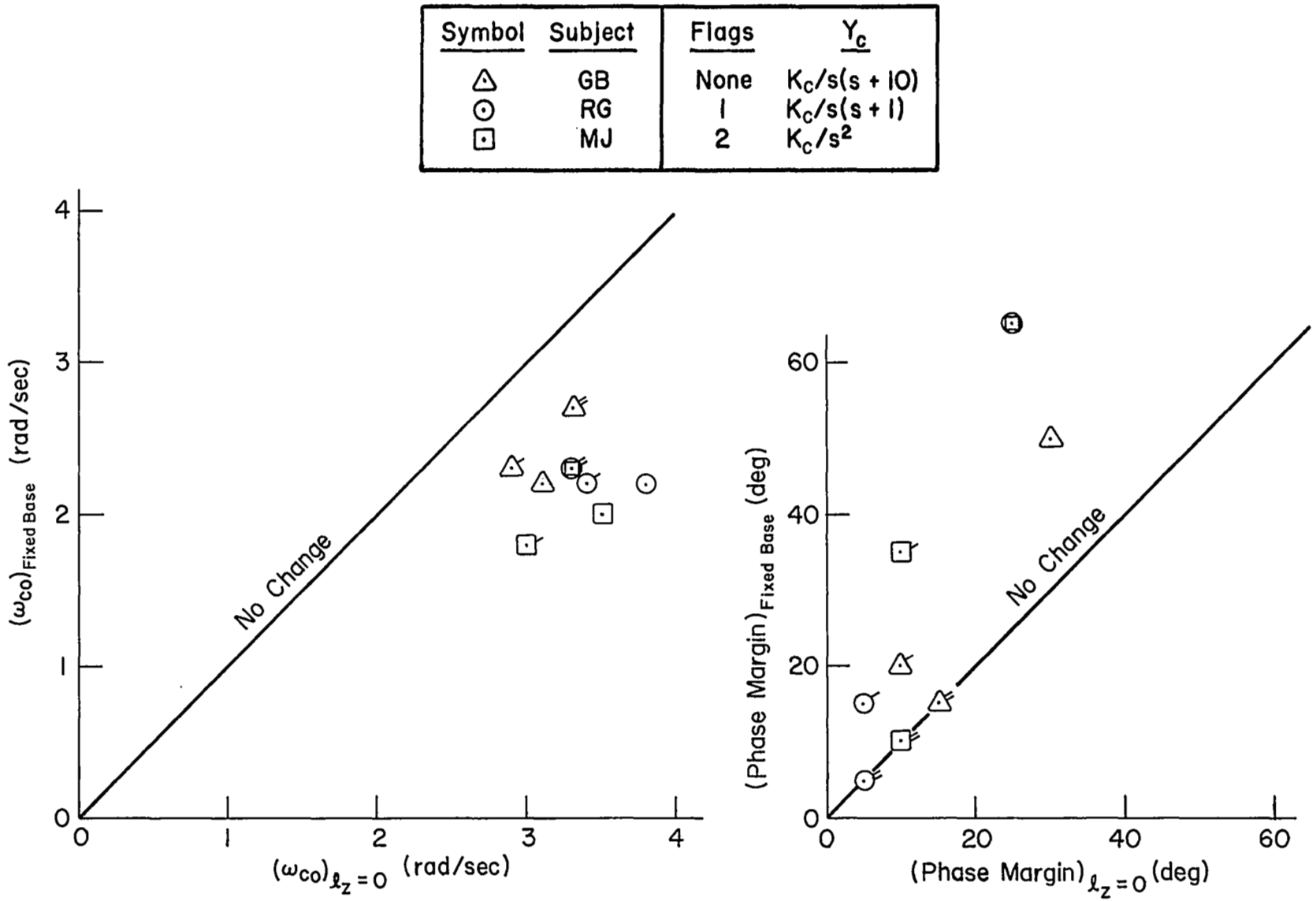

Figure 9. Motion Effects on Crossover Frequency and Phase Margin

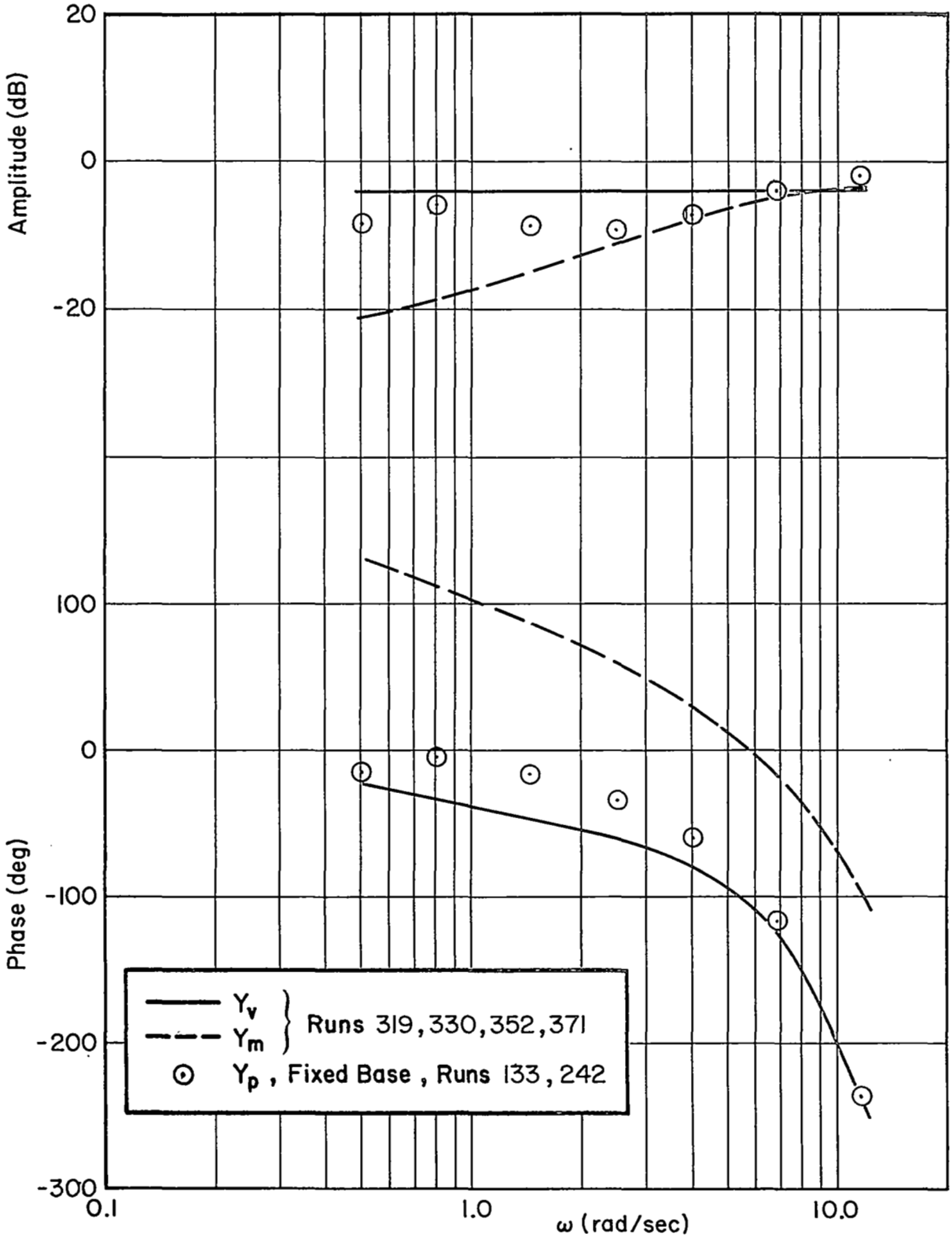

Figure 10. Visual and Motion Feedbacks for $Y_c = K_c/s(s+10)$, $\ell_z = 0$

a. Subject: GB

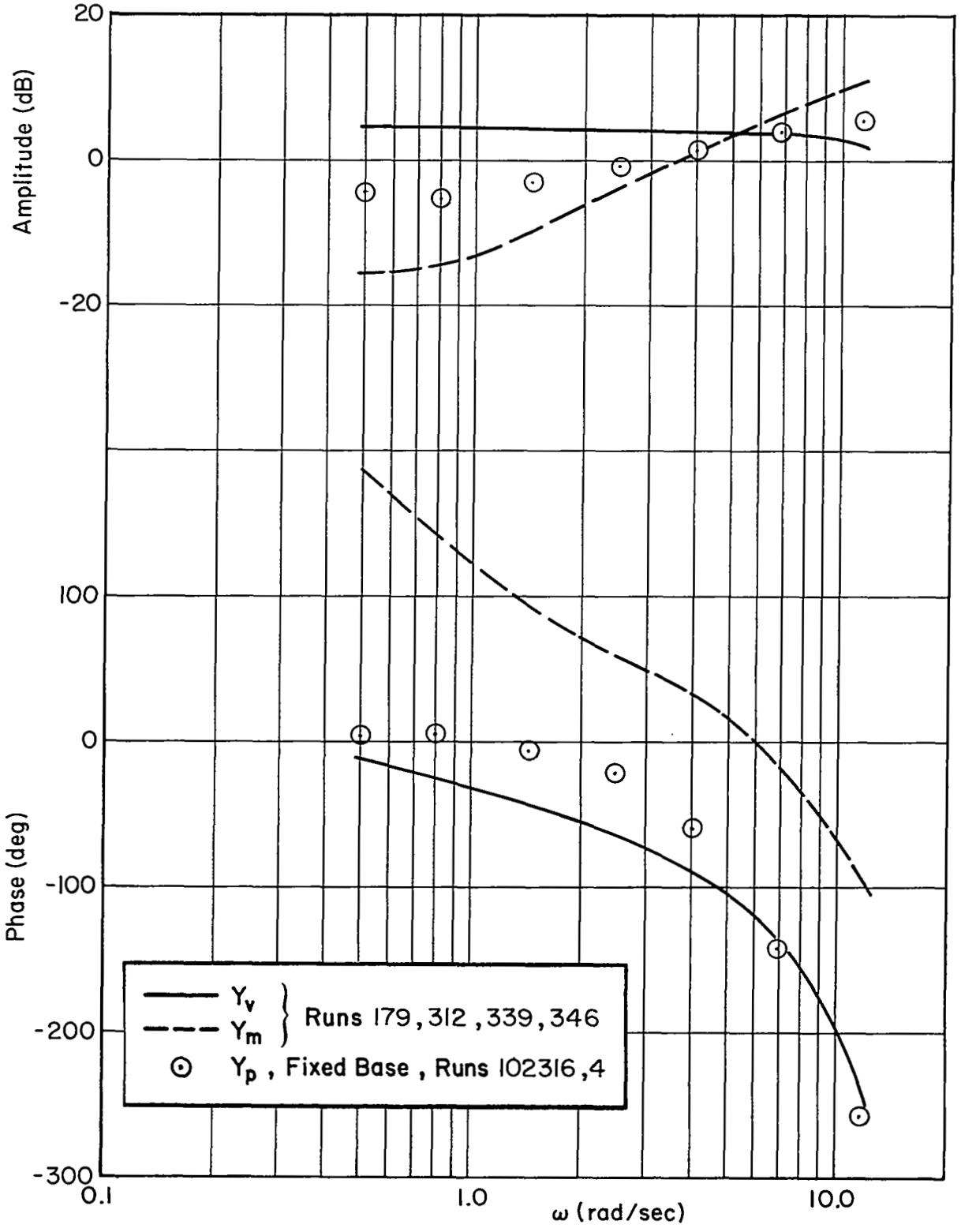

Figure 10 (Concluded)

b. Subject: RG

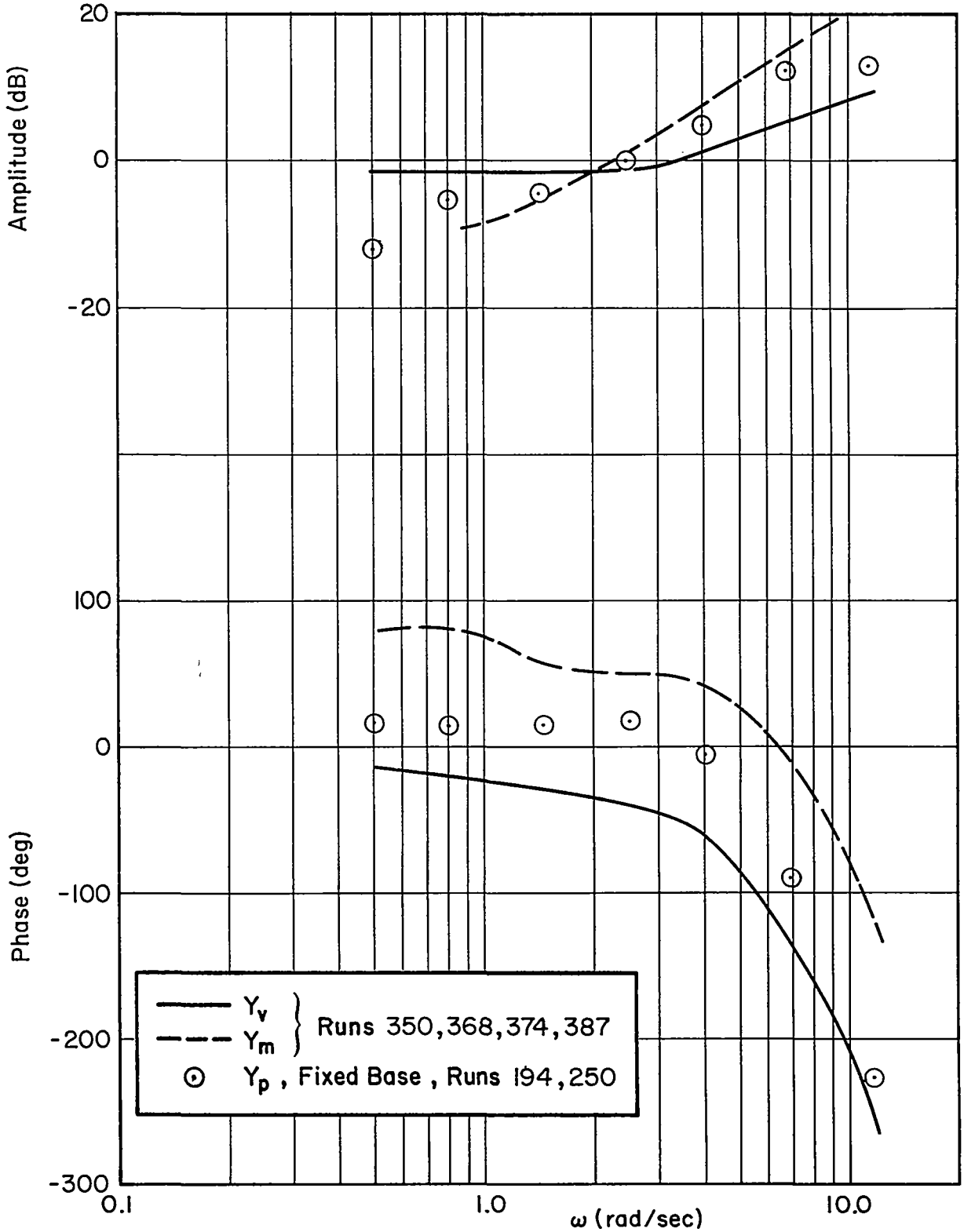

Figure 11. Visual and Motion Feedbacks for $Y_c = K_c/s^2$, $\ell_z = 0$

a. Subject: GB

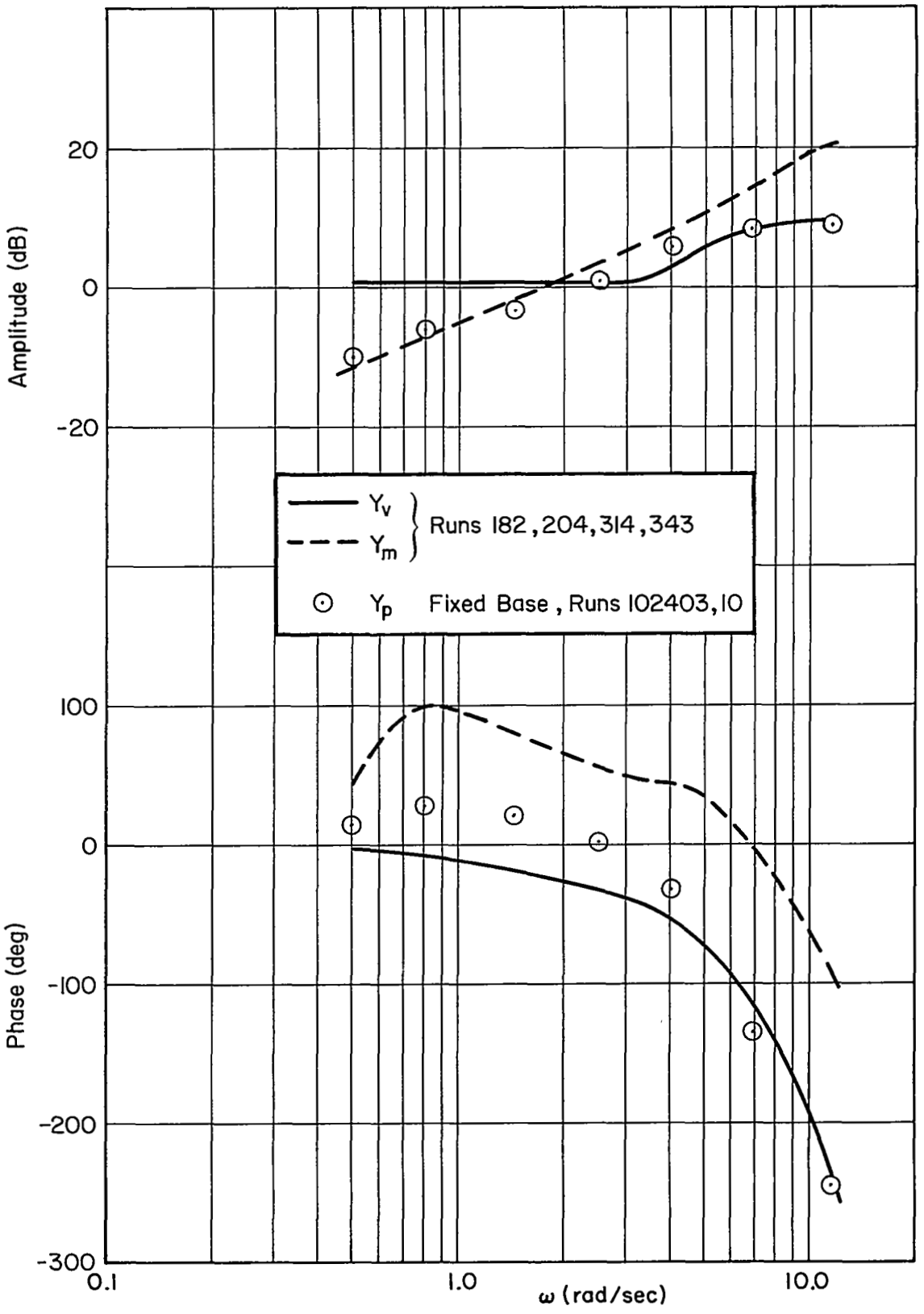

Figure 11 (Concluded)

b. Subject: RG

The motion feedback describing function, Y_m, generally appears to be a very low frequency first-order lead and a time delay of roughly 0.26 sec. Comparison of the visual and motion feedbacks shows a definite difference between the two controlled elements. For $Y_c = K_c/s(s+10)$ the magnitudes of Y_v and Y_m are equal for a frequency of 5 – 9 rad/sec. For the more difficult task, $Y_c = K_c/s^2$, the magnitudes are equal at a frequency of roughly 2 rad/sec. Thus for the task requiring more pilot lead, the relative contribution of the motion feedback is significantly higher.

The Y_m data also provide important clues as to the origin of the motion feedback, whether it is predominantly angular rate, linear acceleration, or a combination. Considering the two vestibular feedback paths, and recalling that the measured Y_m includes the simulator dynamics, Y_m can be expressed as

$$Y_m = \left(\frac{\dot{\varphi}_s}{\varphi}\right)\left(\frac{\dot{\varphi}_{sub}}{\dot{\varphi}_s}\right)\left(\frac{c}{\dot{\varphi}_{sub}}\right) + \left(\frac{a_y}{\varphi}\right)\left(\frac{a_{y_{sub}}}{a_y}\right)\left(\frac{c}{a_{y_{sub}}}\right) \qquad (13)$$

The various terms in Eq. 13 are discussed below.

The term $(\dot{\varphi}_s/\varphi)$ is the describing function from the analog computer roll angle, φ, to the simulator roll rate, $\dot{\varphi}_s$, see Fig. 2. It includes the roll washout, Eq. 2, and the roll dynamics of the simulator, Eq. 7. The net describing function $(\dot{\varphi}_s/\varphi)$ is shown in Fig. 12. Note that for 1 – 10 rad/sec the amplitudes of $(\dot{\varphi}_s/\varphi)$ and Y_m have similar shapes but $(\dot{\varphi}_s/\varphi)$ has considerably less phase lag. The significance of this will be discussed shortly.

The next term in Eq. 13, $(\dot{\varphi}_{sub}/\dot{\varphi}_s)$, is the describing function from simulator roll rate to the pilot's subjective roll rate, $\dot{\varphi}_{sub}$. This term represents the dynamics of the semicircular canals. As detailed in Section V.A, the dynamics of the semicircular canals can be approximated by a first-order lag or a time delay of 0.1 sec.

The final term in the semicircular canal feedback, $(c/\dot{\varphi}_{sub})$, covers the pilot dynamics from subjective roll rate to stick deflection. This would include any pilot equalization plus transmission and neuromuscular lags.

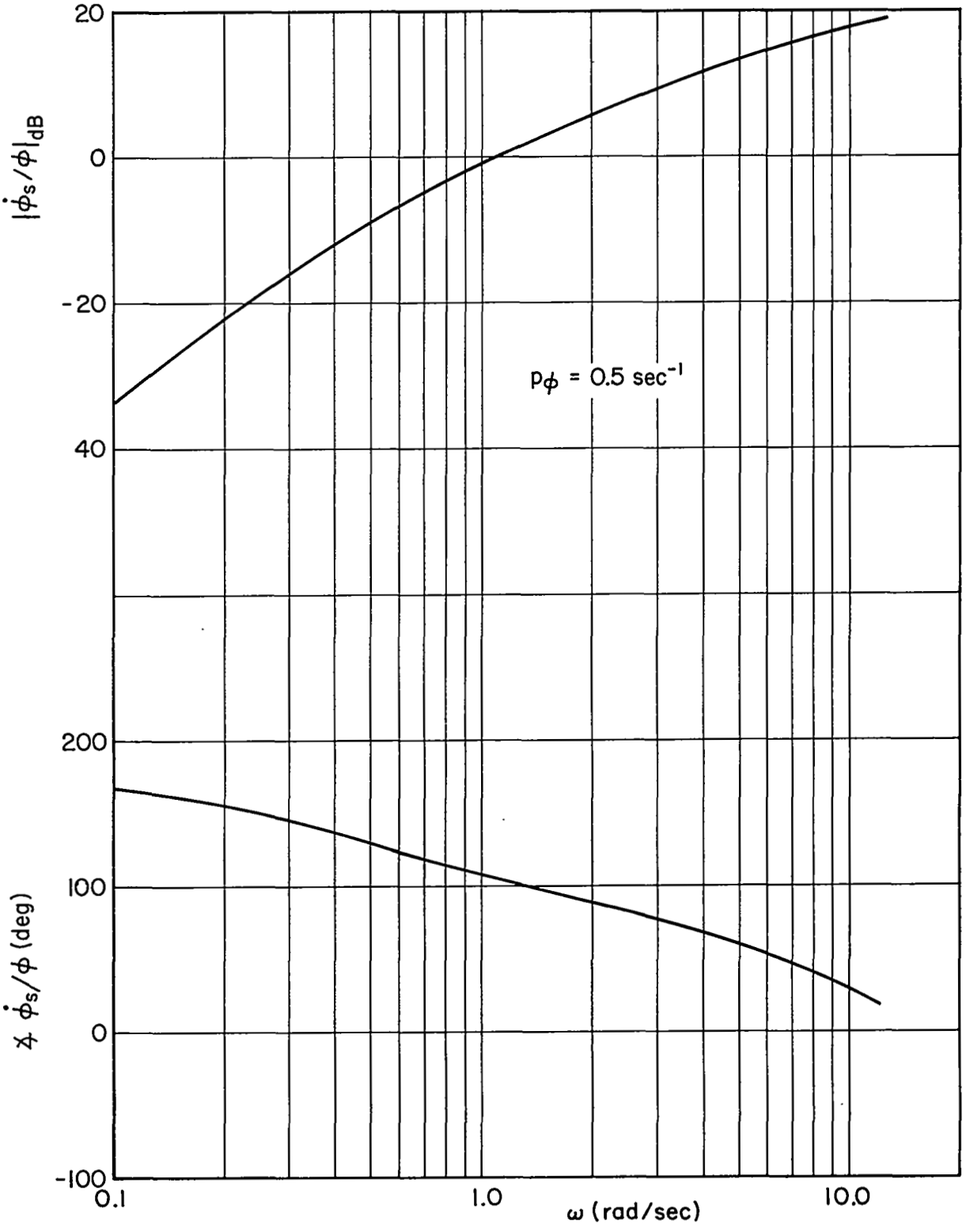

Figure 12. Roll Response Characteristics

The first element in the utricular feedback, (a_y/φ), is the describing function from the analog computer roll angle to the side acceleration (as measured by an accelerometer) at the pilot's head. This response can be computed from Eq. 4 and the simulator characteristics of Eqs. 7 and 8. The results are shown in Fig. 13. Three features of the response characteristics are particularly significant.

- Although the side acceleration response for this case was supposed to be low, simulated head position at the vehicle c.g., there is appreciable response at the higher frequencies. This is due to the frequency response limitations of the lateral position channel of the simulator; at the higher frequencies it is unable to offset the effects of the simulator angular acceleration about an axis approximately 1.5 ft below the subject's head.

- The dynamic limitations of the lateral position channel also result in very abrupt changes in the amplitude and phase which do not appear in the Y_m data.

- The (a_y/φ) response has considerably more lead than the $(\dot{\varphi}_s/\varphi)$ response of Fig. 12.

The next element in the utricular path represents the dynamics of the utricle itself, i.e., subjective acceleration/actual acceleration, $(a_{y_{sub}}/a_y)$. As detailed in Section V.B, the sensor dynamics can be approximated by a first-order lag with a break frequency of 1.5 rad/sec. Thus, the utricles, viewed as accelerometers, have a much poorer frequency response than the semicircular canals, viewed as rate gyros. As a result, much of the extra lead in the utricular path, (a_y/φ) versus $(\dot{\varphi}_s/\varphi)$, is lost when the differences in sensor characteristics are included.

The final term in the utricular path, $(c/a_{y_{sub}})$, is the pilot describing function from subjective acceleration to stick deflection. This includes any pilot equalization plus transmission and neuromuscular lags.

Having considered the various elements in both of the motion feedback paths, we are now in a position to examine their relative contributions to the measured Y_m's. The key item here is the abrupt variations in the

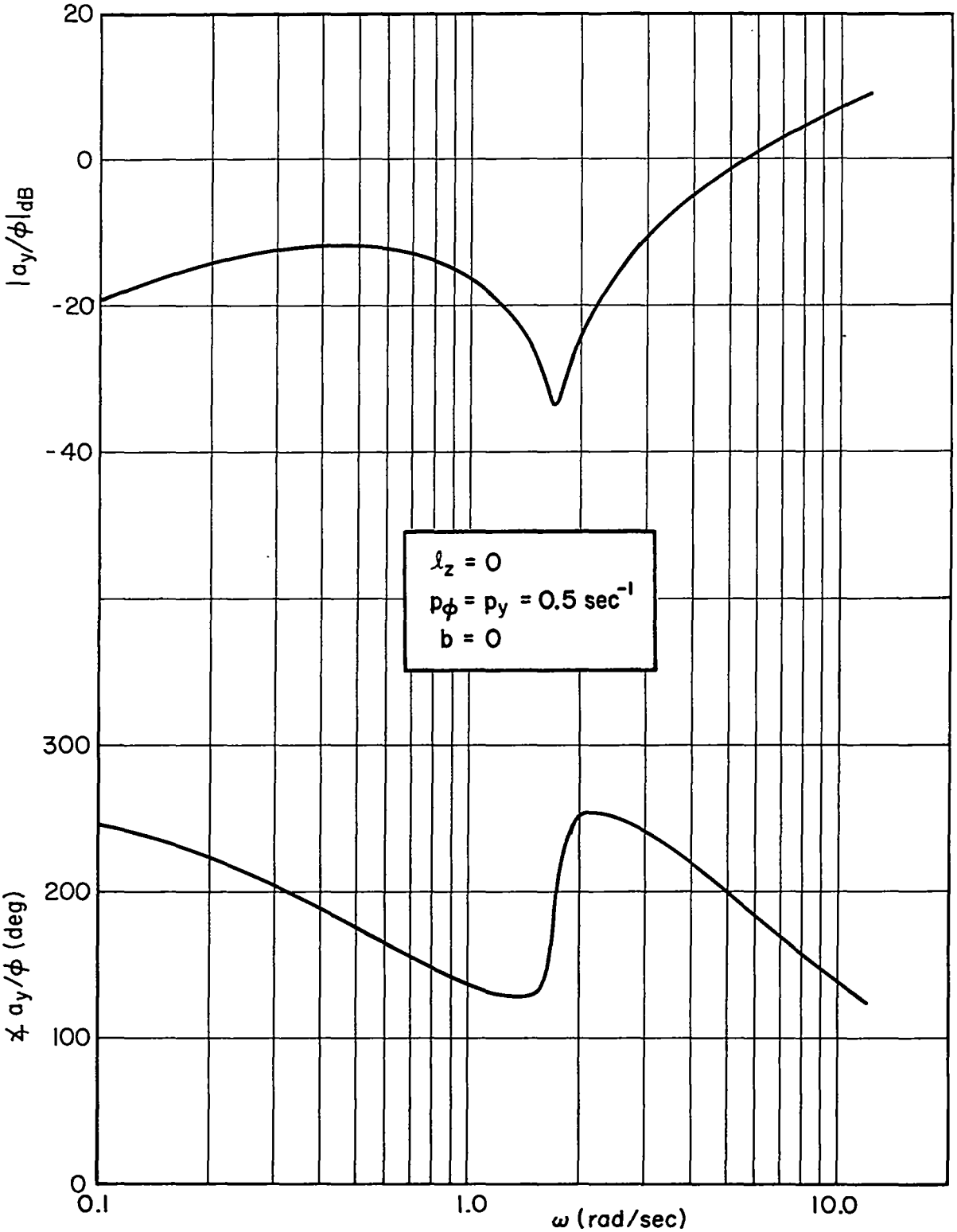

Figure 13. Lateral Acceleration Response Characteristics

amplitude and phase of the lateral acceleration response, (a_y/φ). If there were a significant utricular contribution to the motion feedback, one would expect similar variations in the Y_m data. Since there are none, it is concluded that the utricular contribution is, at most, minor. This conclusion will be further justified by the results described in Section III.C, which show very little effect for rather large changes in the linear motion cues. Furthermore, the Y_m data are matched very well by a simple model having only the semicircular canal path.

The Y_m data of Figs. 10 and 11 can be approximated by a pure lead and a time delay of 0.26 sec. By approximating the two known elements in this feedback, one can estimate the third element, i.e.,

$$Y_m = \left(\frac{\dot{\varphi}_s}{\varphi}\right)\left(\frac{\dot{\varphi}_{sub}}{\dot{\varphi}_s}\right)\left(\frac{c}{\dot{\varphi}_{sub}}\right) \tag{14}$$

$$Kse^{-0.26s} \doteq (se^{-0.1s})(e^{-0.1s})\left(\frac{c}{\dot{\varphi}_{sub}}\right) \tag{15}$$

or

$$\left(\frac{c}{\dot{\varphi}_{sub}}\right) \doteq Ke^{-0.06s} \tag{16}$$

Thus, the pilot describing function from subjective roll rate to stick deflection is approximately a gain and a time delay of 0.06 sec. Since this describing function includes both transmission and neuromuscular lags, 0.06 sec seems rather low. One possible explanation is that the total lag is actually somewhat larger but the pilots have adopted a high frequency lead to partially compensate for the lag.

2. Remnant Data

Two simple overall measures of remnant are the relative correlated error, $\rho_{a_e}^2$, and the relative correlated output, $\rho_{a_c}^2$. Data on both of these parameters are shown in Fig. 14. Several features of this data are interesting.

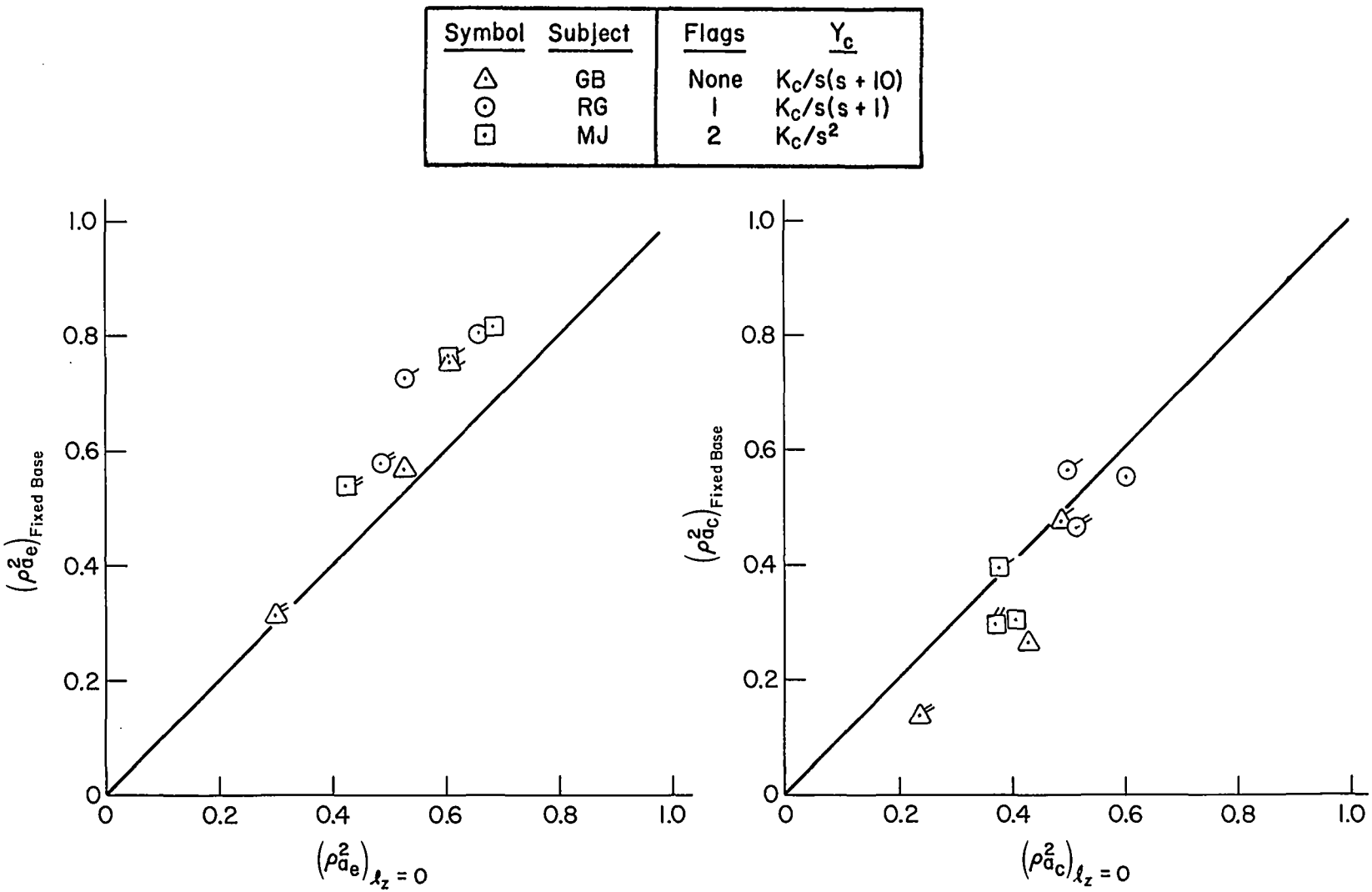

Figure 14. Motion Effects on Relative Correlated Error and Output

- $\rho_{a_e}^2$ is always higher fixed base than moving base
- $\rho_{a_c}^2$ is generally lower fixed base than moving base
- With one exception, $\rho_{a_e}^2$ is greater than $\rho_{a_c}^2$

However, these data per se shed light only on the smoothed-over effects of motion cues on pilot remnant. To provide more detailed information we will examine the power spectra of the pilot's output.

Remnant can be modeled as either noise injected at the pilot's input, n_e, or output, n_c, see Fig. 15. If input frequencies are excluded, then the power spectra of the pilot's output is given by

$$\Phi_{cc} = \left| \frac{Y_p}{1 + Y_p Y_c} \right|^2 \Phi_{n_e n_e} \tag{17}$$

$$\Phi_{cc} = \frac{1}{|1 + Y_p Y_c|^2} \Phi_{n_c n_c} \tag{18}$$

The choice of model forms is somewhat arbitrary, see Ref. 7. Note that to match the measured spectra, Φ_{cc}, the two models are related by

$$\Phi_{n_c n_c} = |Y_p|^2 \Phi_{n_e n_e} \tag{19}$$

Power spectra of the pilot's output were measured for the 12 runs listed in Table IX. These runs cover fixed and moving base, the two

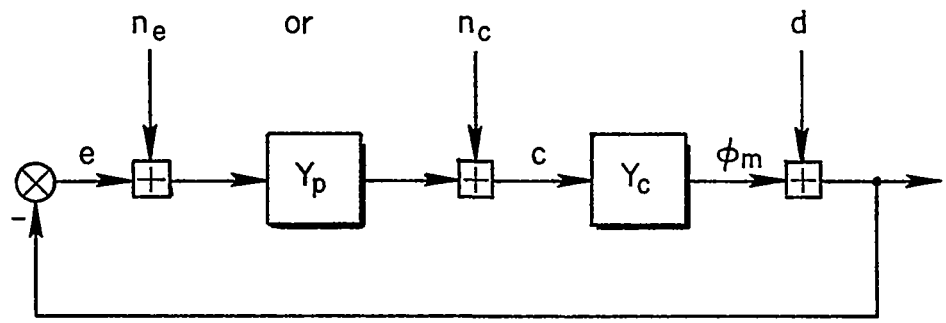

Figure 15. Remnant Models

TABLE IX

RUNS SELECTED FOR REMNANT ANALYSIS

Y_c		MOTION		SUBJECT		RUN NUMBERS
$K_c/s(s+10)$	K_c/s^2	FIXED BASE	$\ell_z = 0$	RG	MJ	
x		x		x		102316 102504
x			x	x		102315 102503
	x	x		x		102403 102510
	x		x	x		102402 102509
x		x			x	264
x			x		x	263
	x	x			x	269
	x		x		x	268

extremes in controlled element dynamics, two subjects, and two replications for one subject. Two examples of the spectra are shown in Fig. 16 (components at input frequencies have been removed). For 11 of the 12 runs,* it was found that over the frequency range for which good describing function and spectral data were available (1 – 10 rad/sec) the power spectral shape closely matched $1/|1 + Y_p Y_c|^2$. This indicates that the remnant can be viewed as a flat spectra from 1 – 10 rad/sec injected at the pilot's output. Furthermore, beyond 10 rad/sec $|Y_p Y_c| << 1$ so that the spectra Φ_{cc} and $\Phi_{n_c n_c}$ are nearly equal. All the data then indicate a $\Phi_{n_c n_c}$ spectra which is flat out to roughly 20 rad/sec. The only effect of changes in controlled element or motion cues was to change the magnitude of $\Phi_{n_c n_c}$.

*The twelfth run ($Y_c = K_c/s(s+10)$, $\ell_z = 0$, Subject: MJ) did not have the peak in the spectra corresponding to the closed-loop dominant mode. No explanation for this phenomenon is known.

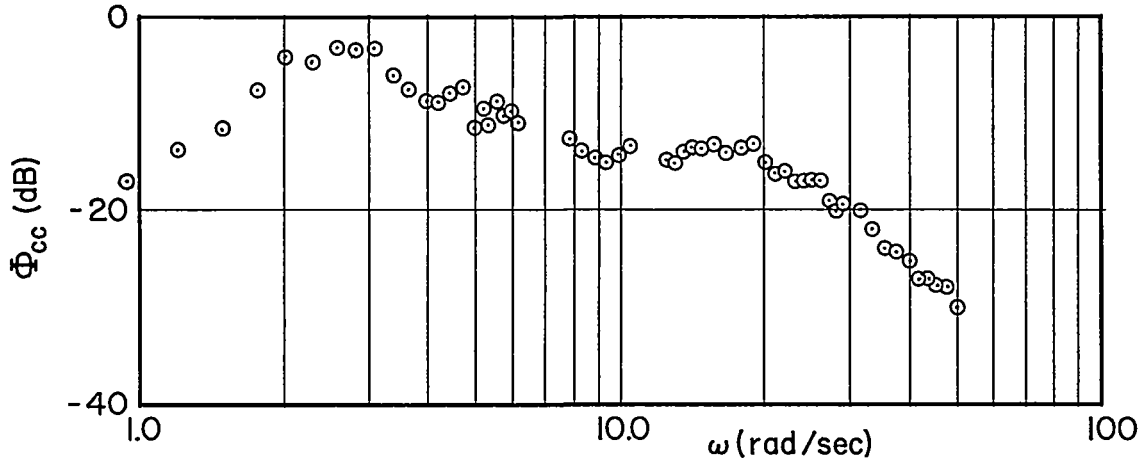

a) Fixed Base

$Y_c = K_c / s^2$ Subject : MJ

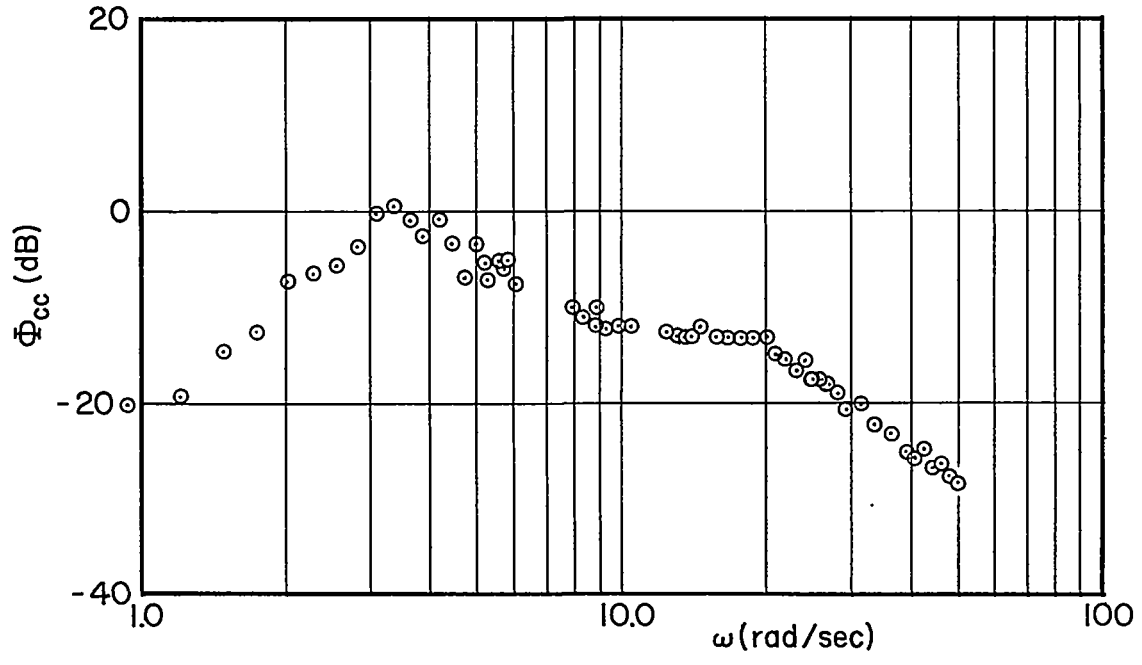

b) $\ell_z = 0$

Figure 16. Sample Power Spectra of Pilot Output

The effects of motion cues on the open-loop remnant are listed in Table X. In one case there was no change but in the others the moving-base remnant was a factor of 2 or more greater than the fixed-base values.

TABLE X

MOTION EFFECTS ON REMNANT

Y_c		MOTION		SUBJECT		$\Phi_{n_c n_c}$ for $\omega = 1-20$ rad/sec (deg^2/rad/sec)	$\frac{(\Phi_{n_c n_c})_{\ell_Z = 0}}{(\Phi_{n_c n_c})_{\text{fixed base}}}$
$\frac{K_c}{s(s+10)}$	K_c/s^2	FIXED BASE	$\ell_Z = 0$	RG	MJ		
x		x		x		0.037	2.2
x			x	x		0.081	
	x	x		x		0.13	1.0
	x		x	x		0.13	
x		x			x	0.0071	2.8*
x			x		x	0.020*	
	x	x			x	0.040	2.0
	x		x		x	0.079	

*Data questionable because of missing peak in Φ_{cc} at dominant closed-loop mode.

It should be noted that the above results do not agree with the data of Ref. 7 or the Ref. 8 analysis of the Ref. 9 data. Those reports presented remnant data for fixed-base tracking for a variety of controlled elements and input bandwidths. They concluded that the highest degree of similarity in the remnant data existed for the remnant injected at the pilot's input, n_e. The results reported here show the greatest similarity for remnant injected at the pilot's output. No explanation for this apparent discrepancy is currently available.

3. Performance Data

The effects of motion on performance will be discussed in terms of the normalized mean-square error, $\overline{e^2}/\overline{d^2}$. However, to provide a closer

tie to the describing function and remnant results, $\overline{e^2}/\overline{d^2}$ will be divided into two components. One component, $\overline{e_i^2}/\overline{d^2}$, includes only the error components at input frequencies. The remaining component, $\overline{e_n^2}/\overline{d^2}$, is that due to remnant. Data on motion effects on the two components and the total are shown in Fig. 17. The most significant features of these results are:

- $\overline{e_i^2}/\overline{d^2}$ is much less with motion than fixed base; ratio of moving/fixed base values is 0.27−0.52. This is compatible with the observed increases in crossover frequency discussed earlier.
- $\overline{e_n^2}/\overline{d^2}$ is reduced with motion, ratio of 0.40−0.98, but the percentage reduction is always less than for $\overline{e_i^2}/\overline{d^2}$. Any increases in the injected remnant are apparently more than compensated for by the increased crossover frequency.
- Total error, $\overline{e^2}/\overline{d^2}$, is considerably reduced by the addition of motion cues, ratio of 0.32−0.51.
- For each of the three subjects, motion effects on $\overline{e_i^2}/\overline{d^2}$, $\overline{e_n^2}/\overline{d^2}$, and $\overline{e^2}/\overline{d^2}$ were greater for $Y_c = K_c/s^2$ than for $Y_c = K_c/s(s+10)$.

C. EFFECTS OF VARIATIONS IN THE LINEAR MOTIONS

For a given controlled element, the linear motion cues could be varied independently of the angular cues by changing the parameters in the position washout and equalization circuits, see Fig. 2. A number of these variations were tested for controlled elements $Y_c = K_c/s(s+10)$ and $Y_c = K_c/s^2$. The parameters which were varied were ℓ_z, p_y, and b, Eq. 6. The resulting change in the describing function for roll angle to lateral acceleration at pilot's head is shown in Fig. 18. The main point of Fig. 18 is that rather large variations in the linear cues were tested. Yet, as we will see, the variations did not produce any significant changes in the tracking data.

There was, however, an effect on the pilots' subjective impressions of the simulation. For those parameter combinations which produced higher lateral accelerations there were pilot complaints of a tendency toward disorientation. The comments of Subject GC relative to disorientation are listed in Table XI.

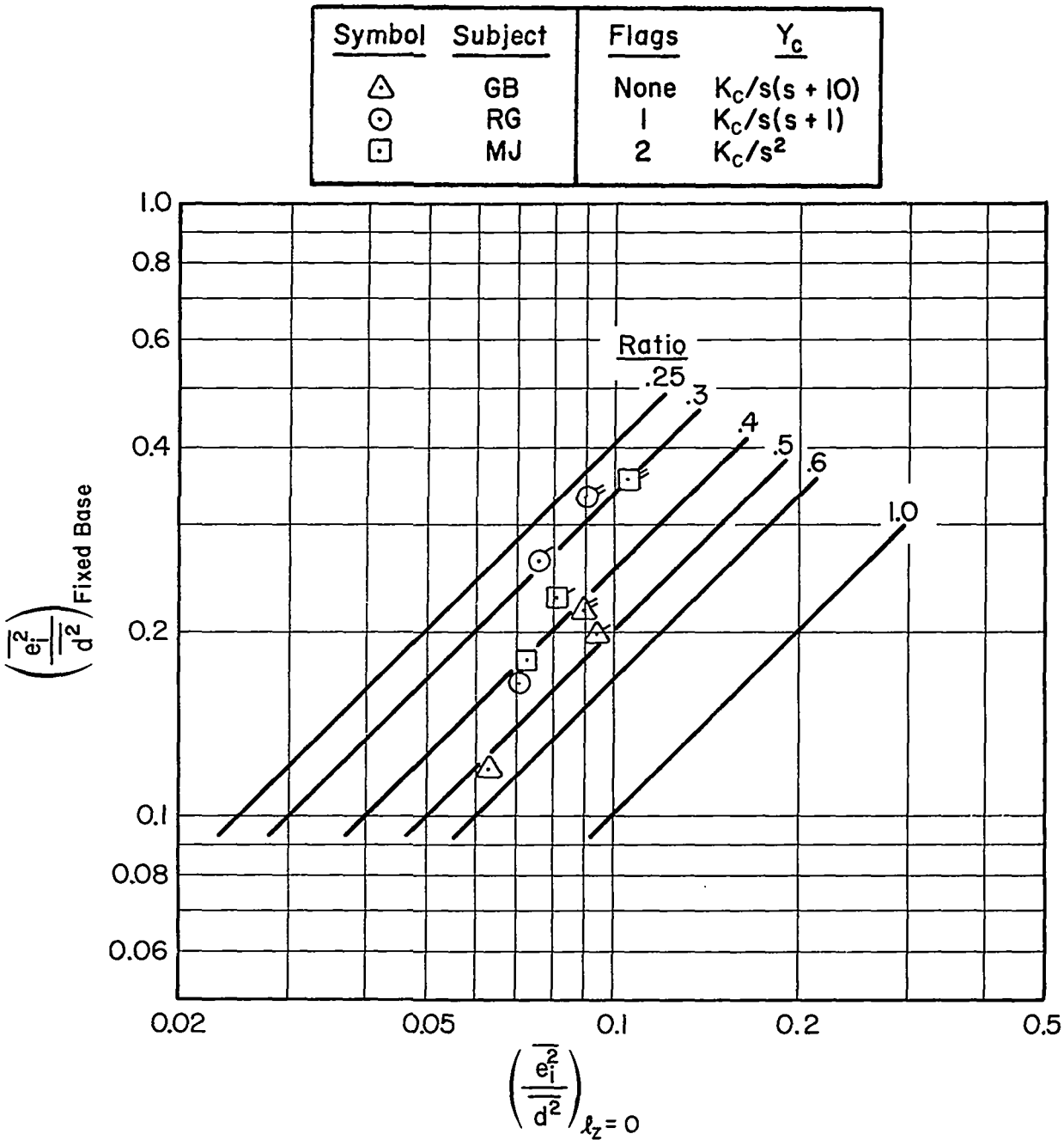

Figure 17. Motion Effects on Performance

a. $\overline{e_i^2}/\overline{d^2}$

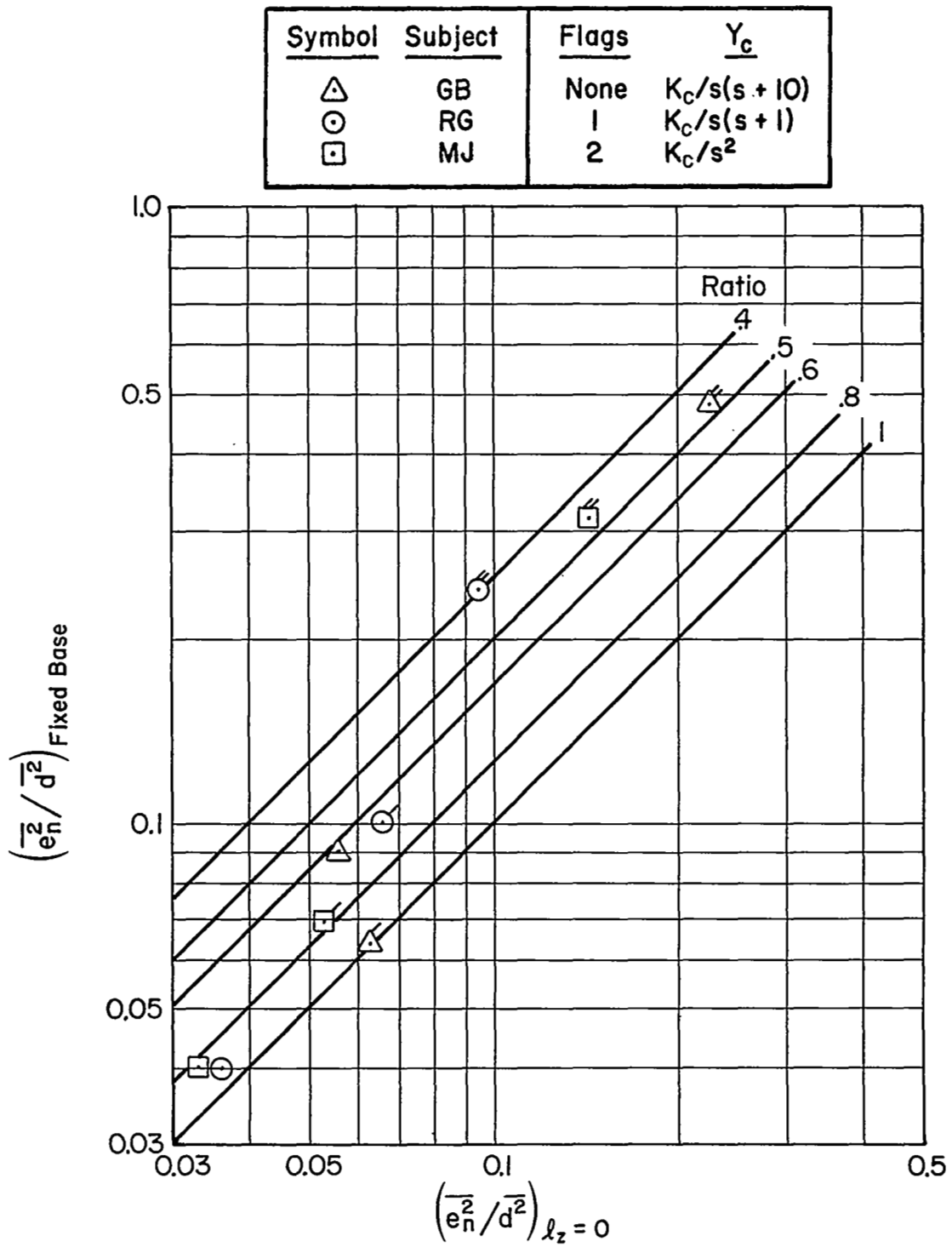

Figure 17 (Continued)

b. $\overline{e_n^2}/\overline{d^2}$

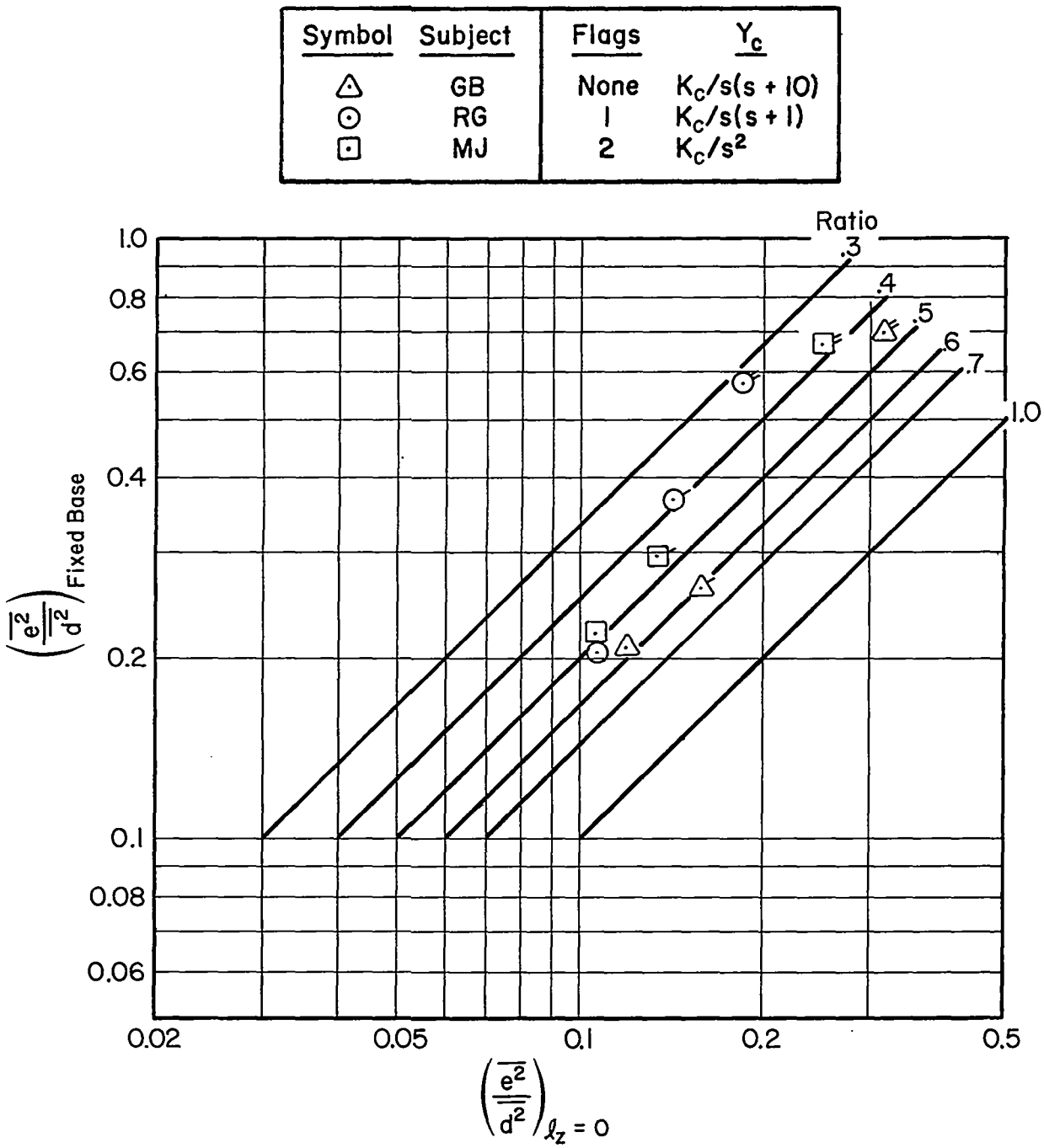

Figure 17 (Concluded)

c. $\overline{e^2}/\overline{d^2}$

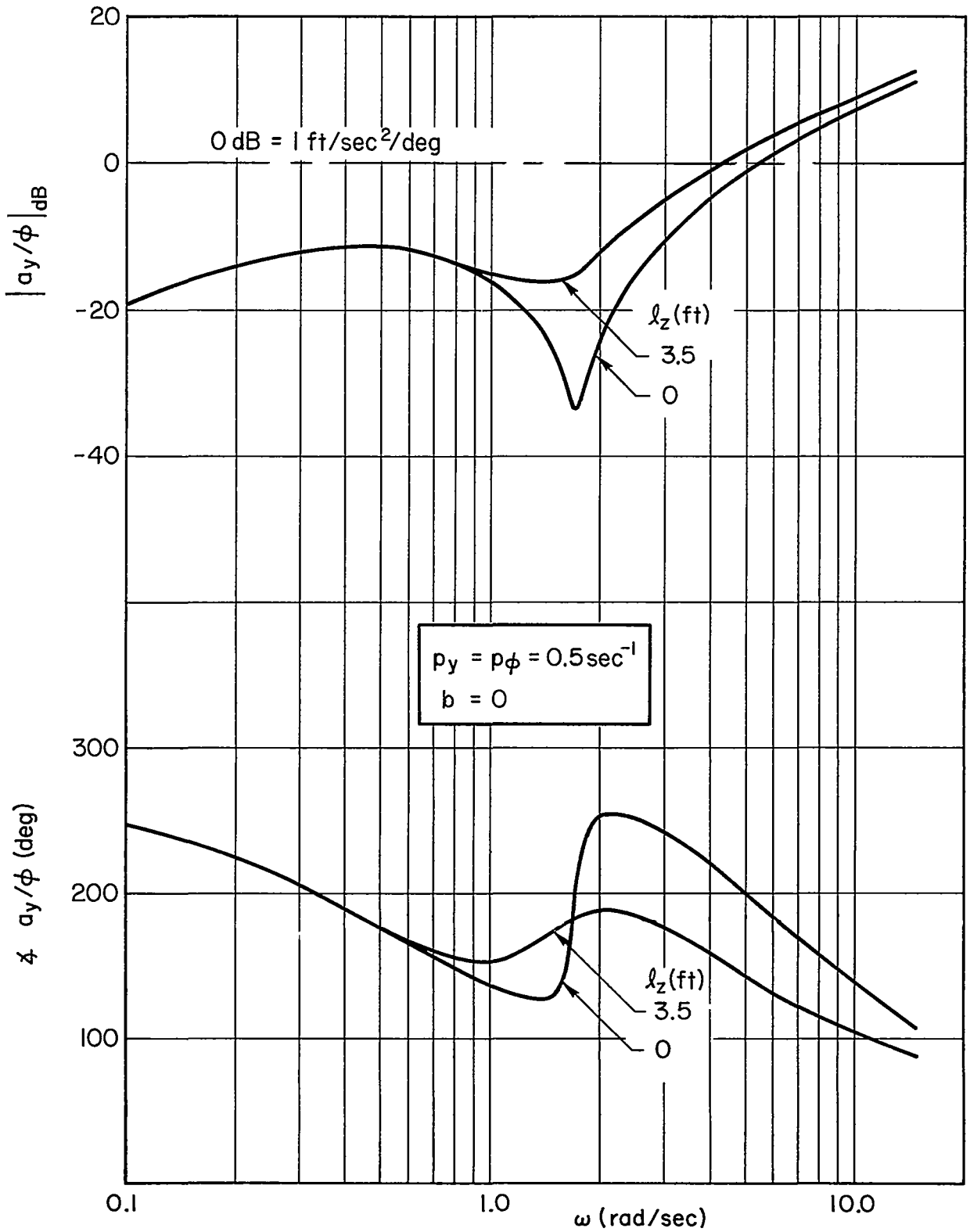

Figure 18. Effects of Parameter Variations on Lateral Acceleration Response

a. ℓ_z Variations

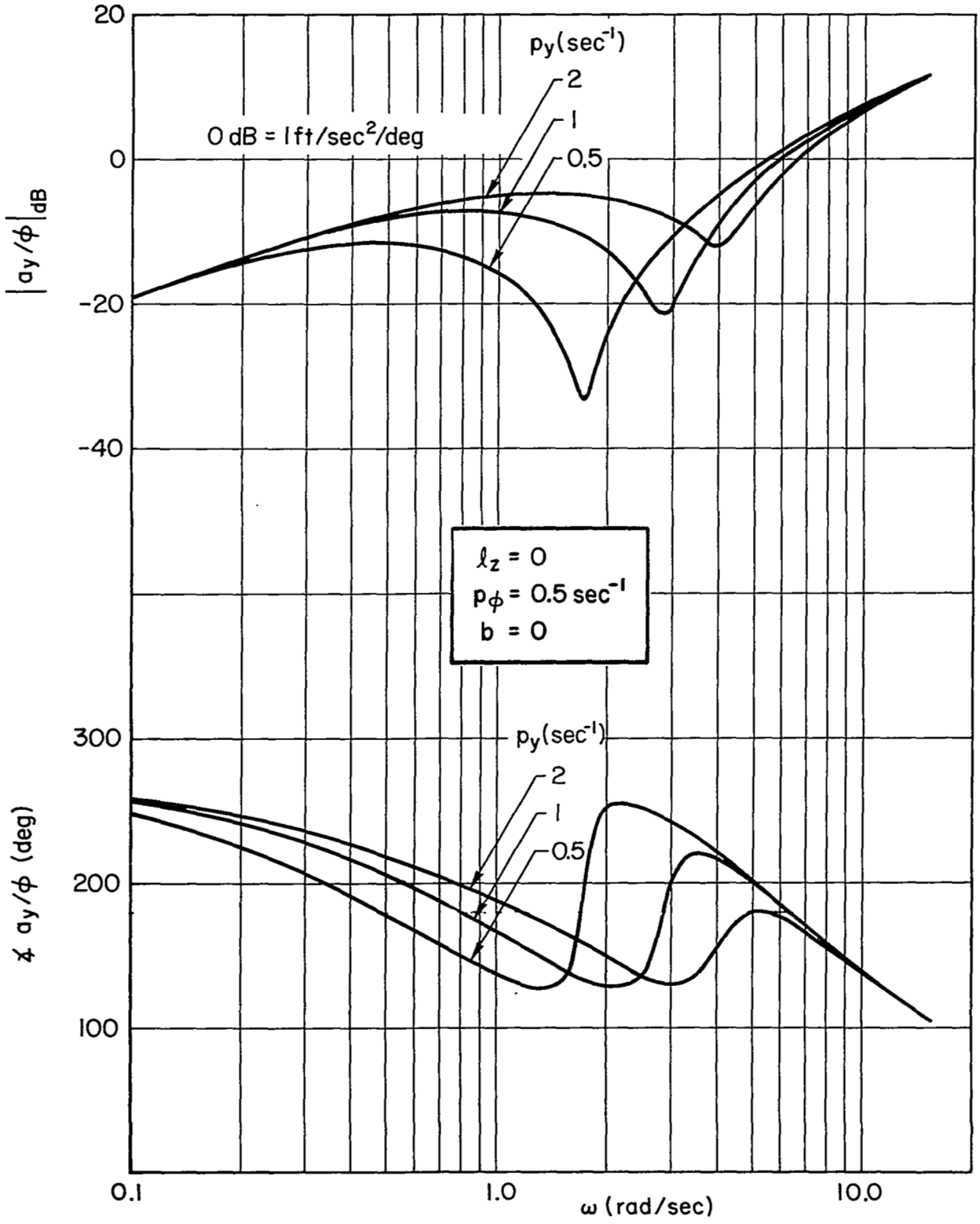

Figure 18 (Continued)

b. p_y Variations for $\ell_z = 0$

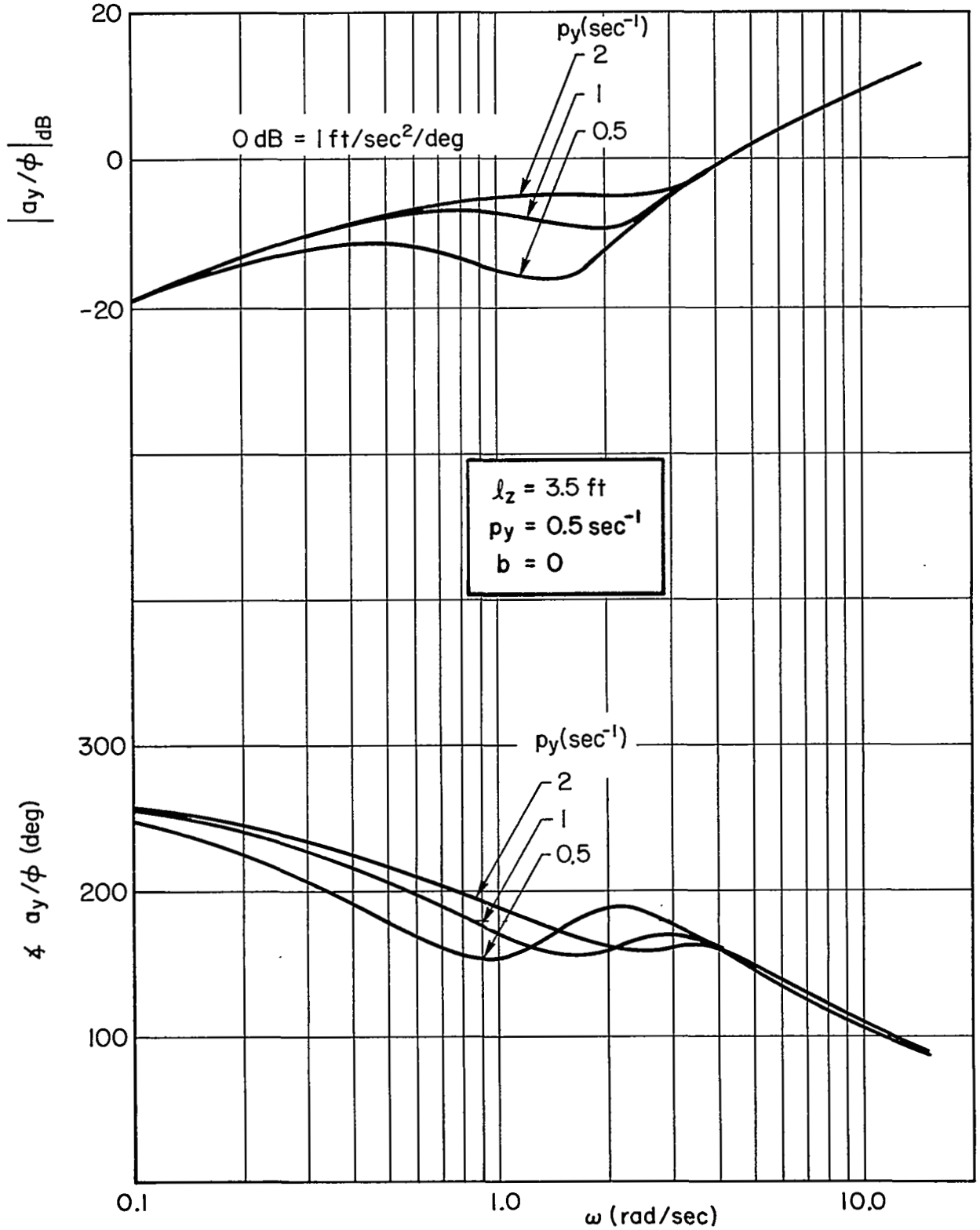

Figure 18 (Continued)

c. p_y Variations for $\ell_z = 3.5$ ft

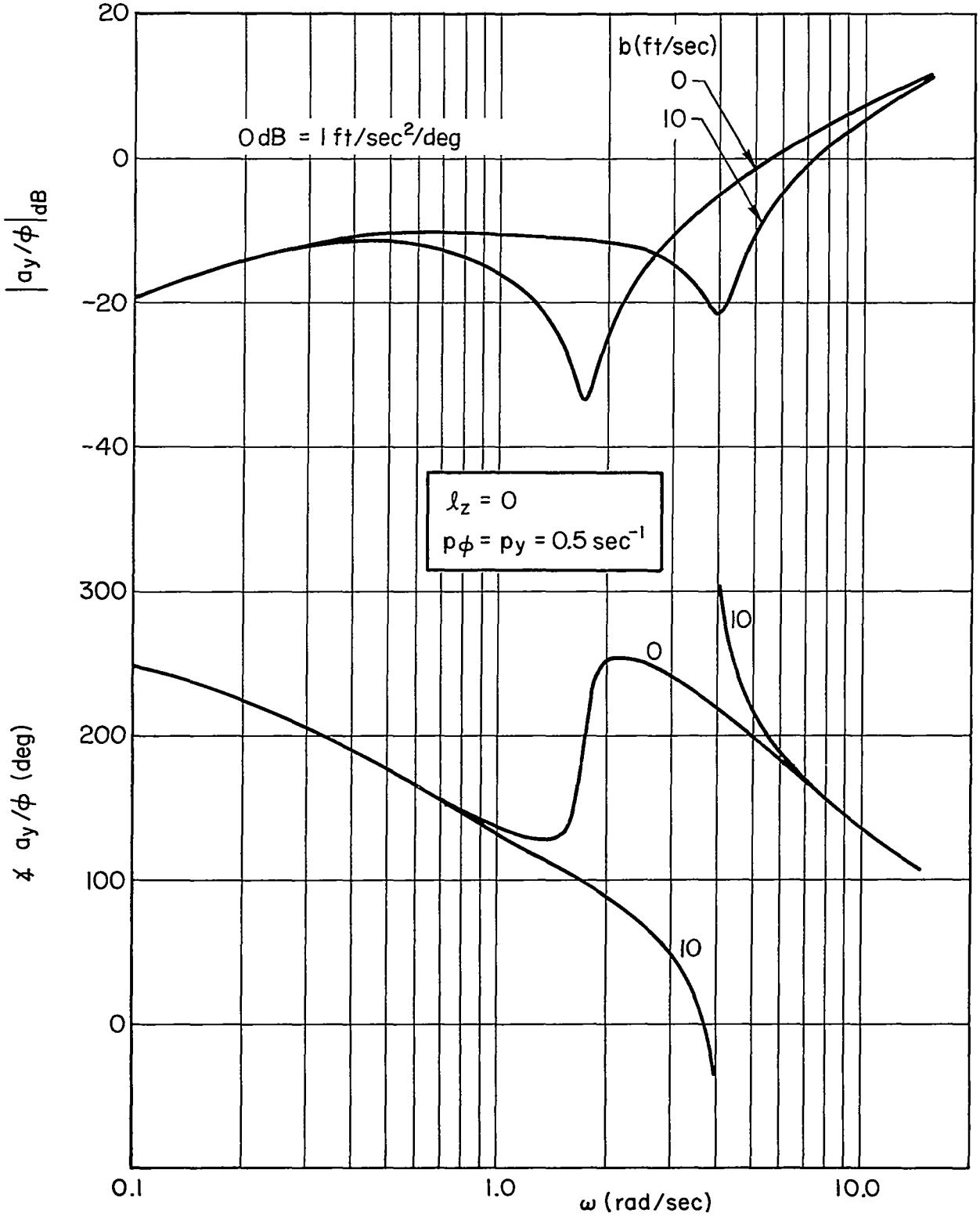

Figure 18 (Concluded)

d. b Variation

TABLE XI

PILOT COMMENTS ON DISORIENTATION

SUBJECT: GC $p_\varphi = 0.5$ sec^{-1} b = 0

Y_c	ℓ_z (ft)	p_y (sec^{-1})	PILOT COMMENT
$\frac{K_c}{s(s+1)}$	3.5	0.5	I'm having a very slight tendency toward disorientation from the lateral feedback here.
$\frac{K_c}{s^2}$	3.5	0.5	Must have added incentive to keep the errors small — to keep the large head motion which, at the largest or highest rates, gives some feeling of disorientation.
$\frac{K_c}{s(s+10)}$	0	1	Fairly distracting and somewhat disorienting motion involved in this simulation.
$\frac{K_c}{s^2}$	0	1	Still definitely disturbing and somewhat disorienting, nauseating, so to speak.
$\frac{K_c}{s(s+10)}$	0	2	Disorienting
$\frac{K_c}{s^2}$	3.5	2	...there's a feeling of disorientation

Overall pilot describing functions, Y_p, were computed for 30 runs in which the linear acceleration cues were varied from those of the $\ell_z = 0$ runs considered earlier in Section III.B. None of these data showed any significant effects of the changes in the linear cues. Because of the negative results only a small sample of that data is presented here in Fig. 19.

The separated visual and motion describing functions were computed for 15 two-input runs in which ℓ_z was 3.5 ft. Figure 20 compares these results with the $\ell_z = 0$ data discussed earlier. The phase data show no discernible effects of the ℓ_z variation but there are some differences

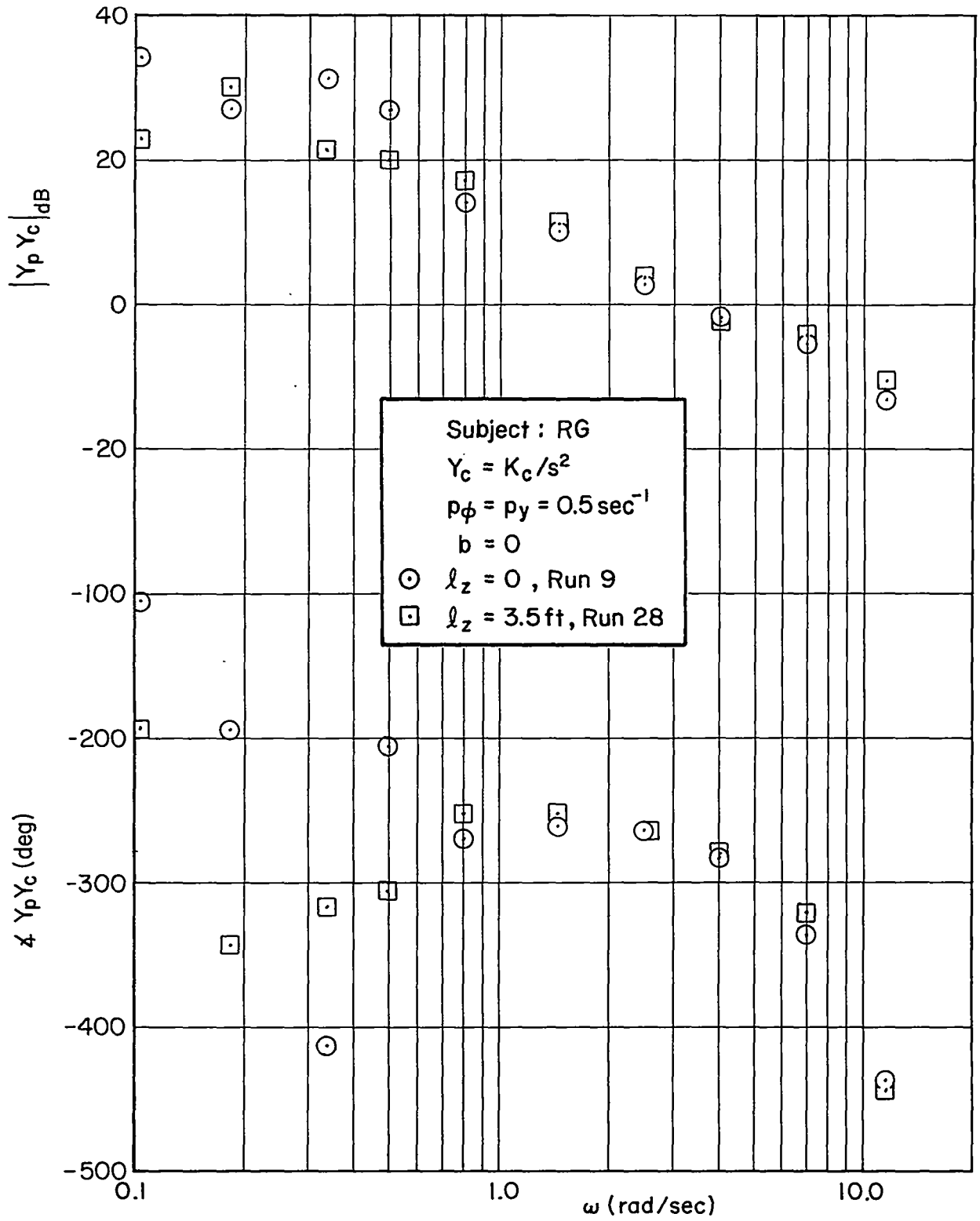

Figure 19. Effects of Parameter Variations on Overall Describing Function

a. ℓ_z Variations

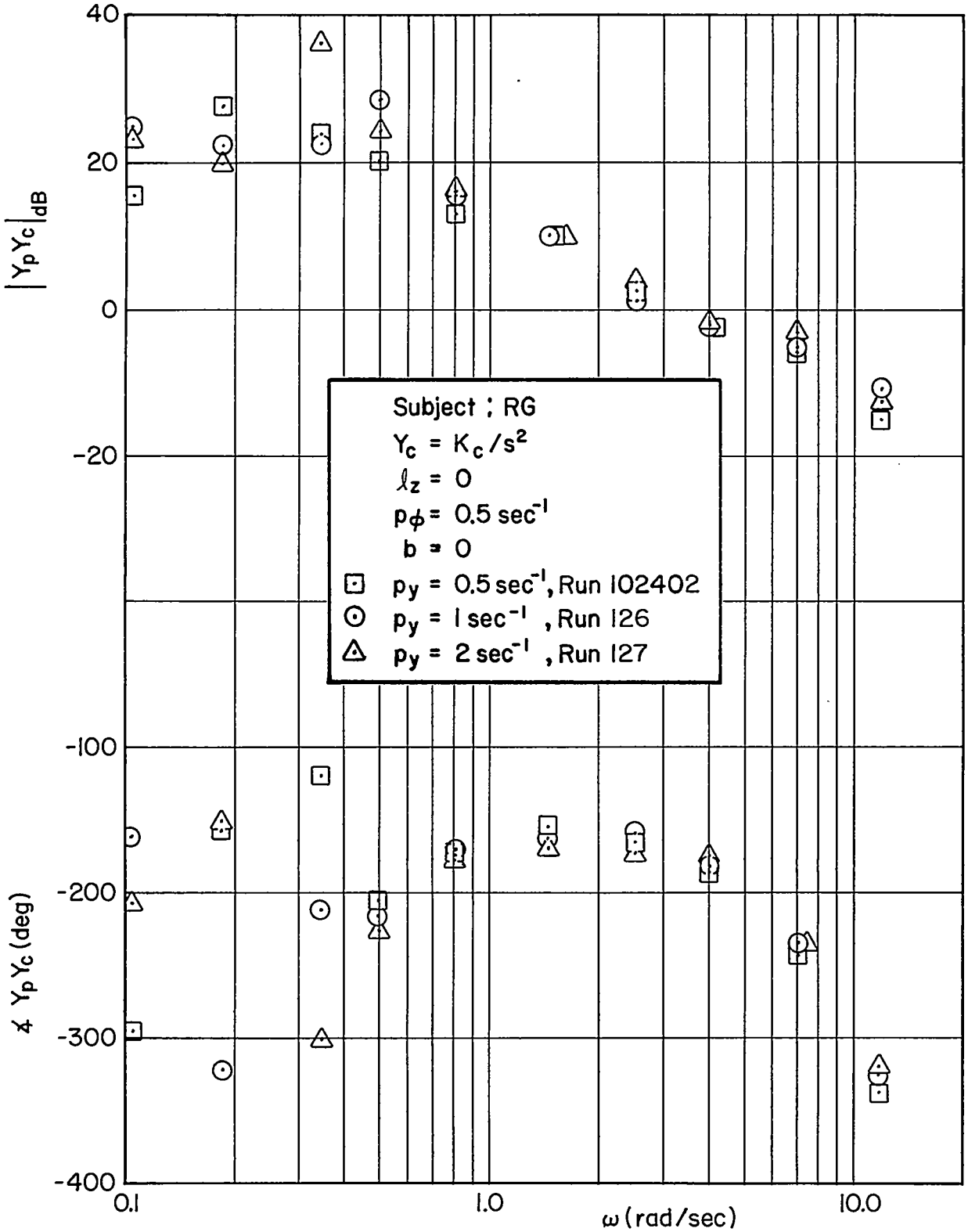

Figure 19 (Continued)

b. p_y Variations for $\ell_z = 0$

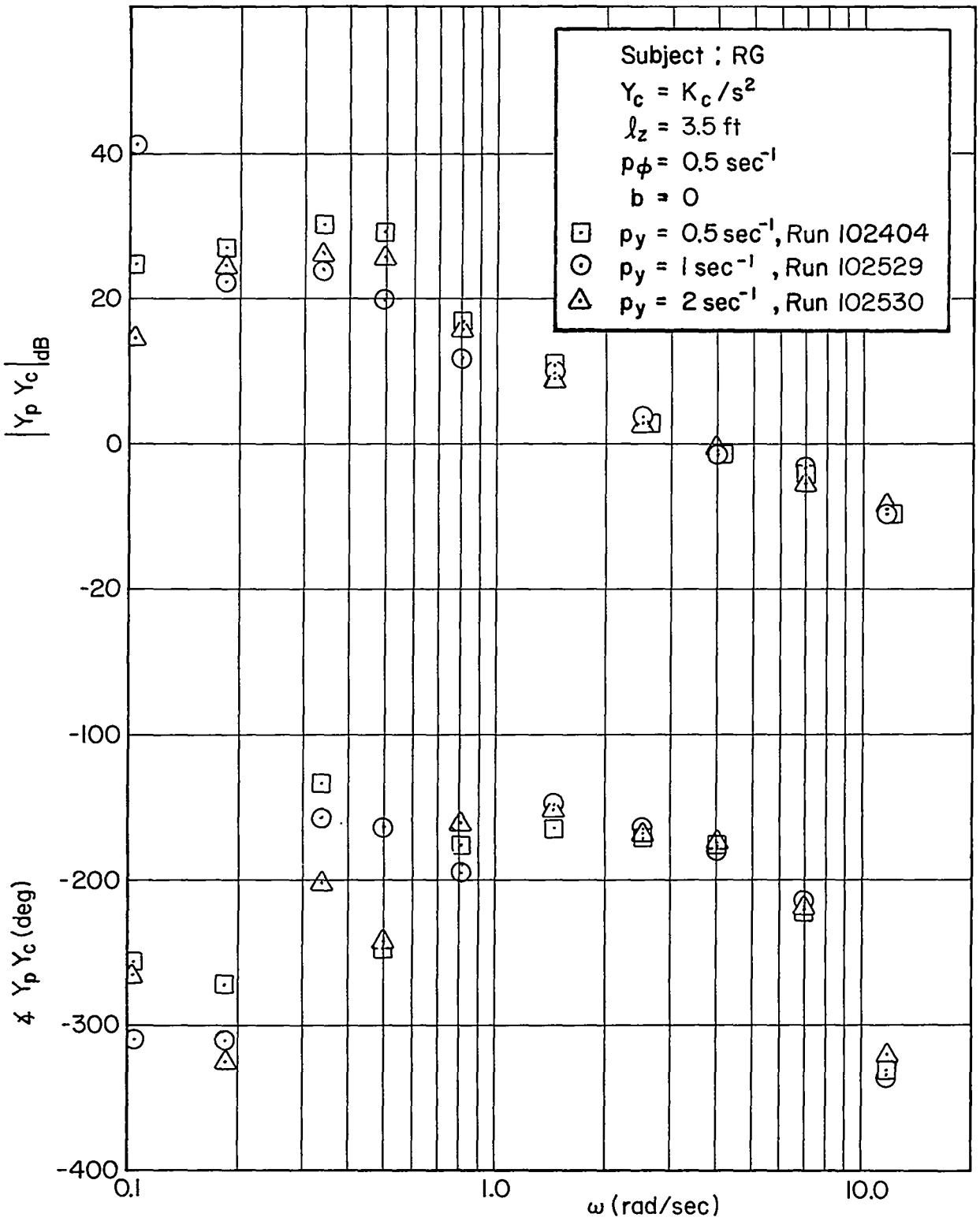

Figure 19 (Continued)

c. p_y Variation for $\ell_z = 3.5$ ft

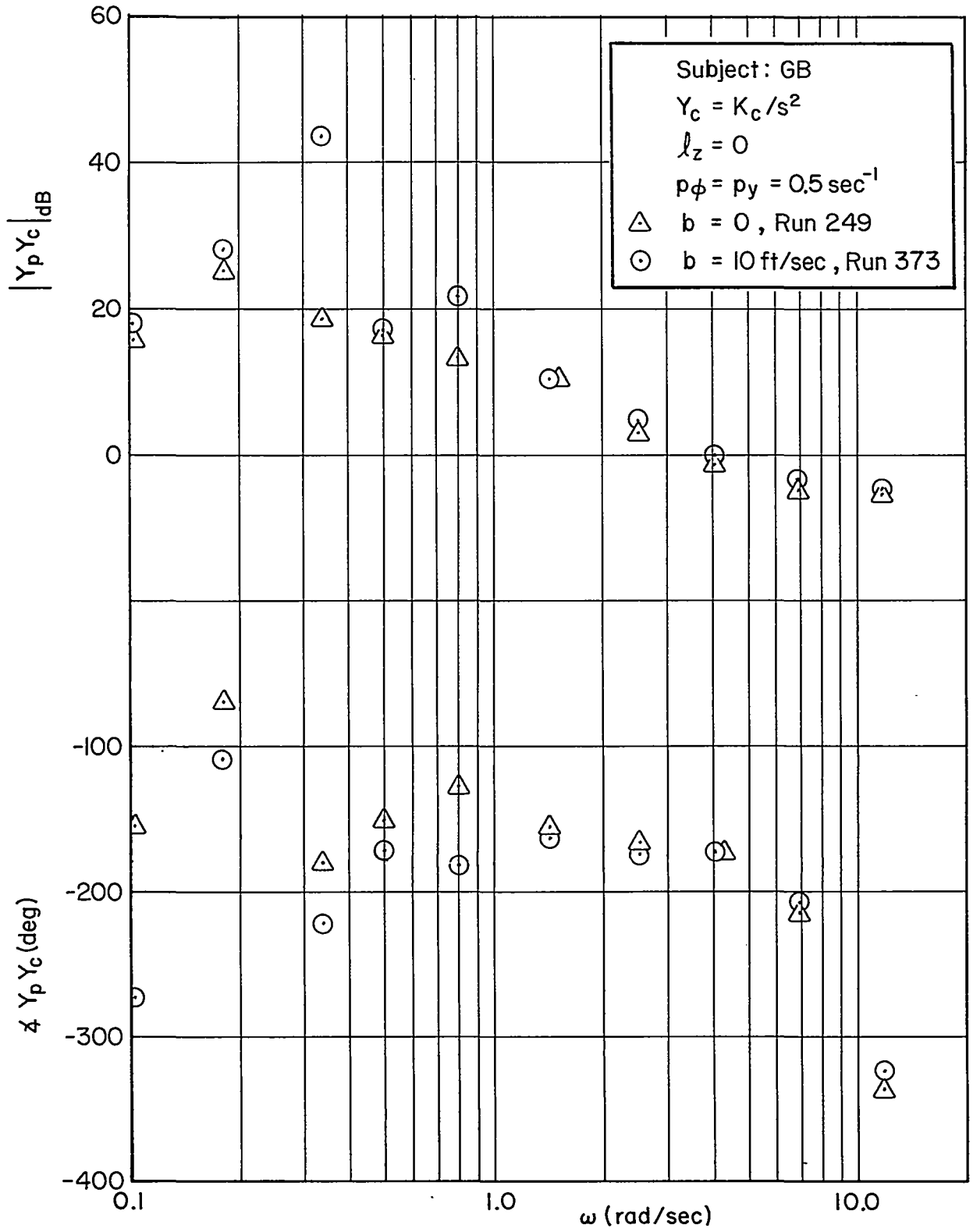

Figure 19 (Concluded)

d. b Variations

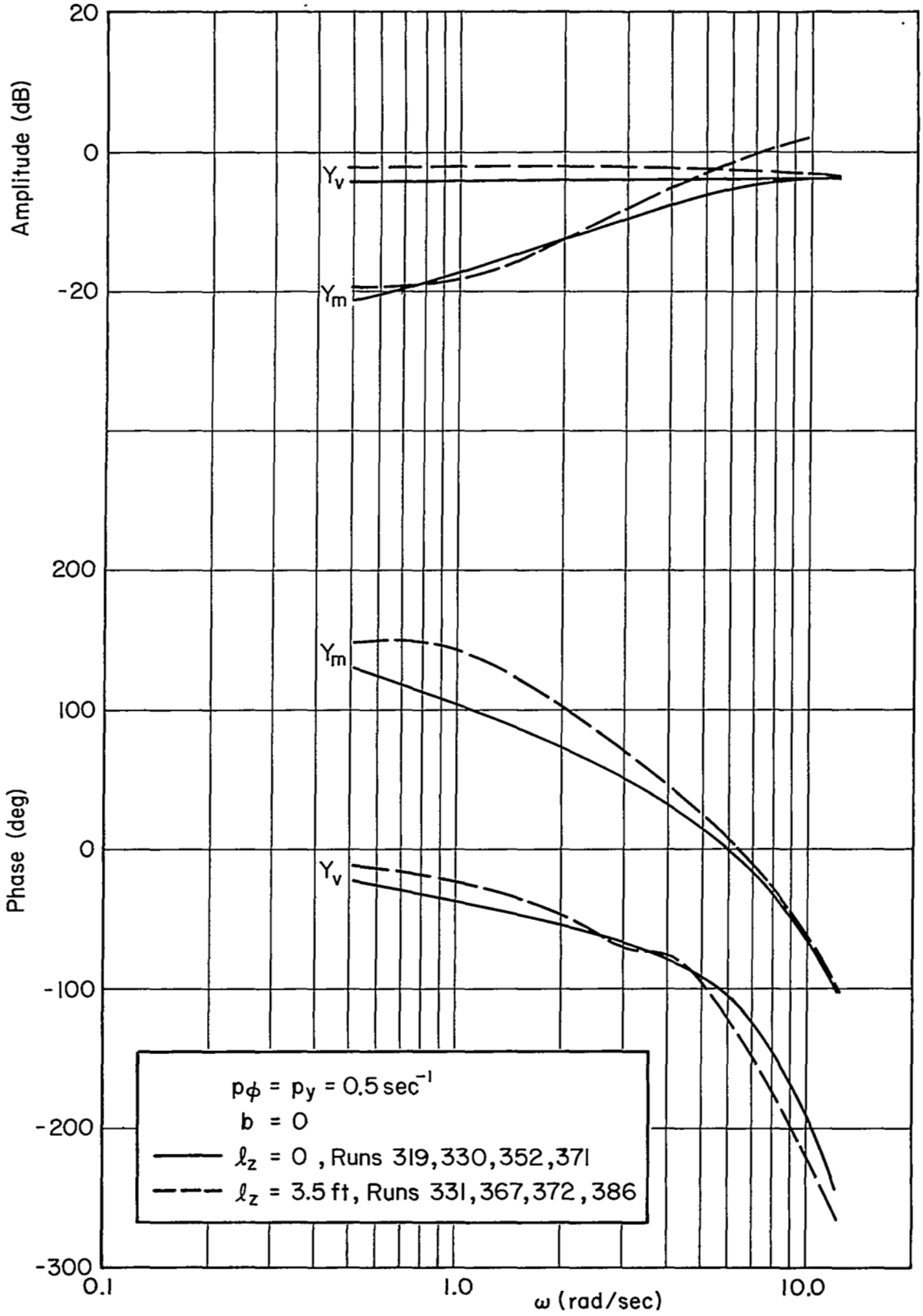

Figure 20. Effects of ℓ_z on Visual and Motion Feedbacks

a. $Y_c = K_c/s(s + 10)$, Subject: GB

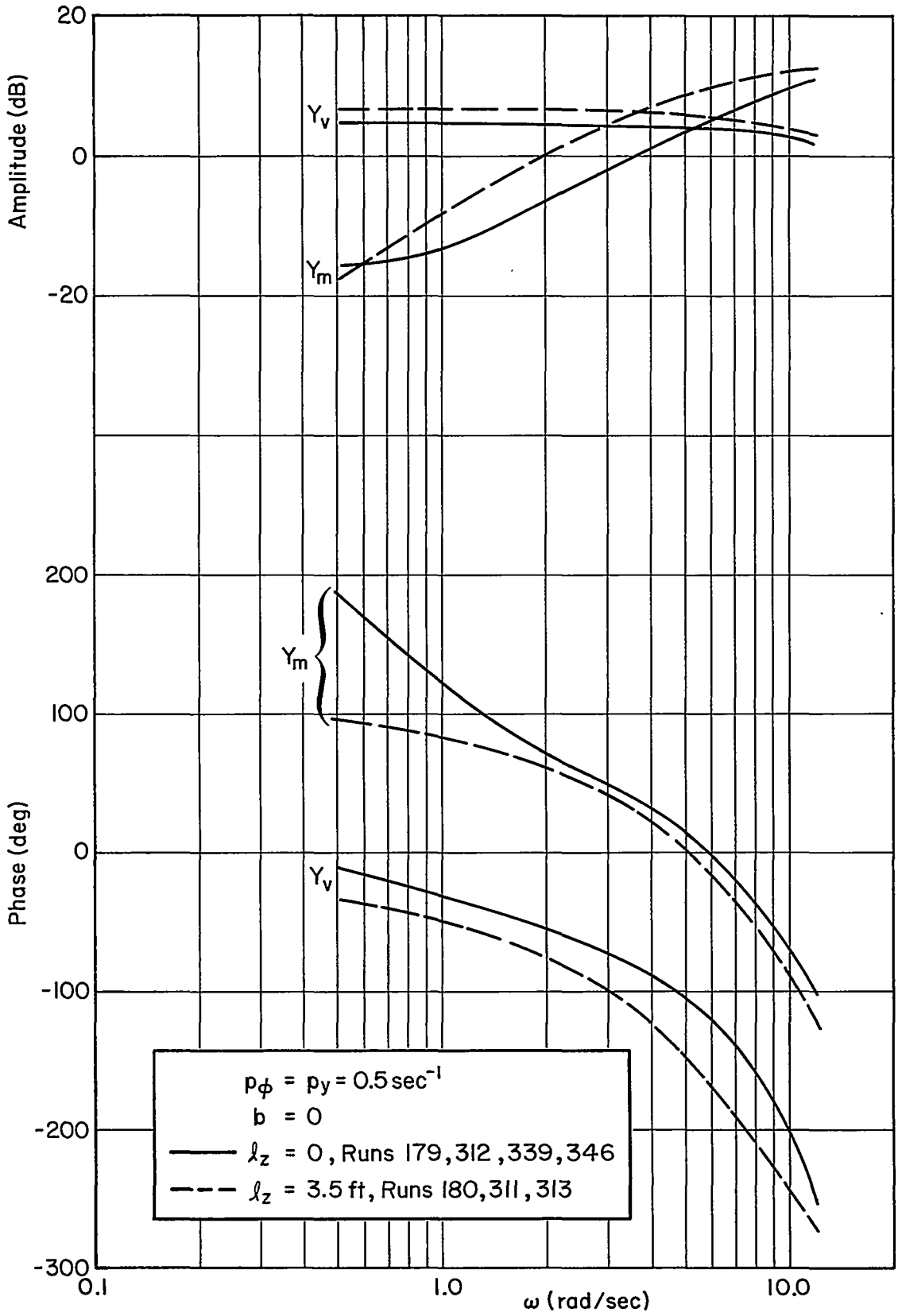

Figure 20 (Continued)

b. $Y_c = K_c/s(s+10)$, Subject: RG

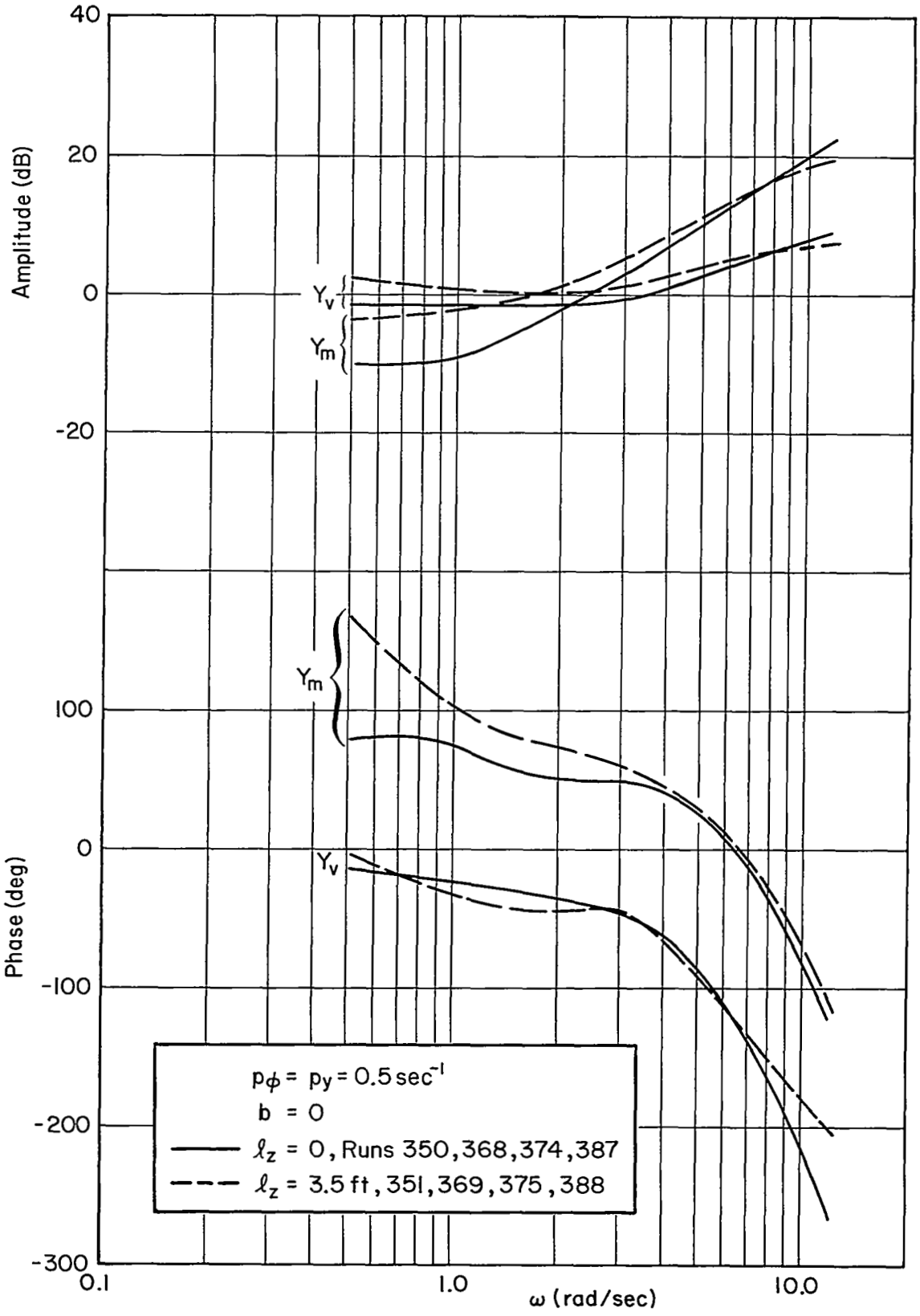

Figure 20 (Continued)

c. $Y_c = K_c/s^2$, Subject: GB

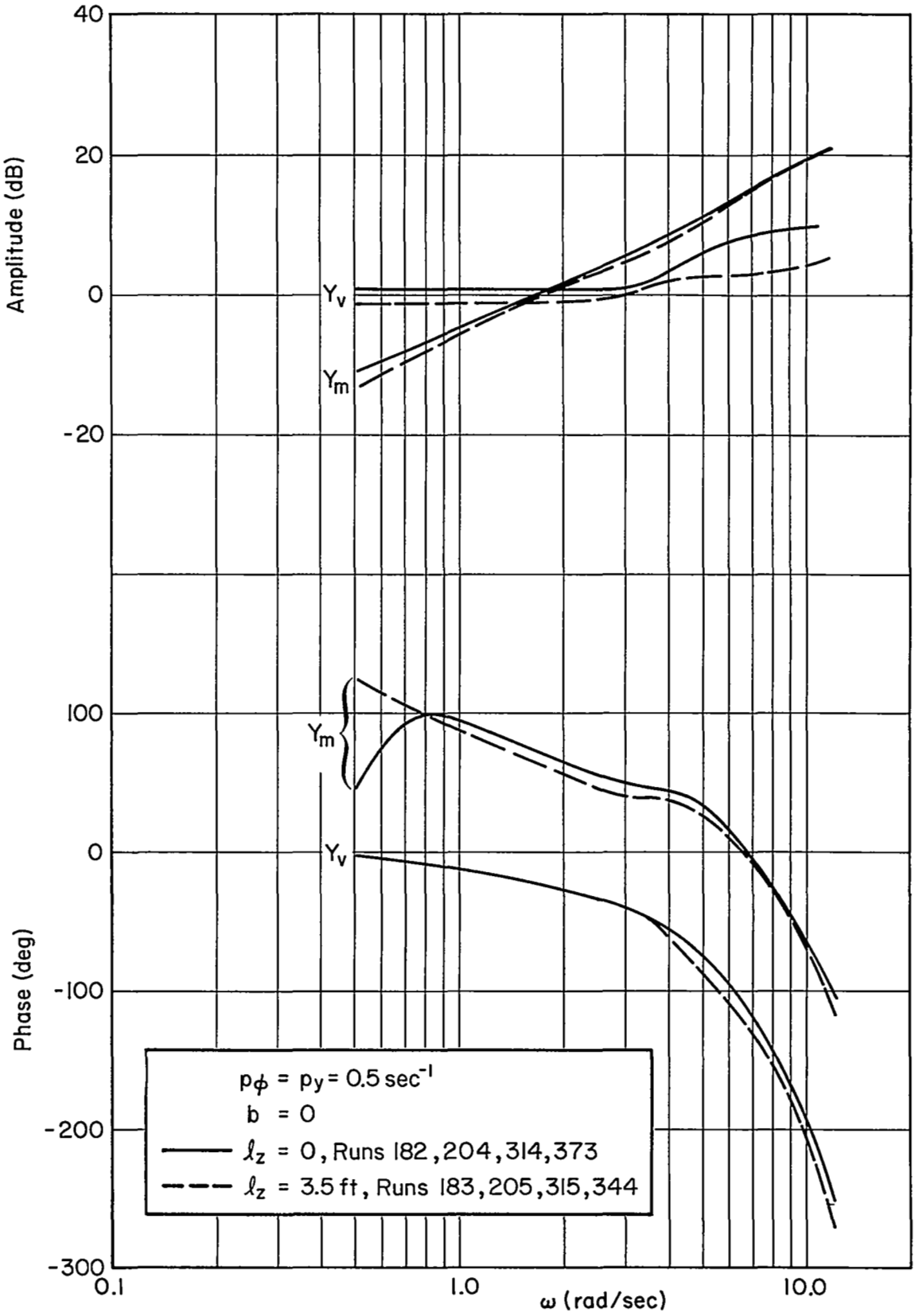

Figure 20 (Concluded)

d. $Y_c = K_c/s^2$, Subject: RG

in the magnitudes. In three cases the Y_v and Y_m magnitudes for $\ell_z = 3.5$ ft are generally larger than for $\ell_z = 0$, while in the fourth case the situation is reversed. An increase in the computed magnitude of Y_v results in an increase in the computed magnitude of Y_m because they differ in phase by roughly $100 - 150$ deg and their sum, Y_p, is the same for $\ell_z = 0$ or 3.5 ft (recall Fig. 19a). Since the amplitude differences due to ℓ_z are not completely consistent, the differences shown in Fig. 20 may be more an indication of the accuracy of the two-input data reduction than of an ℓ_z effect. This interpretation is supported by the lack of definite ℓ_z effects on any of the other metrics.

The effects of changing the linear motion cues on tracking performance were also checked. Since the $\overline{e^2}/\overline{d^2}$ data are available only for those runs which were processed on the digital computer (a fraction of the total experimental runs), the comparison was made using the on-line performance measure, mean-absolute error, $\overline{|e|}$. This parameter is available for all runs. The data are shown in Fig. 21. No definite effect of changing either ℓ_z or p_y can be discerned. However, there may be a small improvement in performance for $b \neq 0$. Yet, the Y_p describing function data for the two runs with $b = 10$ ft/sec which were analyzed show minor, if any, differences from $b = 0$ runs (data for one of these runs is given in Fig. 19d). The slight performance change may actually be a training effect since the $b \neq 0$ runs were only made after all replications with the other configurations indicated in Fig. 21.

D. EFFECTS OF ROLL WASHOUT

Variations in the roll washout will, of course, alter the rotary motion cues seen by the pilot. However, they also change the linear acceleration cues because the pilot is not on the roll axis of the simulator. The net effects on both the rotational and linear motion cues are shown in Fig. 22. With increasing p_φ, the amplitude of the roll response at the lower frequencies is decreased and the phase lead is increased. The reduced amplitude should degrade the pilot's use of this cue but the increased lead is helpful. The variations in the linear cues are large but from the results discussed in the previous subsection, we would expect them to have little effect.

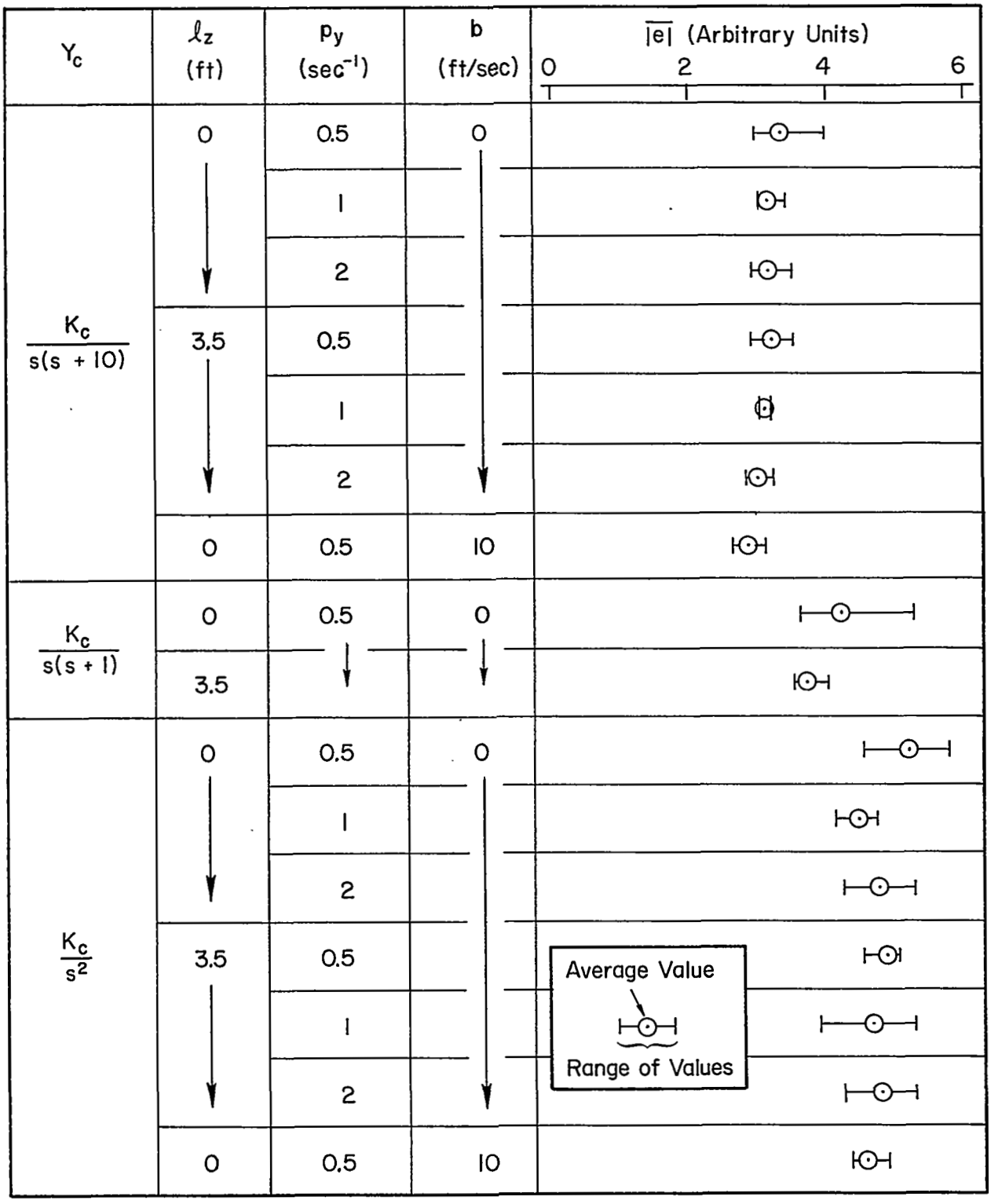

$p\phi = 0.5 sec^{-1}$

Figure 21. Performance Data for Variations in Linear Motions

a. Subject: GB

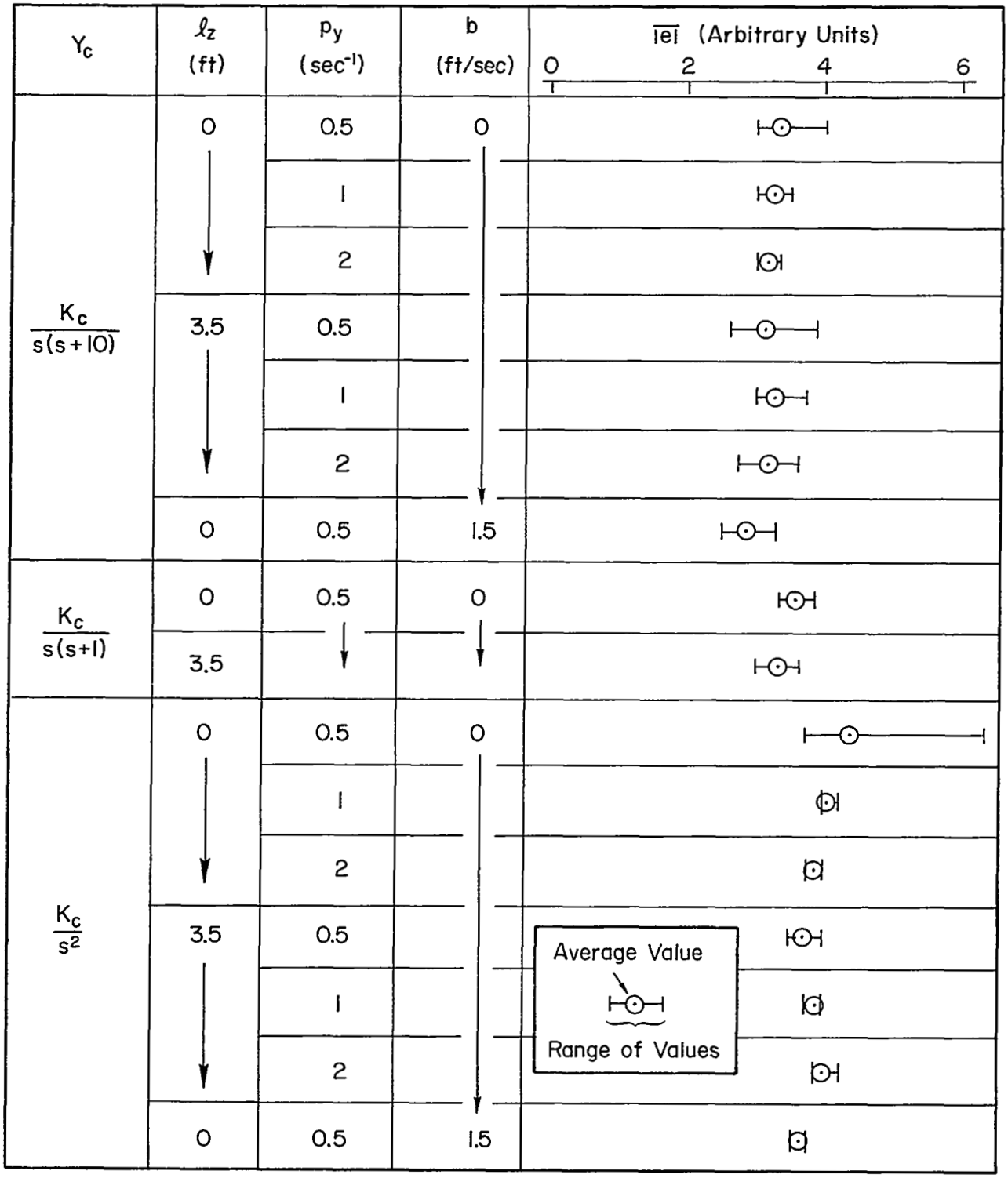

Figure 21 (Continued)

b. Subject: RG

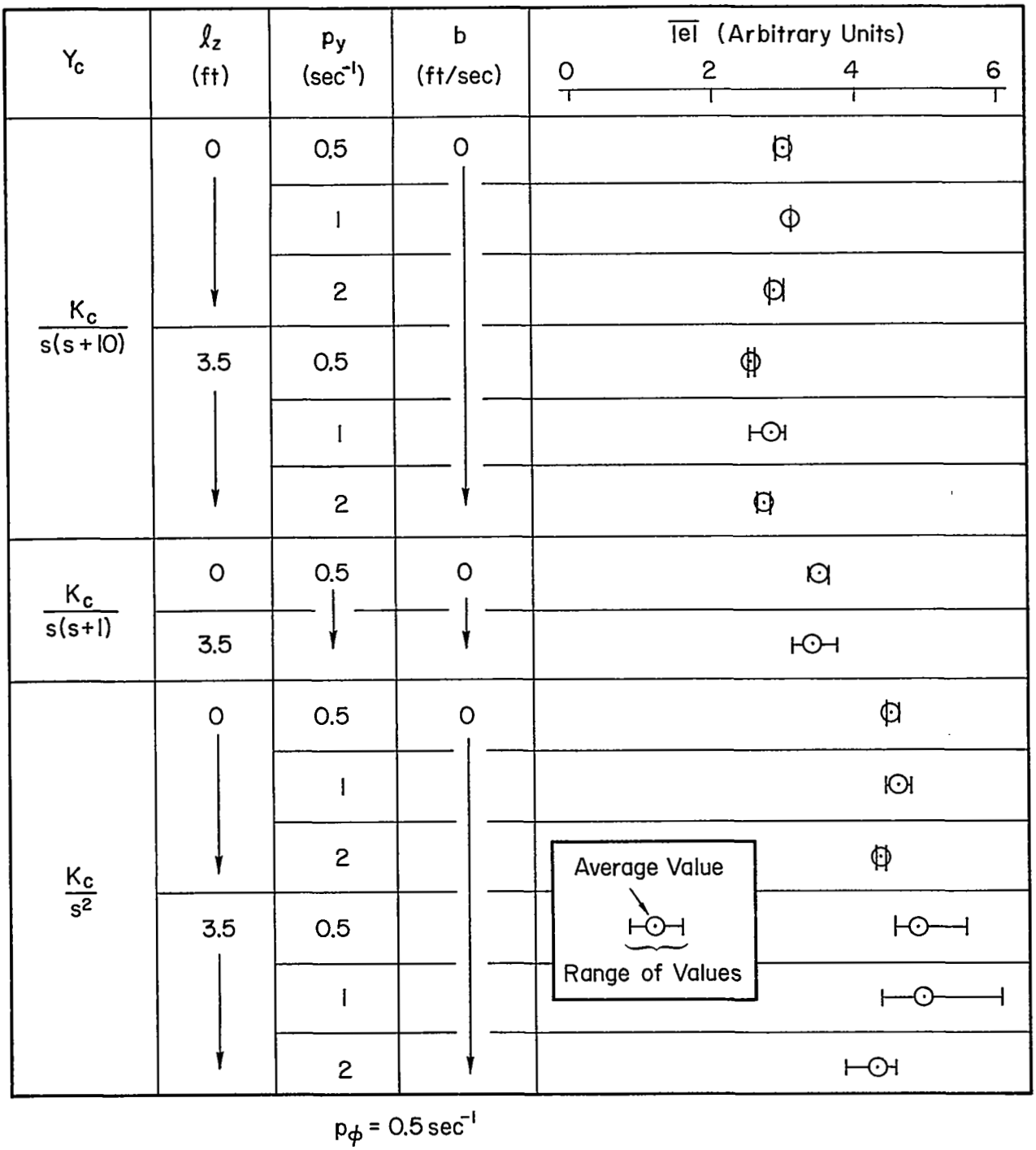

Figure 21 (Concluded)

c. Subject: MJ

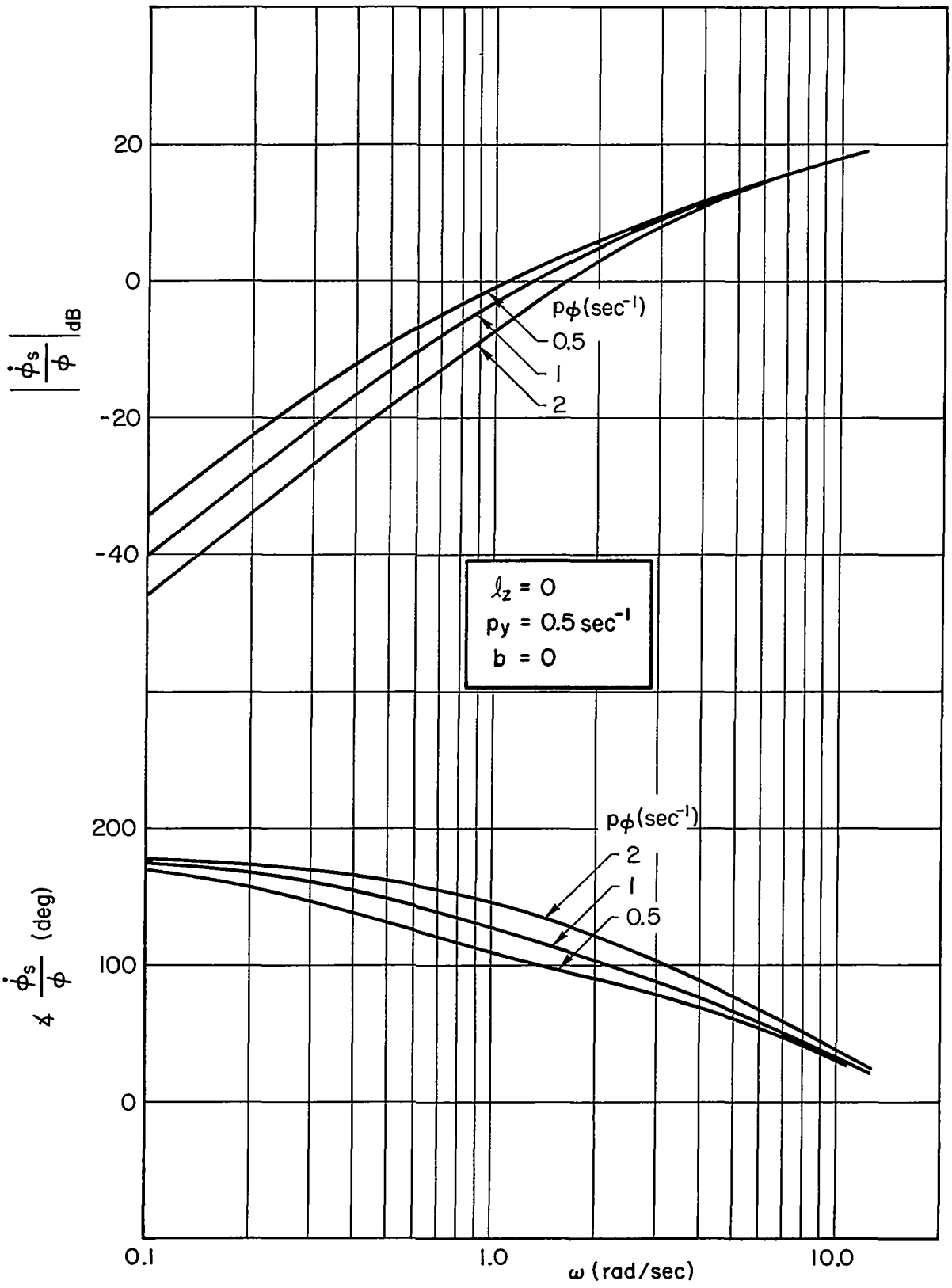

Figure 22. Effects of Roll Washout on Simulator Response Characteristics

a. Roll

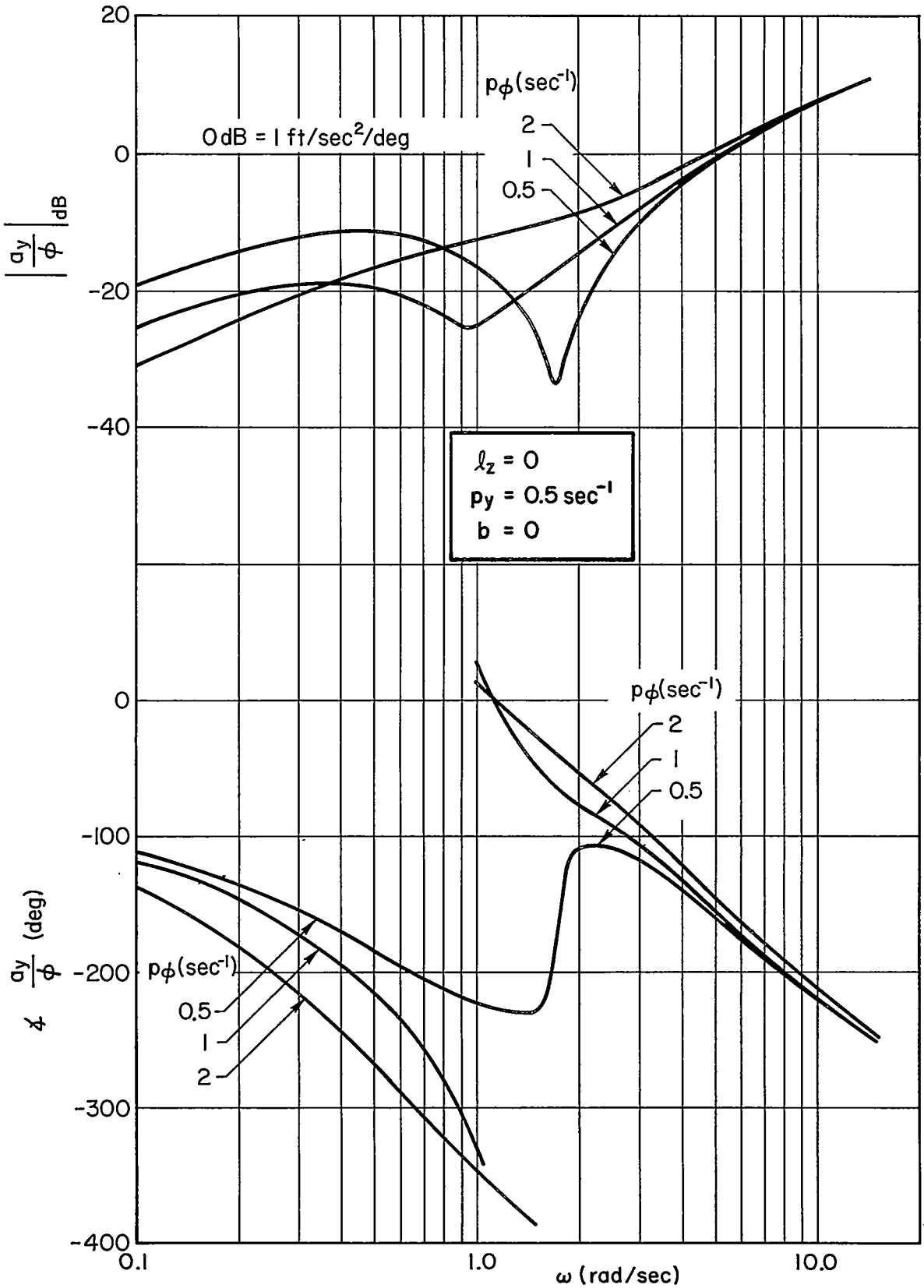

Figure 22 (Concluded)

b. Lateral Acceleration

Overall pilot describing function, Y_p, data was obtained only for Subject RG. The results are shown in Fig. 23. There appears to be a very slight reduction in gain, and therefore crossover frequency, for $p_\varphi = 2$ sec^{-1}.

The performance data also shows rather small changes due to p_φ variations, see Fig. 24, but a definite difference in the effects on the three subjects.

- GB's performance is not affected by p_φ
- RG's performance is degraded when p_φ is increased to 2 sec^{-1} (which correlates with the Y_p data)
- MJ's performance is degraded when p_φ is increased to 1 sec^{-1} but does not get any worse for 2 sec^{-1}

GB's relative insensitivity to the roll washout correlates with the results of Section III.B which showed that the basic effects of the motion cues on his performance (ω_{co} and $\overline{e^2}/\overline{d^2}$) were less than for the other two subjects. This may well be due to the subject's different backgrounds; GB's flight experience is strictly in multi-engine aircraft, while RG's and MJ's is primarily in fighters. One might expect motion cues to be more important in a highly maneuverable fighter than in a large, sluggish aircraft.

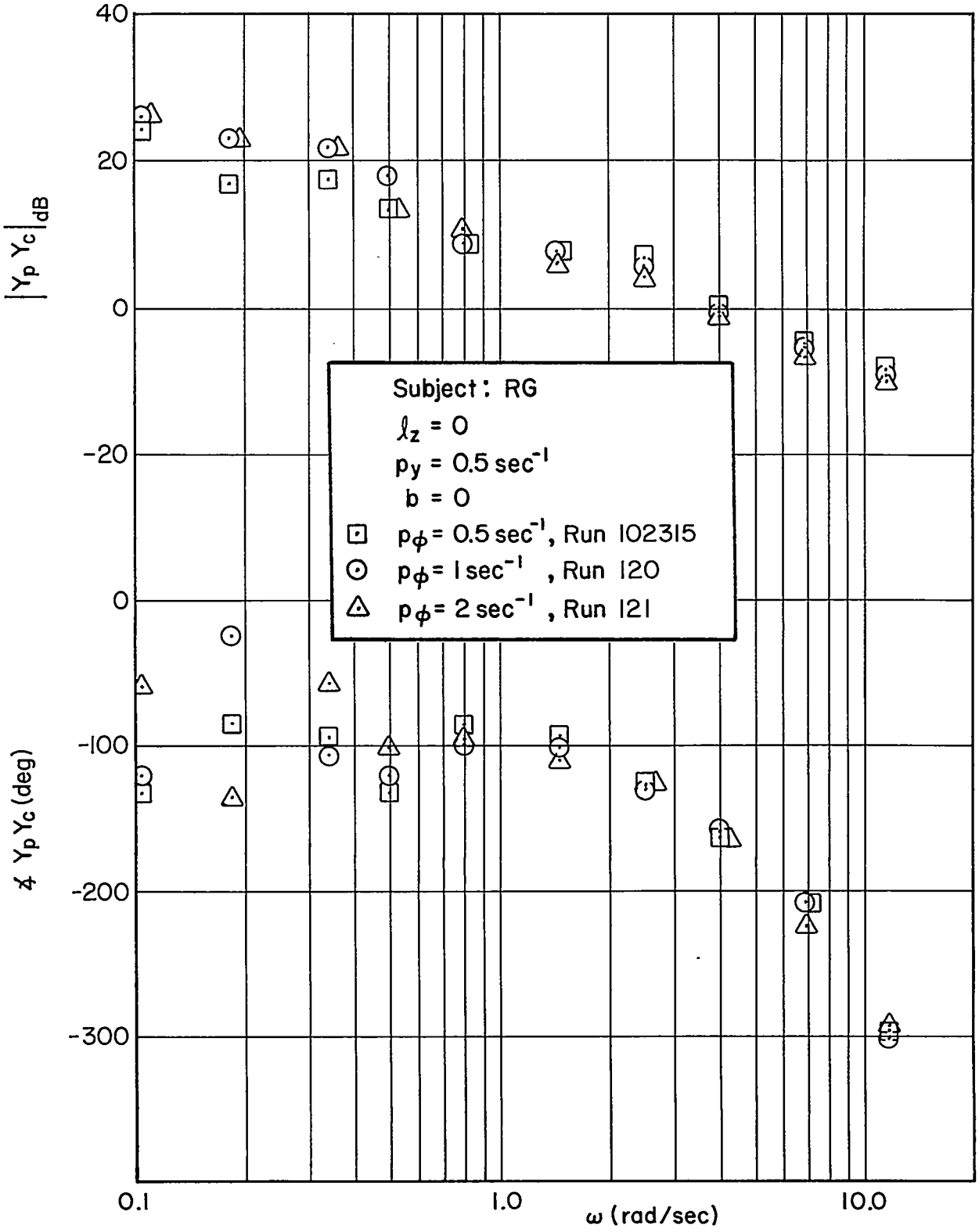

Figure 23. Roll Washout Effects on Overall Describing Function

a. $Y_c = K_c/s(s + 10)$

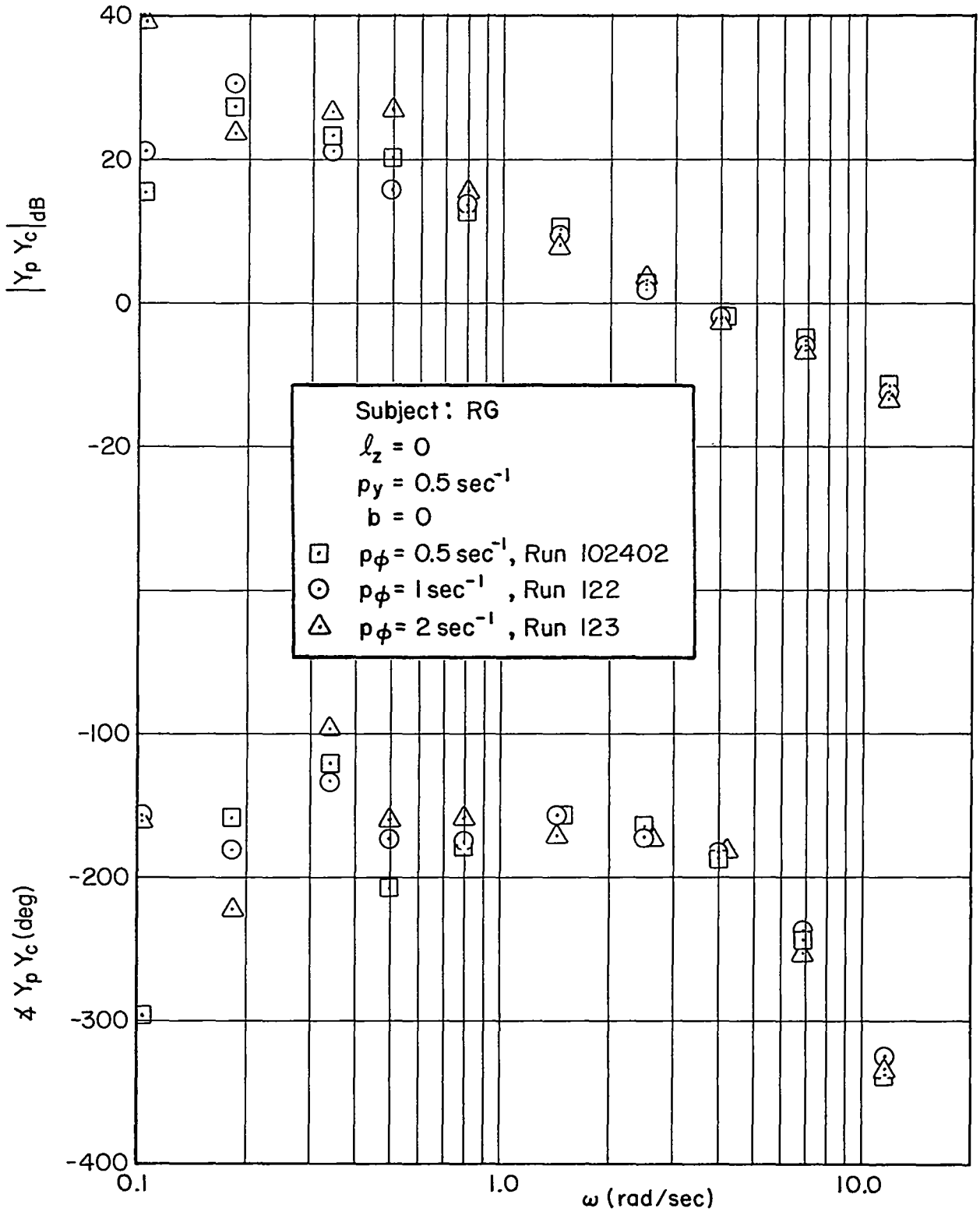

Figure 23 (Concluded)

b. $Y_c = K_c/s^2$

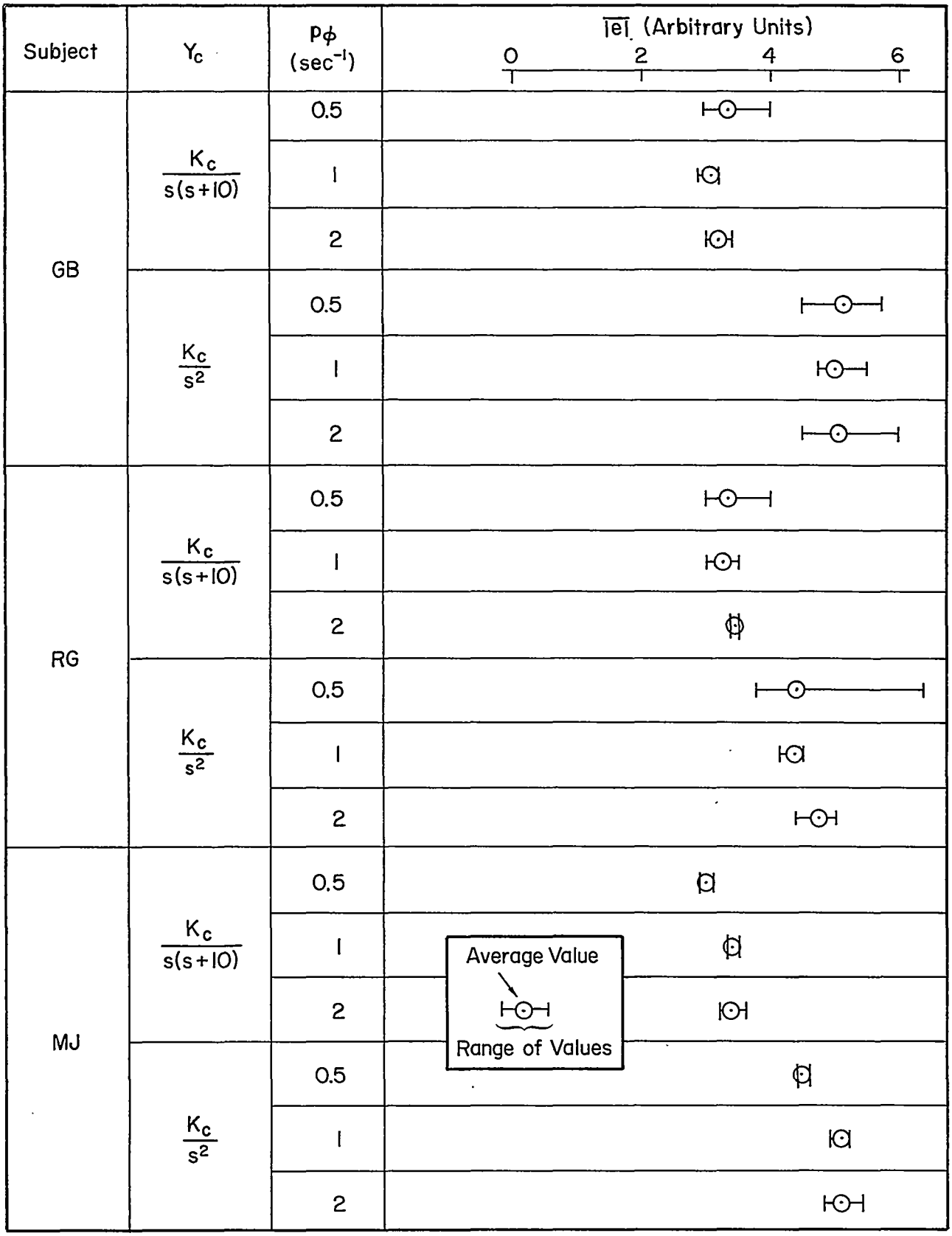

Figure 24. Performance Data for Variations in Roll Washout

SECTION IV

CORRELATION WITH PREVIOUS DATA

A. DESCRIBING FUNCTION RESULTS

The previous experiments in which pilot describing functions are compared for fixed-base and moving-base (or flight) are summarized in Table XII. In all cases the describing functions were measured from the displayed error to the pilot's control output. This corresponds to the Y_p data presented here.

Some of the comments in Table XII refer to command or disturbance inputs. Figure 25 illustrates the distinction between the two for a compensatory display. With a command input, the visual system senses only the difference between the input and the vehicle motion, while the vestibular system senses the actual vehicle motion. Thus there is a conflict between the two modalities. With a disturbance input, both the visual and vestibular systems sense the vehicle motions.

For one reason or another, the results of the first four references listed in Table XII are inconclusive when attention is centered on motion effects. The results of Ref. 3 demonstrate the important difference between a command and a disturbance input. With a command input and a compensatory display, the in-flight describing functions were approximately the same as those for fixed-base. With the conflict between the visual and vestibular sensations, the pilots apparently ignored the motion cues.

With the disturbance input there were definite changes in the describing functions, gain was increased, crossover frequency was higher, and the high frequency lags were less. Unfortunately, the differences cannot be conclusively attributed to motion cues alone, as there was also a difference in the display. For the ground and flight tests with the command input, the pilots tracked using an artificial horizon (conventional attitude ball). For the flight tests with the disturbance input, the pilots tracked using the natural horizon. While the results cannot be conclusively attributed to motion cues, the differences are quite similar to the motion effects obtained in Refs. 2 and 4, and the experiment described here.

TABLE XII

SUMMARY OF PREVIOUS DESCRIBING FUNCTION DATA

REF.	MOVING-BASE DEVICE	GENERAL RESULTS	REMARKS
10	Princeton Navion	Flight τ's higher than ground by 0.1-0.2 sec. Pilot's longitudinal gain in flight approximately 1/2 ground value.	Results not generally pertinent to motion cue effects because of: 1. Command input 2. Different subjects for in-flight and ground data 3. Considerable distractions during in-flight tests
11	NASA TV-2	Inconclusive. Amplitude and phase differences were inconsistent.	Data reduction inaccurate. Used error, rather than input, cross spectra.
12	Air Force Variable-Stability T-33	Only conclusive difference was lower gain on ground for frequencies less than approximately 0.3 rad/sec.	Considerable variability in the flight data.
13	MIT NE-2 Motion Simulator	Moving-base gains lower and lags larger than fixed-base.	Author attributes differences to a combination of "simulator nonlinearities, a poorly-marked and less sensitive moving-base display grid, and perhaps vestibular confusion and insensitivity to very small deflections."
2	MIT NE-2 Motion Simulator	1. For rotation about vertical axis, τ reduced 0.1 sec relative to fixed-base. 2. For rotation about horizontal axis, τ reduced 0.2 sec and crossover frequency doubled relative to fixed-base.	Controlled-element gain for rotation about horizontal was twice that for rotation about vertical axis. Fixed-base data were not taken with higher gain. Result 2 assumes no significant effects of gain increase.
3	Air Force Variable-Stability T-33	1. Small differences between ground and flight with command input. 2. Flight with disturbance input had significantly higher crossover frequencies and less high frequency phase lag.	For flight tests, instruments (gyro horizon) were used to track command input, but natural horizon was used for disturbance input.
4	MIT NE-2 Motion Simulator	Describing functions and performance measures given for 40 controlled elements. Generally, the addition of motion significantly increased the pilot gain, reduced high frequency phase lags, and improved performance.	Motion was roll about a horizontal axis with subject's head nearly on the axis.

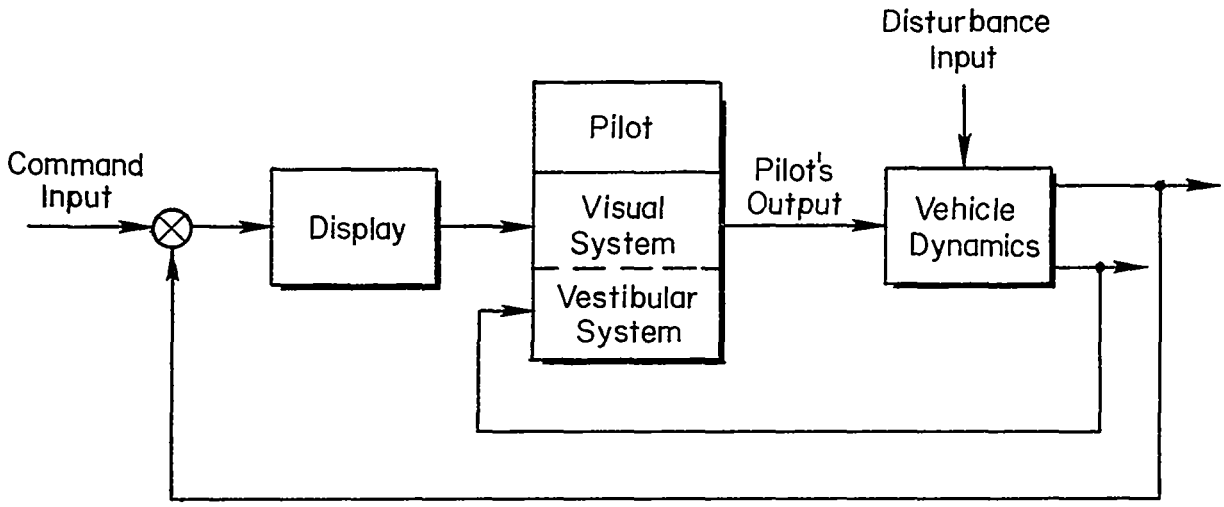

Figure 25. Loop Structure for Compensatory Display

Reference 2 has describing function data for three test conditions with $Y_c = K_c/s$: fixed-base, rotation about a vertical axis, and rotation about a horizontal (roll) axis. In all three cases, the pilot's amplitude ratio is nearly constant over the frequency range of the data presented, 0.3-5 rad/sec, and the phase is very closely approximated by a time delay, τ, with its transfer characteristic, $e^{-\tau s}$. The crossover frequencies for the three cases were 2.7, 2.7, and 5 rad/sec. The time delays were 0.2, 0.1, and 0 sec. While the fixed-to-moving-base differences are similar to those reported here, the crossover frequencies are appreciably higher and the phase lags are appreciably less. The crossover frequency and phase lag differences between the two experiments may be due to differences in subjects, manipulator dynamics, and input characteristics. The Ref. 2 tests used a much broader bandwidth input and the Ref. 4 results showed some reduction in phase lag as input bandwidth is increased.

Reference 4 presents data for a wide range of controlled elements with (and without) one set of motion cue characteristics, whereas the present experiments treated fewer controlled elements but varied the motion cue characteristics. Consequently, the two experiments complement each other quite nicely if the fundamental results on motion effects agree. Three of the Ref. 4 controlled elements are similar to those used here. They are

$$\frac{K_c}{s} e^{-0.1s} \quad , \quad \frac{K_c}{s(s+1)} e^{-0.1s} \quad , \quad \frac{K_c}{s^2} e^{-0.1s}$$

In the Ref. 4 tests several different controlled element gains were used for each of the above dynamics, while in the present experiments the pilots selected what they felt was an optimum gain. In the following comparisons, only the Ref. 4 data for the gain which gave the best performance will be considered.

A comparison of crossover frequencies is shown in Fig. 26. The crossover frequencies of Ref. 4 are generally appreciably higher; however, the increments due to motion cues are about the same in both tests. A comparison of the describing function data shows that the major difference in the two tests is the lower phase lags measured in Ref. 4. This correlates with the higher crossover frequencies.

A detailed comparison between the phase measurement from the two tests is difficult because the two sets of data show somewhat different phase variations with frequency. For example, the Ref. 4 moving-base results for $Y_c = (K_c/s)e^{-0.1s}$ show less phase lag at the highest frequency data point (7.7 rad/sec) than at the previous point (4.3 rad/sec). Perhaps the most meaningful comparison between the two experiments, relative to motion effects, is the change in phase lag at the highest frequency data point of Ref. 4. The results for both Ref. 4 and the present test (based on frequency interpolation of the data in Figs. 6-8) are listed in Table XIII. Note the considerably greater phase difference for the present data.

Comparison of Ref. 4 and our data has shown some discrepancies in the details and quantitative results; however, the gross effects of motion cues are the same for both. Considering the many differences in experimental conditions, the discrepancies should not be too surprising. Perhaps the most significant difference in the two tests was the background of the subjects. The Ref. 4 subjects (5 undergraduate students, 1 graduate student, and 1 housewife) were considerably younger than ours. In addition, five of the Ref. 4 subjects were nonpilots and the other two were private pilots; on the other hand, our subjects were all seasoned professional pilots.

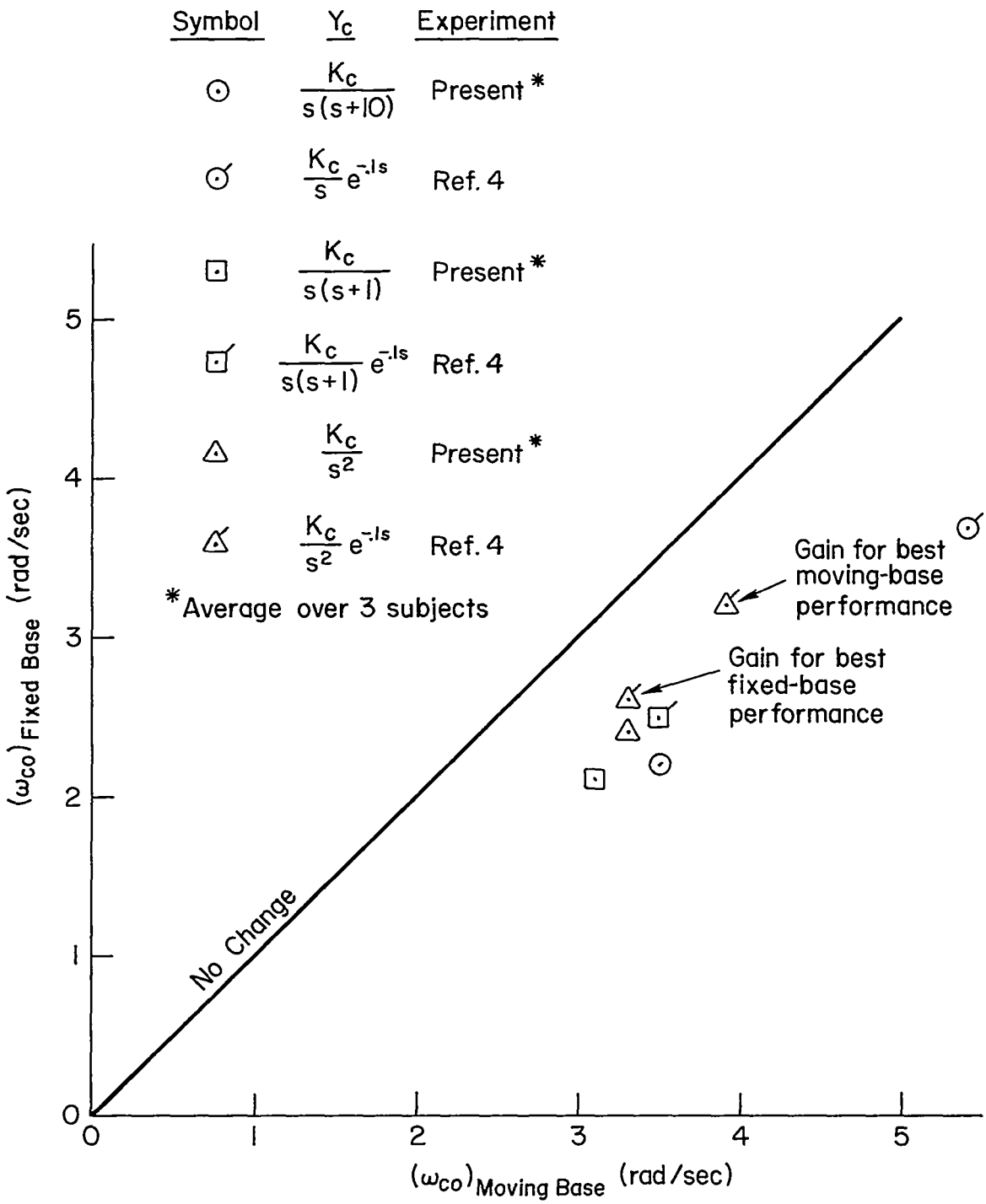

Figure 26. Comparison of Crossover Frequencies with Ref. 4 Data

TABLE XIII

COMPARISON OF PHASE LAGS WITH REF. 4

Y_c	$\left[(\angle Y_p)_{\text{Moving Base}} - (\angle Y_p)_{\text{Fixed Base}}\right]_{\omega = 7.7 \text{ rad/sec}}$ (deg)		
	REF. 4	PRESENT TEST	
		RANGE	AVERAGE
$(K_c/s)e^{-0.1s}$ or $K_c/s(s+10)$	25	37-74	50
$\frac{K_c}{s(s+1)} e^{-0.1s}$ or $K_c/s(s+1)$	37	39-78	64
$(K_c/s^2)e^{-0.1s}$ or K_c/s^2	41* 31**	43-81	62

*K_c for best fixed-base performance.

**K_c for best moving-base performance.

That the background of the subjects can seriously affect the results was demonstrated in Ref. 14. This report describes another experiment on motion cue effects using the MIT NE-2 Motion Simulator. The task was roll angle and lateral position control of a hovering helicopter. The most interesting result of that test was that two experienced helicopter pilots couldn't control the simulator fixed-base, but could moving-base; yet two of three nonpilot subjects did better fixed-base than moving-base. The author concluded, "For inexperienced subjects, the motion cue is effectively a disturbance... The experienced operator, however, depends strongly upon the motion cue..."

B. PERFORMANCE MEASURES

Comparing performance data from various experiments can be more difficult than comparing describing function data, as the results are more sensitive to input characteristics. Nevertheless, the previous data on motion effects on tracking performance will be reviewed below. The major emphasis

will be on the general trends of motion cue effects rather than on the exact numerical results.

A pitch tracking task was used in Ref. 15. A command input and a pursuit display were used. With the pursuit display the pilot had both visual and vestibular feedbacks of the vehicle motion so that the discrepancy present with a compensatory display and command input should not have been a problem. The controlled element dynamics were

$$Y_c = \frac{K_c(s + 1)}{s(s^2 + 2\zeta_c\omega_c s + \omega_c^2)(s + 10)} \tag{20}$$

The effects of motion cues on performance are shown in Fig. 27.

Note that for good (small error) configurations the motion cues did not improve the performance. This may have been due to the motions being below the threshold of the semicircular canals; the input was only 0.6 deg rms. For the more difficult controlled elements there is a substantial improvement due to the motion cues. It is also clear from Fig. 27 that the controllability boundaries would be broader with motion than without.

Performance data were also taken in the Ref. 2 experiments described earlier. For $Y_c = K_c/s$, the $\overline{e^2}/\overline{d^2}$ were

- 0.075 fixed-base
- 0.050 moving base, rotation about vertical axis
- 0.044 moving base, rotation about horizontal axis

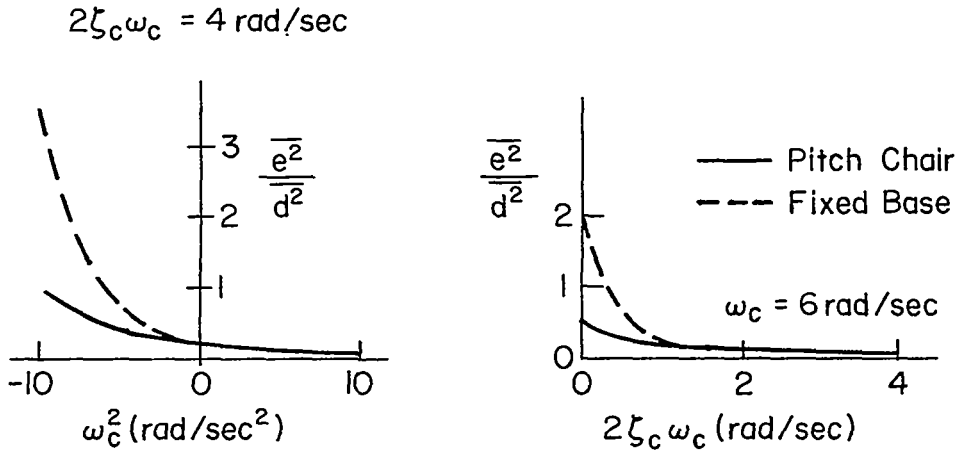

Figure 27. Performance Data from Ref. 15

This gives a ratio of moving/fixed-base performance of 0.67 or 0.59. This is in fair agreement with our ratio of 0.48-0.58 for $Y_c = K_c/s(s+10)$; see Fig. 17c.

Reference 2 also gives performance data for control of an unstable controlled element,

$$Y_c = \frac{K_c\omega_c^2}{s^2 - \omega_c^2} \tag{21}$$

For this test there was no input and the moving-base case was rotation about a horizontal axis. The results are shown in Fig. 28. As before, motion cues are very helpful for the more difficult controlled elements (larger ω_c's) and increase the controllability limit. The lack of improvement with motion for the smaller ω_c's is surprising, for if we extrapolate the curve of Fig. 28, we would conclude that motion cues are not helpful for $Y_c = K_c/s^2$. On the contrary, both the Ref. 4 data and ours show that motion cues do substantially improve performance for $Y_c = K_c/s^2$. The explanation may well be the same as that suggested for the Ref. 15 results, the motions were below the semicircular canal thresholds.

As noted earlier, 40 controlled elements were tested in Ref. 4 and performance data were given for all 40. However, the subjects were not allowed to select the optimum gain and the data for

$$Y_c = \frac{K_c}{s(s+a)} e^{-0.1s} \tag{22}$$

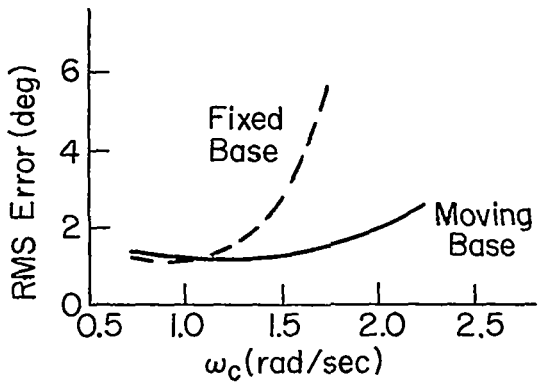

Figure 28. Performance Data from Ref. 2

show a strong effect of gain, K_c, on performance. Consequently, for much of the data it is impossible to separate the effects of controlled element dynamics and gain. We will, therefore, restrict our review to dynamics of the form given by Eq. 22 and for which enough gains were tested to at least approximate the optimum. The performance data for the best gains are shown in Table XIV.

TABLE XIV

PERFORMANCE DATA FROM REF. 4

a (sec^{-1})	$(\overline{e^2}/\overline{d^2})_{\text{Fixed Base}}$	$(\overline{e^2}/\overline{d^2})_{\text{Moving Base}}$	$\frac{(\overline{e^2}/\overline{d^2})_{\text{Moving Base}}}{(\overline{e^2}/\overline{d^2})_{\text{Fixed Base}}}$
−0.5	0.88	0.47	0.53
0	0.81* 1.09**	0.55* 0.44**	0.68* 0.40**
1	0.40* 0.50**	0.32* 0.30**	0.80* 0.60**
5	0.29	0.19	0.66
∞†	0.21	0.12	0.57

*Best gain for fixed base.

**Best gain for moving base.

†$Y_c = (K_c/s)e^{-0.1s}$

The data of Table XIV show no clear trend in motion effects as a function of "a" as opposed to our results, Fig. 17c. Furthermore, a comparison of Table XIV and Fig. 17c shows several interesting results:

- For $Y_c \doteq K_c/s$, both the fixed- and moving-base performances are nearly identical for the two tests.
- For $Y_c \doteq K_c/s(s+1)$, our subjects did somewhat better fixed base than the Ref. 4 subjects, and considerably better moving base. Our data show a larger effect of motion cues.
- For $Y_c \doteq K_c/s^2$, our subjects did better both fixed and moving base than the Ref. 4 subjects, and our data show a larger effect of motion cues.

In light of the differences in the describing function results of Ref. 4 and the present experiment, the general lack of quantitative agreement in the performance data is not surprising.

SECTION V

MULTIMODALITY PILOT MODEL

This section presents an initial hypothesis for a multimodality pilot model, i.e., an approximate mathematical description of pilot control behavior when utilizing both visual and motion cues. Because there are many gaps in the currently available experimental data, certain portions of the model can be only vaguely defined. Future experiments may provide the basis for subsequent refinements and modifications. In the meantime, this model is meant to serve as a working hypothesis.

The primary motion-sensing mechanisms in a normal human are the vestibular organs — the semicircular canals and the utricles (Ref. 1). The semicircular canals respond to angular and the utricles to linear accelerations of the head. There are three essentially orthogonal canals on each side of the head, so that angular accelerations with any direction can conceivably be sensed. The two utricles, on the other hand, are approximately coplanar and thus respond only to a component of the total linear acceleration.

The basic structure of the multimodality pilot model consists of three parallel, noninteracting feedback paths via the visual system, the semicircular canals, and the utricles. It is recognized that the three noninteracting feedback paths are a gross simplification. Interactions between the visual and vestibular systems occur at several levels. For instance, at one level are the compensatory eye motions produced by the vestibular system when the head is moved while, at another level, are the illusions and disorientations resulting from conflicting visual and vestibular sensations. However, for our present purposes the simplified model is adequate.

Characteristics of the visual path are well known. A quasi-linear model for control tasks involving only visual cues is described in detail in Ref. 16. This description includes a describing function model form and adjustment rules for selecting the variable parameters. Possible modifications of the visual path due to the presence of motion cues will be discussed later.

The characteristics of the two motion feedback paths are discussed in Subsections A and B. This is followed, in Subsection C, by a discussion on the integration of the three feedbacks. The final subsection, D, deals with moving-base simulator requirements. The implications of the multimodality pilot model, as well as other factors, are considered.

A. CHARACTERISTICS OF THE SEMICIRCULAR CANAL PATH

While the semicircular canals are basically responsive to angular accelerations, their dynamic characteristics are such that over the range of frequencies normally used in manual control they can be considered as rate gyros which provide the pilot with a subjective impression of angular velocity. The model for the semicircular canal path can be represented by the elements shown in Fig. 29. The sensor is comprised of the semicircular canals which provide the subjective angular velocity. As in the case of visual feedback it is assumed that the pilot

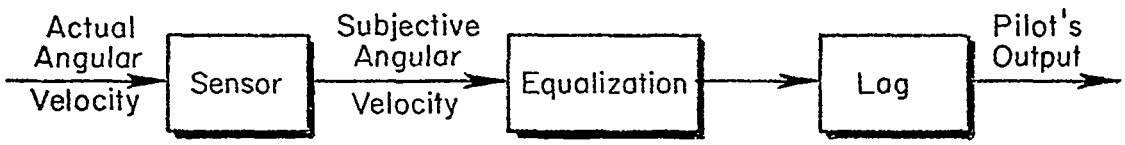

Figure 29. Elements of the Semicircular Canal Path

can provide some equalization on the sensed quantity. The final element shown in Fig. 29 is a lag which includes the net effects of any central processing, transmission, and neuromuscular lags. Portions of this lag are common to all three feedback paths. The characteristics of each of the three elements in Fig. 29 will now be discussed.

A great deal of research has been done on the sensory characteristics of the semicircular canals. A thorough summary of this work is given in Ref. 1. A model of semicircular canal dynamics which is particularly convenient for application to control system analyses is that shown in Fig. 30. Numerous experiments have demonstrated that the numerical values for the parameters in Fig. 30 have considerable intersubject variability and are a function of the axis of rotation (Ref. 1). Many of these

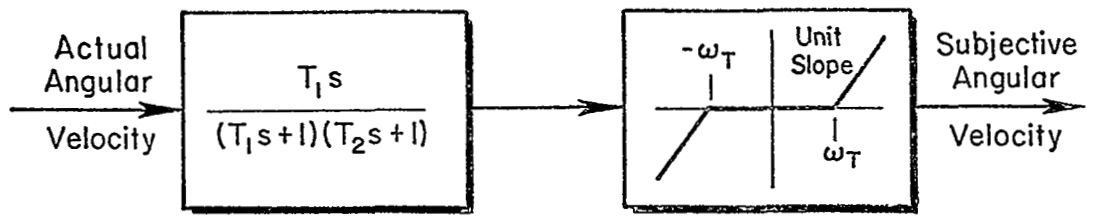

Figure 30. Semicircular Canal Dynamics

experiments have dealt with the larger time constant, T_1. From this work the estimated values for pilots are (Ref. 1):

$$T_1 \doteq \begin{cases} 6.5 \text{ sec for roll} \\ 5.3 \text{ sec for pitch} \\ 8.0 \text{ sec for yaw} \end{cases} \tag{23}$$

Data for the shorter time constant, T_2, are much more limited. The best estimate is (Ref. 1):

$$T_2 \doteq 0.1 \text{ sec for any axis} \tag{24}$$

Thus, the linear element in Fig. 30 acts like a bandpass filter with low-frequency cutoff at 0.125−0.15 rad/sec and high frequency cutoff at 10 rad/sec, and with nearly unity gain over the frequency range 0.3−5 rad/sec. Over this range the semicircular canals function as a rate sensor.

Numerical values for the threshold shown in Fig. 30 are based on experiments to determine the minimum detectable constant angular acceleration or step velocity change. For a step acceleration input of magnitude α, the output of the linear element in Fig. 30 would be

$$T_1\alpha\left[1 - \left(\frac{T_1}{T_1 - T_2}\right)e^{-t/T_1} + \left(\frac{T_2}{T_1 - T_2}\right)e^{-t/T_2}\right]$$

The steady-state response is then $T_1\alpha$. The minimum detectable angular acceleration, α_{min}, is then related to the threshold by

$$T_1\alpha_{min} = \omega_T \tag{25}$$

Using the α_{min} values from Ref. 2, i.e.,

$$\alpha_{min} \doteq \begin{cases} 0.5 \text{ deg/sec}^2 \text{ for roll or pitch} \\ 0.14 \text{ deg/sec}^2 \text{ for yaw} \end{cases} \tag{26}$$

and the time constants from Eq. 23, the threshold is estimated to be

$$\omega_T \doteq \begin{cases} 3.2 \text{ deg/sec for roll} \\ 2.6 \text{ deg/sec for pitch} \\ 1.1 \text{ deg/sec for yaw} \end{cases} \tag{27}$$

As a matter of interest, these thresholds are an order of magnitude greater than those which would be specified for flight control system rate gyros.

The above expression can also be used to approximate the latency time (time to detect an input acceleration), T_L, by

$$\begin{aligned} \omega_T &= T_1\alpha\left[1 - \left(\frac{T_1}{T_1 - T_2}\right)e^{-T_L/T_1} + \left(\frac{T_2}{T_1 - T_2}\right)e^{-T_L/T_2}\right] \\ &\doteq T_1\alpha\left(1 - e^{-T_L/T_1}\right) \end{aligned} \tag{28}$$

Equation 28 has been shown to match measured latency times quite accurately, e.g., Ref. 2.

Values for the threshold can also be estimated from the minimum detectable step change in velocity. For a step velocity change of magnitude, ω, the output of the linear element of Fig. 30 is

$$\frac{T_1\omega}{T_1 - T_2}\left(e^{-t/T_1} - e^{-t/T_2}\right)$$

The maximum value of the output is easily shown (using $T_1 >> T_2$) to be approximately ω. Therefore the threshold, ω_T, is also approximately equal to the minimum detectable step velocity change. Threshold estimates obtained in this manner are in rough agreement with those given in Eq. 27, although there is considerable intersubject variability. (See Ref. 1 for a more complete discussion of this subject.)

In most cases of manual vehicular control, the motions are considerably above the thresholds noted above and the primary concern is in the frequency range of 1–5 rad/sec. Then the sensor dynamics for the semicircular canal path are adequately approximated by

$$\frac{\text{subjective angular velocity}}{\text{actual angular velocity}} \doteq \frac{1}{T_2 s + 1} \doteq e^{-T_2 s} \qquad (29)$$

The other two elements in the semicircular canal path are equalization and lag. Unfortunately, there are no direct data on these two and there is only a limited amount of inferential data. Some of the data of Ref. 4 indicate that relatively large lead equalization (roughly 1 sec) is possible. Whether or not the pilot can generate lead equalization as large as that measured for visual tracking is unknown. In fact, the mechanism for generating lead in visual tasks is still not completely understood. Until more concrete data can be obtained, it will be hypothesized that the lead in the semicircular path can be as large as that used in the visual path.

It is also theoretically possible for the pilot to use lag equalization in the semicircular path. However, the primary function of the path appears to be to supply lead equalization. In none of the cases considered to date has lag equalization been desirable. Therefore, it is assumed that the semicircular canal equalization is of the form $K_1(T_3 s + 1)$.

As indicated above, there are no direct data on the lag element. However, the motion feedback describing function (Y_m) data presented in

Section III provide some clues. As discussed there, the data indicate a net time delay 0.06 sec due to the equalization and lag elements. Since this delay is so small relative to those usually measured in the visual path, it would appear that the actual lag is larger than 0.06 sec but was partially offset by a high frequency lead equalization. The lead time constant could not be appreciably greater than roughly 0.1 sec without producing a noticeable effect on the amplitude data. Consequently, a reasonable estimate for the lag element appears to be a time delay of roughly 0.2 sec.

Combining the above gives the model for the semicircular canal path shown in Fig. 31.

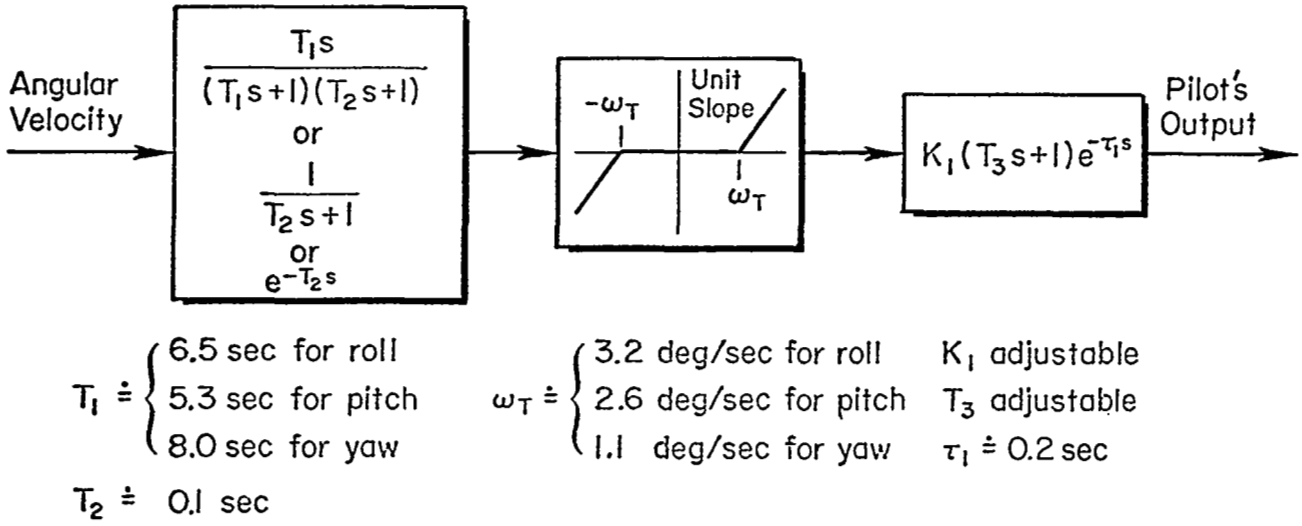

Figure 31. Model for Semicircular Canal Path

B. CHARACTERISTICS OF THE UTRICULAR PATH

The model for the utricular path consists of three elements similar to those used for the semicircular path — sensor, equalization, and lag. While less data is available on the sensor dynamics of the utricles, it is widely accepted that they are sensitive to linear accelerations in the plane of the utricular maculae. This plane is inclined front end upward approximately 30 deg from the horizontal in the upright head.

It should be noted that, like conventional accelerometers, the utricles do not respond to inertial accelerations but to the total applied force. For example, on the ground the utricles respond to tilting the head relative to the gravity vector just as an accelerometer attached to the head would. For simplicity, the inputs to the utricles will hereafter be referred to as accelerations. However, the reader should remember that this means the accelerations which would be sensed by an accelerometer.

The most recent data on utricular sensory dynamics is that given in Ref. 17. That report suggests a model for the sensory dynamics of the form

$$\frac{\text{subjective acceleration}}{\text{actual acceleration}} = \frac{(T_5/T_4)(T_4 s + 1)}{(T_5 s + 1)(T_6 s + 1)} \qquad (30)$$

where $T_4 \doteq 13$ sec

$T_5 \doteq 5.2$ sec

$T_6 \doteq 0.67$ sec

Over the frequency range of interest in most vehicular-control situations Eq. 30 can be adequately approximated by

$$\frac{\text{subjective acceleration}}{\text{actual acceleration}} \doteq \frac{1}{T_6 s + 1} \qquad (31)$$

The utricular threshold is so small, on the order of 0.01g or less, that it will have a negligible effect in most vehicular control situations. There are also very few data on latency times but Ref. 2 does show latency times on the order of 1 sec for accelerations of 0.1g.

Information on the equalization and lag elements is limited to the Ref. 18 analysis of some of the data from Ref. 2. The results for the one case involving a utricular feedback indicated the presence of a first-order lead at 3 rad/sec and a time delay of 0.3 sec. The lead

is identified as pilot equalization and the time delay as the low frequency approximation to the dynamics of the lag element. This analysis provides some evidence to support the inclusion of pilot adjustable lead in the utricular path. However, there are no data on the adjustable range of the lead or the possibility of lag equalization. The possible desirability of lag equalization cannot be ruled out because of the extremely wide range of acceleration numerator zeros which can occur in vehicle transfer functions. These zeros are strong functions of the vehicle stability and control properties and the pilot's location. It is, at least theoretically, possible that in some cases lag equalization would be helpful.

The assumed model for the utricular path is shown in Fig. 32.

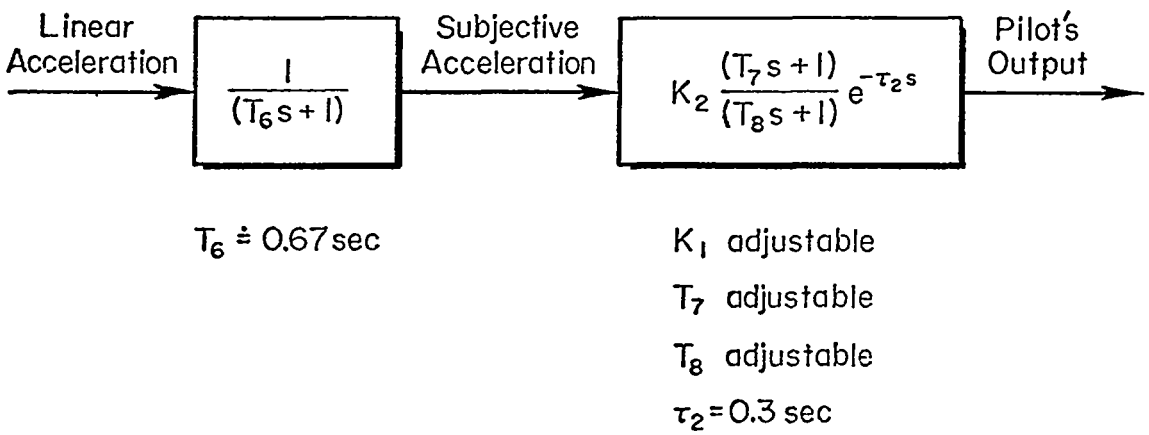

Figure 32. Model for Utricular Path

C. FEEDBACK INTEGRATION

The first problem to be considered here is the conditions under which motion cues can or cannot be utilized. The earlier experiments discussed in Section IV indicate that motion cues will be used unless the task has both a command input and a compensatory display. In this case the visual and vestibular cues conflict and the pilots appear to ignore the motion cues. With a simple, predictable input the pilot may be able to separate the input and the vehicle response, and avoid the visual/vestibular

conflict. Thus, the above restrictions are expanded to: motion cues will be used except when tracking a random-appearing command input with a compensatory display.

The next question is the relative contributions of the semicircular canal and utricular paths. The results presented in Section III indicate that the contribution of the utricular feedback in the present experiment was minor or none. Yet, there are other conditions under which the utricular feedback is definitely utilized. For example, both Refs. 2 and 4 included control of a simulator, which rolled about a horizontal axis, without any visual feedback. This could only be accomplished by using the utricles to provide an indication of the vertical. The resulting performance for tracking with motion cues alone is interesting.

Of the more than 40 controlled elements tested in Refs. 2 and 4, the performance for motion-alone tracking was, with one exception, poorer than for visual and motion cues. In many cases the performance was even poorer than for the visual-alone (fixed base) tracking. These results, combined with those of Section III, suggest that the utricular feedback is generally of minor importance, but in certain special cases it may be used if an appropriate visual feedback is not available. A specific example of the latter condition would be directional control of an aircraft in which there was no visual indication of side acceleration.

The rationale for the relatively minor role of utricular feedback has two factors. First, the sensor dynamics in the utricular path are considerably poorer than those in the semicircular canal path. Thus, the utricular path is generally not much better than the semicircular canal path even though the a component of the utricular feedback is angular acceleration as opposed to angular velocity in the semicircular canal path. The advantage of the extra derivative is largely lost due to the poorer sensor dynamics.

The second factor is the consistent usefulness of the sensed signal. Sensed accelerations may be very sensitive to location and changes in flight condition. This is a familiar problem to automatic control system designers. It may well be that pilots have learned that the utricular feedback is not consistently useful and so generally suppress it. On

the other hand, no such problem exists with the semicircular canal feedback. When trying to control attitude, attitude rate information is always useful.

Having decided that the utricular feedback is generally of minor importance, the key problem in feedback integration is the adjustment of the visual and semicircular canal feedbacks. The following remarks on this subject are based on the results of Section III.

For attitude tracking tasks, the overall effects of motion on the equivalent visual describing function are adjustments in the crossover frequency and effective time delay. One can then use the existing Quasi-Linear Pilot Model to estimate the fixed-base pilot describing function. To allow for motion cues, one increases the crossover frequency by approximately 1 rad/sec and reduces the effective time delay by approximately 0.15 sec. This gives the overall effects of high fidelity angular cues. Separation of the visual and angular feedbacks is also possible.

The adjustment of the variable (by the pilot) parameters in the visual and semicircular canal feedbacks is directly analogous to synthesis of an autopilot for the same task. Given the two feedbacks with certain fixed characteristics in each, the variable parameters are adjusted just as if one were designing an autopilot. The resultant adjustments are most simply described in terms of the relative magnitudes of the two feedbacks as a function of frequency.

The relative magnitudes of the visual and semicircular canal feedbacks depend on the controlled element dynamics; however, the visual path always dominates at low frequencies and the semicircular canal path at high frequencies. For controlled elements which do not require low frequency pilot lead ($Y_c \doteq K_c/s$ in the region of crossover), the two feedbacks are of comparable magnitude in the frequency region just above crossover, 5 – 10 rad/sec. For controlled elements which do require low frequency pilot lead ($Y_c \doteq K_c/s^2$ in the region of crossover), the two feedbacks are of comparable magnitude in the frequency region just below crossover, 1.5 – 2 rad/sec. In all cases, the lead provided by the angular path allows allows the low frequency gain of the visual path to be higher than it would be fixed base and the lead somewhat lower.

D. MOVING-BASE SIMULATOR REQUIREMENTS

In establishing requirements for a moving-base simulator, consideration must be given to the effects of motion cues on:

- Tracking
- Failure detection
- Realism

The data presented here are primarily relevant to the first item, tracking. As this is also the one about which we can be the most quantitative, it will be discussed first. The other two items will be considered subsequently.

With regard to tracking performance, it is generally much more important to have the rotational cues than the linear ones. If tracking performance were the sole criterion, the linear motions might even be eliminated altogether as long as the task did not require a linear acceleration feedback which had no visual equivalent.

On the other hand, the rotary motions should be faithfully reproduced, at least over an appropriate frequency range. A reasonable high frequency limit is 10 rad/sec. This is the bandwidth of the vestibular sensor and is considerably above any manual-control crossover frequencies. For the low frequency limit, it does not appear necessary to go as low as the sensor washout, roughly 0.1 rad/sec. None of our subjects were aware of the 0.5 rad/sec washout in roll and increasing it to 1 rad/sec had very little effect. A conservative lower frequency limit would be 0.5 rad/sec and even 1 rad/sec would be reasonable.

Tracking requirements are also affected by controlled element dynamics. For an easy control task, one requiring little pilot lead, the effects of motion cues are considerably less than for a difficult task, one requiring large pilot lead. Fixed-base results may be completely adequate, although slightly conservative, for a vehicle with good handling qualities. On the other hand, fixed-base results for a vehicle with poor handling qualities or a marginally controllable task will be overly conservative.

While completely general tracking requirements are difficult to define, the following procedure could be used to estimate requirements for a specific situation:

- Define the system—pilot task, vehicle dynamics, displays, and inputs
- Determine potential visual and motion feedbacks
- Analyze the flight situation using the Multimodality Pilot Model and, if necessary, the Multiloop Pilot Model (Ref. 19)
- Reanalyze with a variety of simulator dynamics included
- Determine limits of simulator dynamics for acceptable performance degradation relative to flight

The second consideration in simulator requirements is failure detection. If the piloting task includes recovery from an aircraft or system failure, such as an engine or stability augmentation failure, motion cues can play an especially important role. The motions accompanying a failure can greatly facilitate the pilot's detection of the failure. This is especially true if the visual modality is already heavily loaded with a demanding task. The motion cues also allow an earlier failure detection. For example, a hardover elevator due to a pitch damper failure could be detected by the normal acceleration and pitch rate motion cues before noticeable effects were displayed on the flight instruments (such as the artificial horizon).

At the present no general requirements based on failure detection are available. As a minimum, the motion should be enough to provide an unambiguous clue to the failure. For example, to simulate a hardover yaw damper malfunction, the simulator should have enough lateral travel so that the pilot can clearly separate the lateral acceleration cue accompanying the failure from those due to gusts. In many cases failure detection may put the most stringent requirement on linear motions.

The third consideration in simulator requirements is realism, i.e., does it feel like an airplane to the pilot? The degree of realism necessary depends on at least two factors, the objectives of the simulations and the experience of the subjects. One would certainly expect different requirements for a simulator to be used in handling qualities research and for one to be used to train airline pilots. The goals are

entirely different as may be the backgrounds of the subjects. Research pilots who have had considerable experience in simulators can learn to mentally extrapolate from rather crude simulations to the flight situations.

Two specific problem areas related to realism are false linear accelerations and washout effects on open-loop maneuvers. An example of the first, would be roll control in a simulator with roll motion but no lateral travel. When the subject rolled the simulator he would sense a lateral acceleration because of gravity, whereas in an airplane the sensed acceleration is generally very small. While the false cue may not affect the pilot's control behavior, it will surely influence his subjective opinion of the simulation realism. An example of the washout problem would be a pull-up maneuver in a simulator with limited vertical travel. The initial acceleration would be correct but, because of the limited travel, it would be necessary to quickly reverse the acceleration. Washout characteristics, which might be completely masked in a tracking task, could become quite obvious in certain open-loop maneuvers.

The above discussion of realism has, of necessity, been entirely qualitative. There are no definite requirements available at the present time. A partial solution, at least in some cases, might be to restrict the simulated tasks and allowable maneuvers to conceal the more unrealistic features of the simulator.

SECTION VI

SUMMARY

This report includes the results of a recent experiment to measure the effects of motion cues on a manual control tracking task. The results of this and previous experiments are then used to derive a Multimodality Pilot Model and to derive some requirements for the design of moving-base simulators.

The Multimodality Pilot Model is presented in Section V. Estimates are given for the dynamic characteristics of the various elements in the two vestibular feedback paths, the semicircular canals and the utricles. The integration of the visual and vestibular feedbacks is discussed.

Also presented in Section V is a discussion of the implications of the above results on the requirements for moving-base simulators. The effects of motion cues on tracking, failure detection, and realism are considered. A few general requirements for tracking are suggested and a procedure for establishing tracking requirements for a specific problem is outlined.

The specific results obtained from the experiments reported here are described below. The piloting task was roll control for a simulated VTOL vehicle hovering in gusty air. Both roll and lateral translation motions were included. The key results are:

1. The crossover model of Ref. 7 applies to moving-base tracking as well as fixed-base if the crossover frequency and effective time delay are modified. With motion, the magnitude of the pilot describing function, Y_p, is increased and the phase lag is reduced (roughly equivalent to a time delay reduction of $0.1-0.2$ sec); the increased pilot gain increases the crossover frequency by $0.5-1.5$ rad/sec.

2. With motion, the visual feedback gain at low frequency is increased and the visual lead is reduced.

3. For the task examined the motion feedback appears to be primarily through the semicircular canals with very little utricular feedback.

4. The visual feedback dominates at low frequencies and the motion feedback dominates at high frequencies. For controlled elements which do not require low frequency pilot lead, the two feedbacks are of comparable magnitude in the frequency region of 5 – 10 rad/sec. For controlled elements which require low frequency pilot lead, the two feedbacks are of comparable magnitude in the frequency range of 1.5 – 2 rad/sec.

5. The open-loop remnant injected at the pilot's output has a flat spectrum over the frequency range 1 – 10 rad/sec. With motion, the magnitude of the spectrum is increased by a factor of up to 3.

6. With motion, mean-square error at input frequencies is reduced to 0.27 – 0.52 of the fixed-base value due to increased crossover frequency.

7. With motion, remnant component of mean-square error is reduced to 0.40 – 0.98 of the fixed-base value; increase in crossover frequency has more effect than increase in open-loop remnant.

8. Performance improvement due to motion cues is greater for controlled elements which require low frequency pilot lead than for those which do not.

9. A roll washout of 0.5 rad/sec has a negligible effect and even washouts as large as 2 rad/sec have rather minor effects.

APPENDIX

TWO-INPUT DATA REDUCTION TECHNIQUE

This appendix covers a summary of the procedures employed in the reduction of the experimental data for the two-input tests. The appendix contains

- The derivation of the necessary equations from the system block diagram
- The description of the successive steps taken in the construction of Bode plots for the transfer functions of the visual and the motion feedbacks, Y_v and Y_m
- A typical example of the construction of Y_v and Y_m

The block diagram for the two-input tests is shown in Fig. 33.

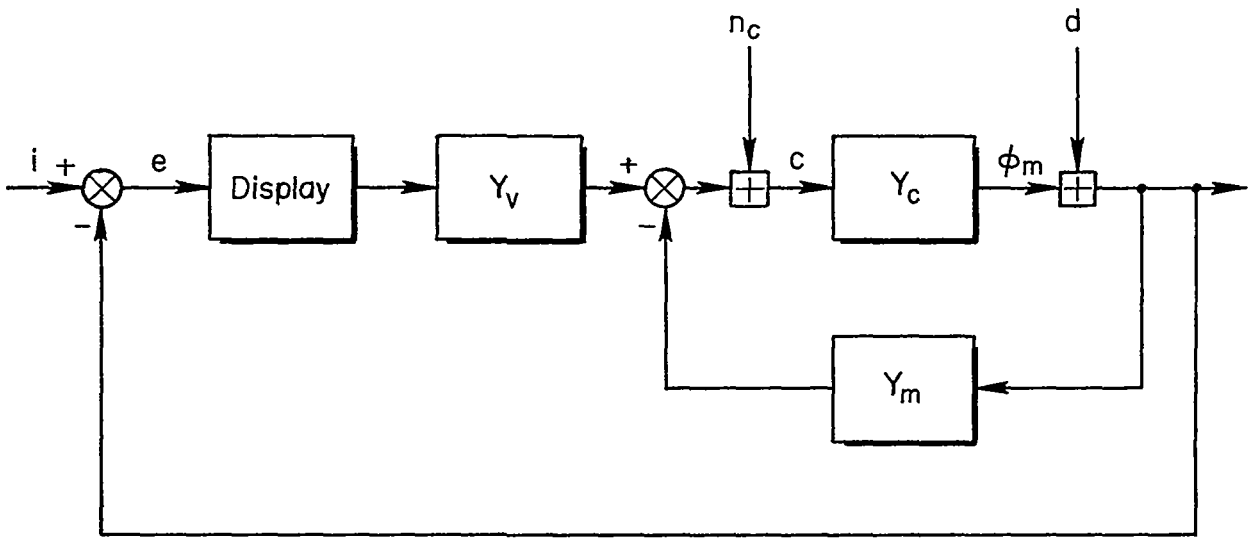

Figure 33. Two-Input Block Diagram

SUMMARY OF EQUATIONS

The following equations can be set up directly from the block diagram:

$$e = i - \varphi_m - d \tag{32}$$

$$c = n_c + Y_v e - Y_m(\varphi_m + d) \tag{33}$$

$$\varphi_m = Y_c c \tag{34}$$

Inserting into Eq. 33 the expressions for e and φ_m, Eqs. 32 and 34, leads to

$$c = n_c + Y_v[i - Y_c c - d] - Y_m(Y_c c + d) \tag{35}$$

from which c as a function of the two inputs i, d, and the open-loop remnant n_c is obtained as

$$c = \frac{Y_v i - d(Y_v + Y_m) + n_c}{1 + Y_c(Y_v + Y_m)} \tag{36}$$

From Eqs. 32, 34, and 36, the system error is readily expressed as

$$e = \frac{i(1 + Y_c Y_m) - n_c Y_c - d}{1 + Y_c(Y_v + Y_m)} \tag{37}$$

By considering the inputs one at a time, the following four transfer functions can be derived from Eqs. 36 and 37.

$$\frac{c}{i} = \frac{Y_v}{\Delta''} \tag{38}$$

$$\frac{c}{d} = -\frac{(Y_v + Y_m)}{\Delta''} \tag{39}$$

$$\frac{e}{i} = \frac{1 + Y_c Y_m}{\Delta''} \tag{40}$$

$$\frac{e}{d} = -\frac{1}{\Delta''} \tag{41}$$

$$\text{where} \qquad \Delta'' = 1 + Y_c(Y_v + Y_m)$$

Moreover, because of Eq. 34, the following two relations

$$\frac{c}{i} = \frac{1}{Y_c}\frac{\varphi_m}{i} \tag{42}$$

$$\frac{c}{d} = \frac{1}{Y_c}\frac{\varphi_m}{d} \tag{43}$$

must hold. These two equations are of particular importance for the cross-checking of the low frequency region of c/i and c/d.

On the basis of the Eqs. 38–43 the desired equations for the describing function of the visual path Y_v, the motion path Y_m, and the pilot $Y_p = Y_v + Y_m$ can now be determined.

Dividing Eq. 38 by Eq. 41 yields the expression

$$Y_v = -\left(\frac{c}{i}\right)\left(\frac{e}{d}\right)^{-1} \tag{44}$$

wherein c/i can also be replaced from Eq. 42. Thus

$$Y_v = -\frac{1}{Y_c}\left(\frac{\varphi_m}{i}\right)\left(\frac{e}{d}\right)^{-1} \tag{45}$$

Replacing Y_v in Eq. 39 by Eq. 38, and using Eq. 41 to eliminate Δ'' leads to

$$Y_m = \left(\frac{e}{d}\right)^{-1}\left(\frac{c}{d} + \frac{c}{i}\right) \tag{46}$$

wherein c can be replaced by Eqs. 42 and 43, so that

$$Y_m = \frac{1}{Y_c}\left(\frac{e}{d}\right)^{-1}\left(\frac{\varphi_m}{d}+\frac{\varphi_m}{i}\right) \tag{47}$$

Since

$$Y_p = Y_v + Y_m \quad , \tag{48}$$

Eq. 39 can be used to compute Y_p, eliminating Δ'' by means of Eq. 41, thus

$$Y_p = \left(\frac{c}{d}\right)\left(\frac{d}{e}\right) \tag{49}$$

wherein c/d can be replaced by Eq. 43 to give

$$Y_p = \frac{1}{Y_c}\left(\frac{\varphi_m}{d}\right)\left(\frac{d}{e}\right) \tag{50}$$

The digital computer program which processed the experimental data computed the six ratios,

$$\frac{c}{i} \ , \ \frac{e}{i} \ , \ \frac{\varphi_m}{i} \ , \ \frac{c}{d} \ , \ \frac{e}{d} \ , \ \frac{\varphi_m}{d}$$

These were evaluated by taking the ratios of the Fourier transforms at the ten input frequencies of i or d. Thus, the first three ratios were evaluated at one set of ten frequencies and the other three ratios were evaluated at a different set of ten frequencies. The calculation of Y_v or Y_m requires having these ratios at common frequencies. The interpolation procedure required to accomplish this is described below. Since Eqs. 49 and 50 involve only ratios at d frequencies, Y_p and Y_pY_c were computed directly by the digital computer.

DATA EVALUATION AND FITTING PROCEDURE

Eight sets of experimental data were processed. The eight sets were for Subject GB or RG, $Y_c = K_c/s(s+10)$ or K_c/s^2, and $\ell_z = 0$ or 3.5 ft. Each set (with one exception) consisted of four runs; two replications for $(i/d)_{rms} = 0.25$ or 0.50. The following steps were taken:

a. In the plots of c/i, c/d, e/d, φ_m/i, and φ_m/d, smooth curves were faired through the distinct frequency points.

b. Data points and faired curves of c/i and c/d were cross-checked on the basis of Eqs. 42 and 43. Because the data for φ_m/i and φ_m/d are generally more accurate in the low frequency region, this step frequently yielded useful information for adjustments on c/i and c/d.

c. Y_v was constructed pointwise from Eq. 44, using the e/d curves and the adjusted curves for c/i. The point set thus obtained was approximated by a transfer function with smooth amplitude ratio, and clearly discernible time delay. No difficulties arose in the fitting of the constructed point set.

d. Y_p was approximated by a somewhat more elaborate transfer function in a similar way as Y_v. The increased complexity of the fit required special attention to the high frequency characteristics of Y_p, because errors in amplitude fitting in this frequency region could seriously affect the phase angle of the delay operator, thus leading to errors in the effective time delay constant.

e. Y_m was computed pointwise on the basis of the original (nonapproximated) point sets of Y_v and Y_p, using the relation

$$Y_m = Y_p - Y_v \tag{51}$$

and was also computed from Eq. 46 directly.

Computation of Y_m from Eqs. 46 and 51 generally led to excellent agreement in the high frequency region, but some scatter in the low frequency region. This fact is readily explained by comparing Eqs. 46 and 51 for the low frequency region. For this region, Y_m from Eq. 51 is generated by only one subtraction of two sizable vectors with well

defined phasing. By Eq. 46, however, Y_m in the low frequency region is generated by the summation of two very small vectors, and the multiplication of this sum by a large vector. Hence, in the second case, slight error in all individual plots may lead to excessive errors in amplitude and phase of Y_m, so that data points in this region computed by Eq. 51 are definitely to be taken as the more accurate ones.

The results of processing the eight sets of data and the pertinent fits of Y_v and Y_p are summarized in Table XV.

TABLE XV

SUMMARY OF TWO-INPUT DATA

Y_c	ℓ_z (ft)	SUBJECT	DESCRIBING FUNCTION APPROXIMATIONS	
			Y_p	Y_v
$\frac{K_c}{s(s+10)}$	0	GB	$0.0623(s+9)s^{-0.29s}$	$0.635e^{-0.35s}$
	3.5	GB	$0.0645\frac{(s+4)(s+5.5)}{(s+2)}e^{-0.25s}$	$\frac{11.93}{(s+15)}e^{-0.31s}$
	0	RG	$0.188(s+7.5)e^{-0.25s}$	$1.585e^{-0.35s}$
	3.5	RG	$0.224\frac{(s+4)(s+5)}{(s+2)}e^{-0.25s}$	$\frac{22.2}{(s+10)}e^{-0.35s}$
$\frac{K_c}{s^2}$	0	GB	$1.06\frac{(s+1.5)(s+5)}{(s+10)}e^{-0.31s}$	$5.4\frac{(s+3)}{(s+20)}e^{-0.42s}$
	3.5	GB	$11.46\frac{(s+1.5)(s+5)}{(s+9)(s+12)}e^{-0.24s}$	$2.88\frac{(s+3.5)}{(s+9)}e^{-0.35s}$
	0	RG	$13.45\frac{(s+2)(s+4.5)}{(s+9)(s+12)}e^{-0.24s}$	$3.74\frac{(s+3)}{(s+10)}e^{-0.40s}$
	3.5	RG	$17.9\frac{(s+1.5)(s+4)}{(s+9)(s+15)}e^{-0.27s}$	$2.38\frac{(s+4.5)}{(s+12)}e^{-0.40s}$

DATA REDUCTION EXAMPLE

For the demonstration of the data reduction procedure the following case has been selected:

$$Y_c = \frac{K_c}{s^2} \quad , \quad \ell_z = 3.5 \text{ ft} \quad , \quad \text{Subject: RG} \quad , \quad \text{Runs: } 183, 205, 315, 344$$

The procedure follows the various steps listed earlier.

a. The Bode plots for c/i, e/d, and c/d are shown in Figs. 34, 35, and 36, respectively. Prior to fairing continuous curves through the data points, the low frequency data points of c/i and c/d were cross-checked according to Eqs. 42 and 43. The plots of φ_m/i and φ_m/d, by means of which the cross-checking was performed, are not shown.

b. In the three aforementioned plots continuous curves were faired through the data points, shaping the curves so that they represented, within the region of interest, amplitude and phase portraits of transfer function comprising combinations of first- and second-order numerator and denominator factors. Individual data points of the desired transfer function were constructed by using the plots of Figs. 34 and 35 in accordance with Eq. 44, that is

$$Y_v = -\left(\frac{c}{i}\right)\left(\frac{e}{d}\right)^{-1}$$

c. The constructed points of Y_v are shown in Fig. 37. The amplitude ratio $|Y_v|$ was first approximated by a simple transfer function, consisting of lead, lag, or lead/lag terms. For the case in consideration, an excellent amplitude fit was found for the function

$$2.38\,\frac{(s+4.5)}{(s+12)}$$

To this was added a time delay to match the phase data. For the example, the resulting fit was

$$Y_v \doteq 2.38\,\frac{(s+4.5)}{(s+12)}\,e^{-0.4s} \qquad (52)$$

As can be seen in Fig. 37, this is a good approximation.

d. The Bode plot of Y_p with faired curves for the region $0.5 < \omega < 15$ rad/sec is shown in Fig. 38. It was found that this data could be well approximated by

$$Y_p \doteq 17.9 \frac{(s+1.5)(s+4)}{(s+9)(s+15)} e^{-0.27s} \qquad (53)$$

e. The faired, but not fitted, Y_v and Y_p data were used to compute Y_m via Eq. 51. The results are shown in Fig. 39. Also shown is Y_m computed from the faired c/i, e/d, and c/d data and Eq. 46. The two results generally agree very well.

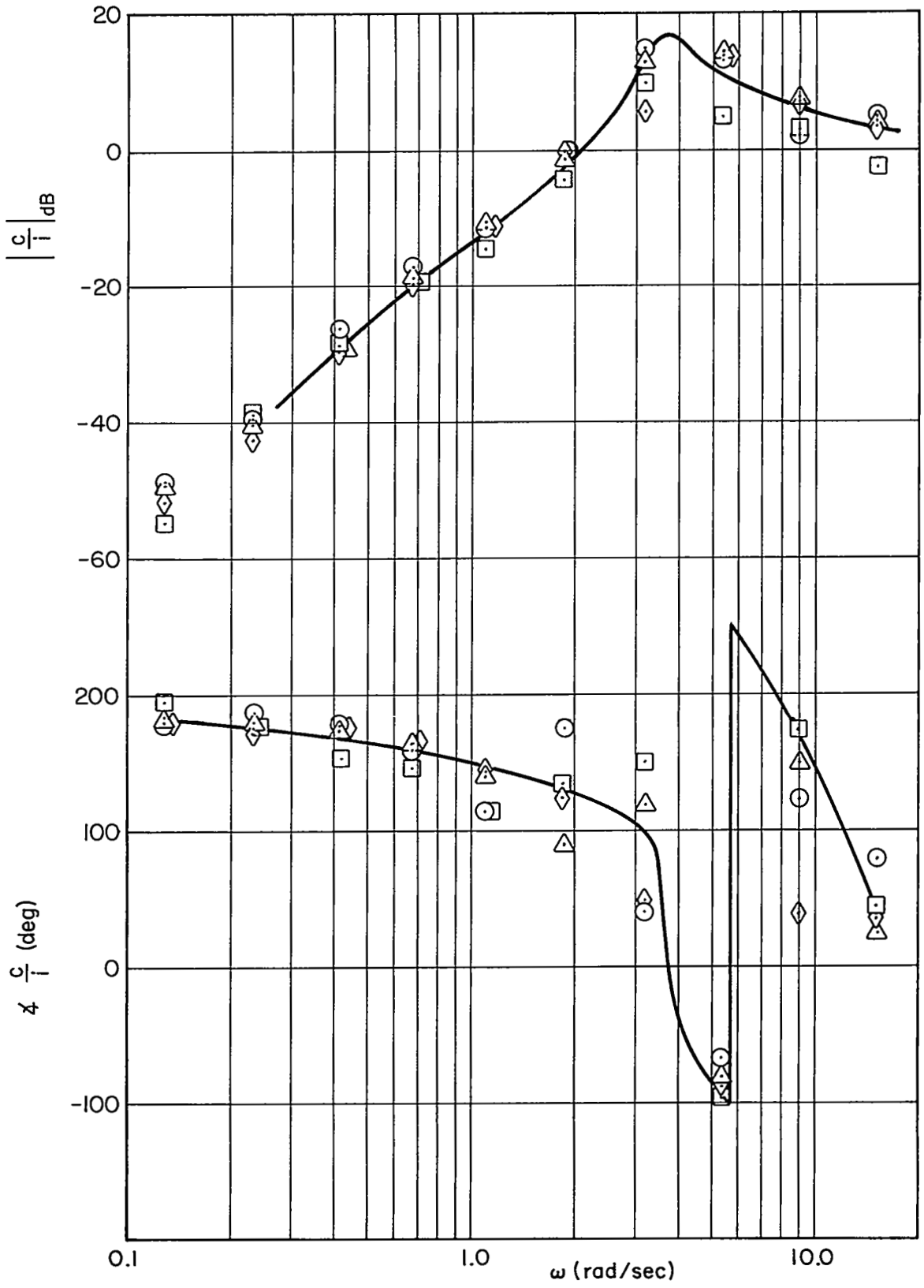

Figure 34. Example c/i Data

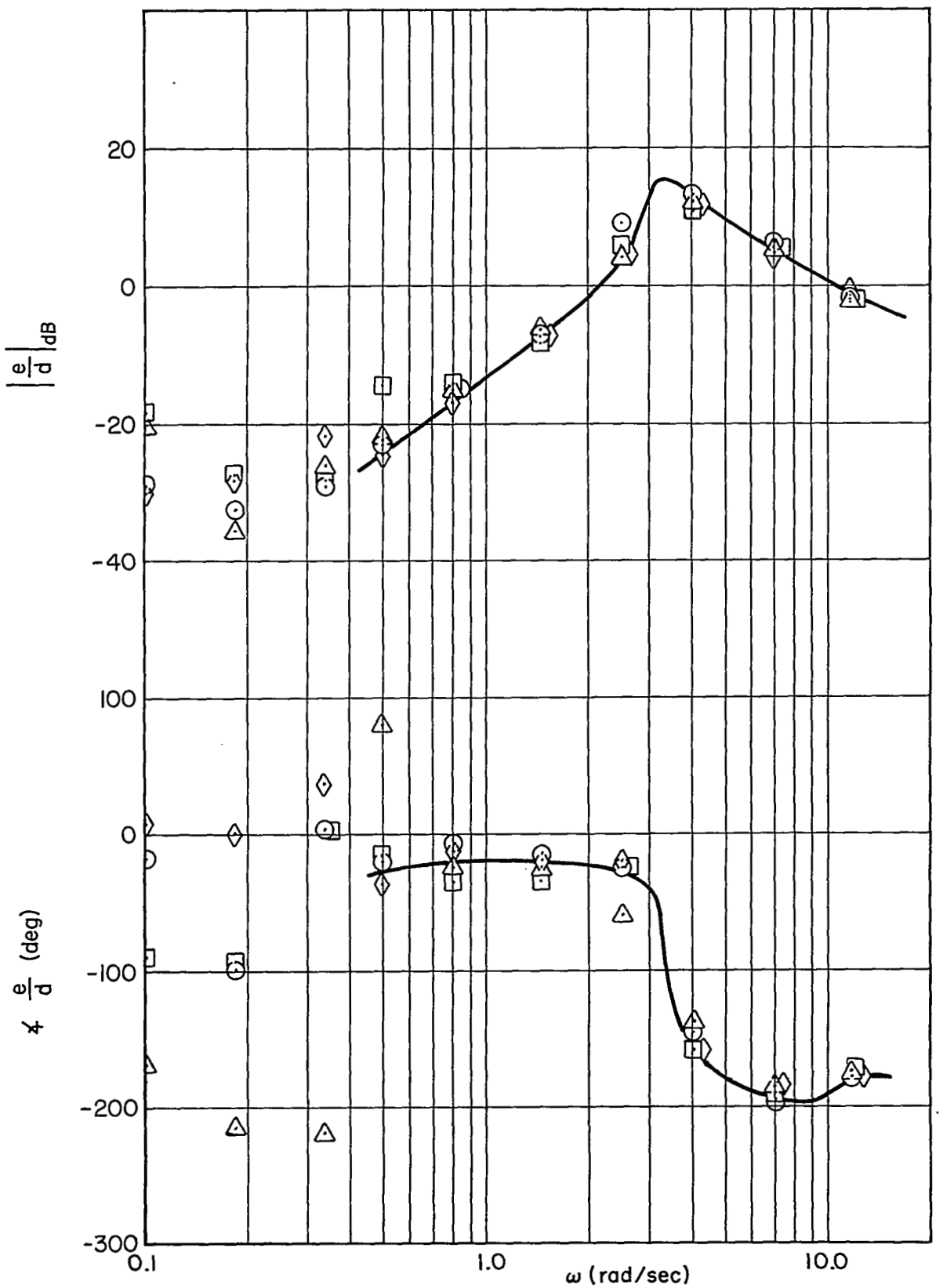

Figure 35. Example e/d Data

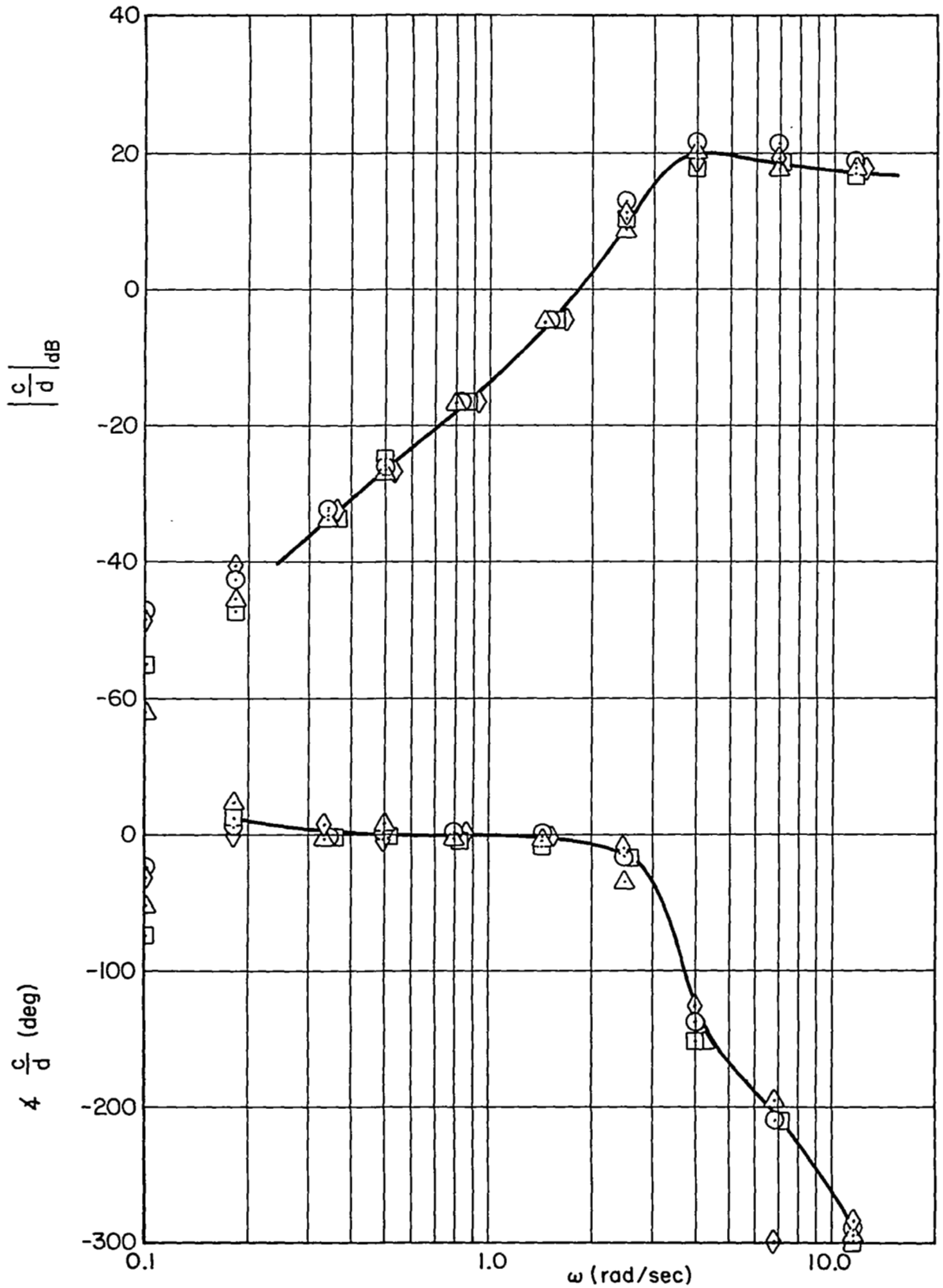

Figure 36. Example c/d Data

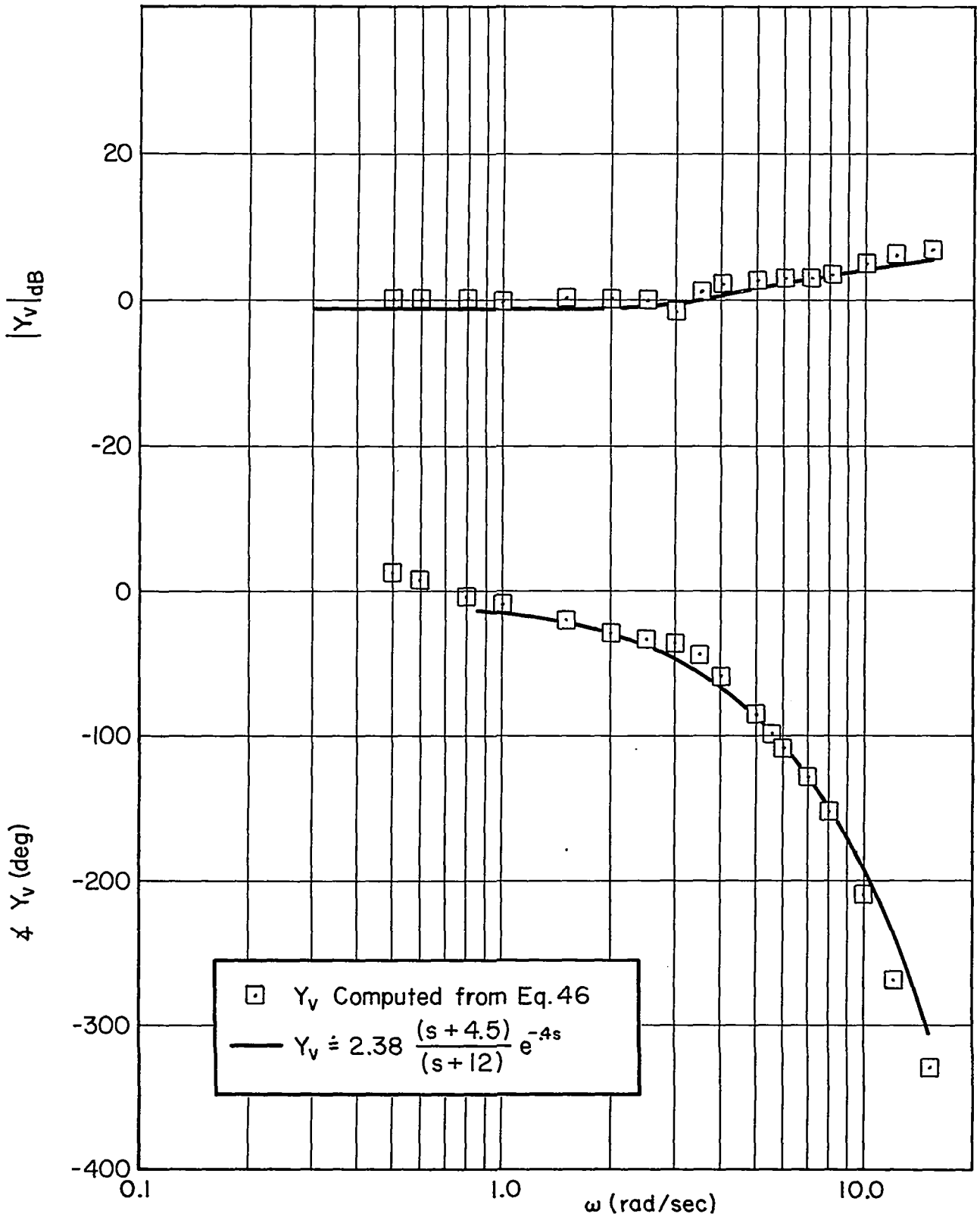

Figure 37. Example Y_v Fit

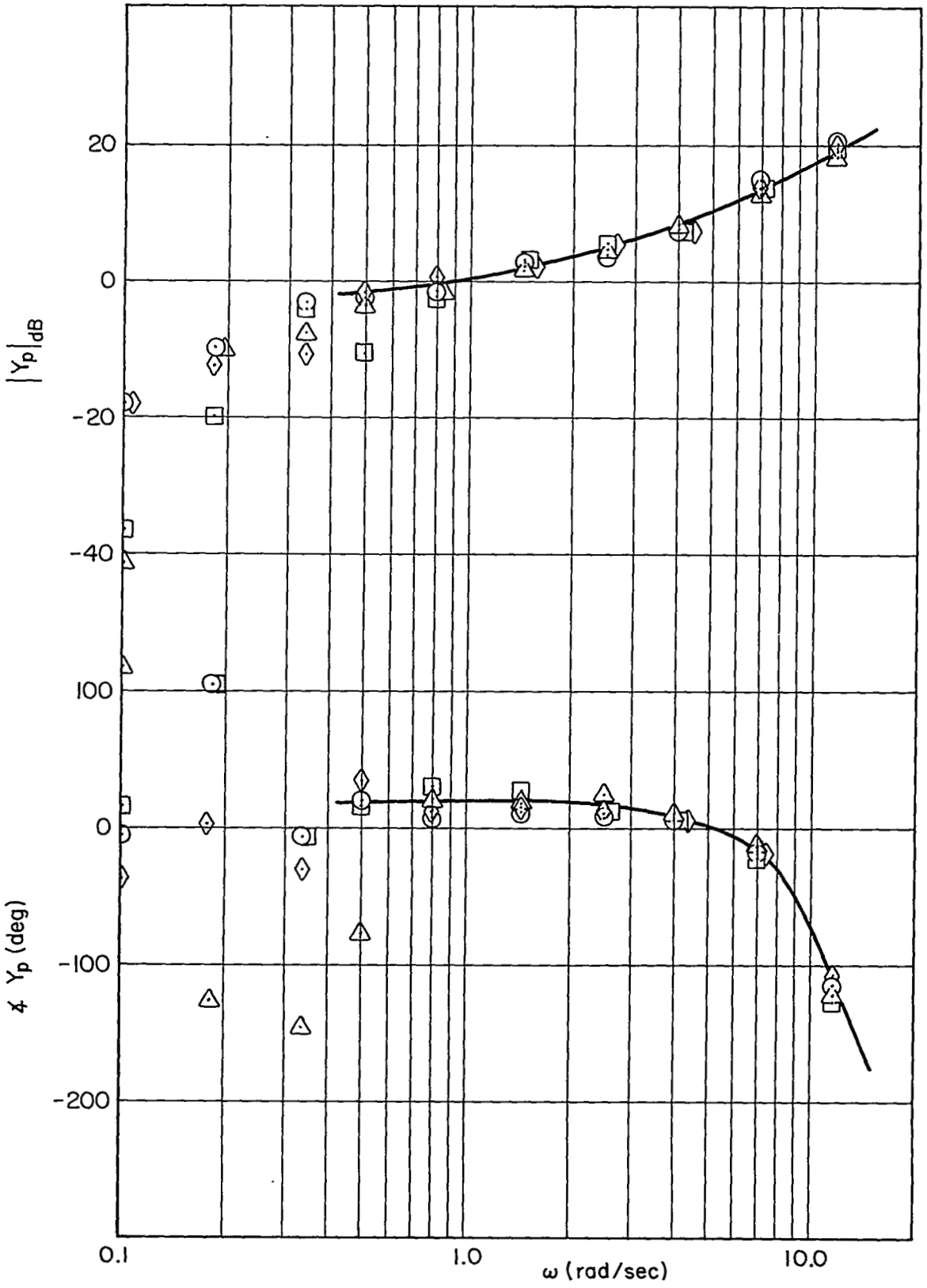

Figure 38. Example Y_p Data

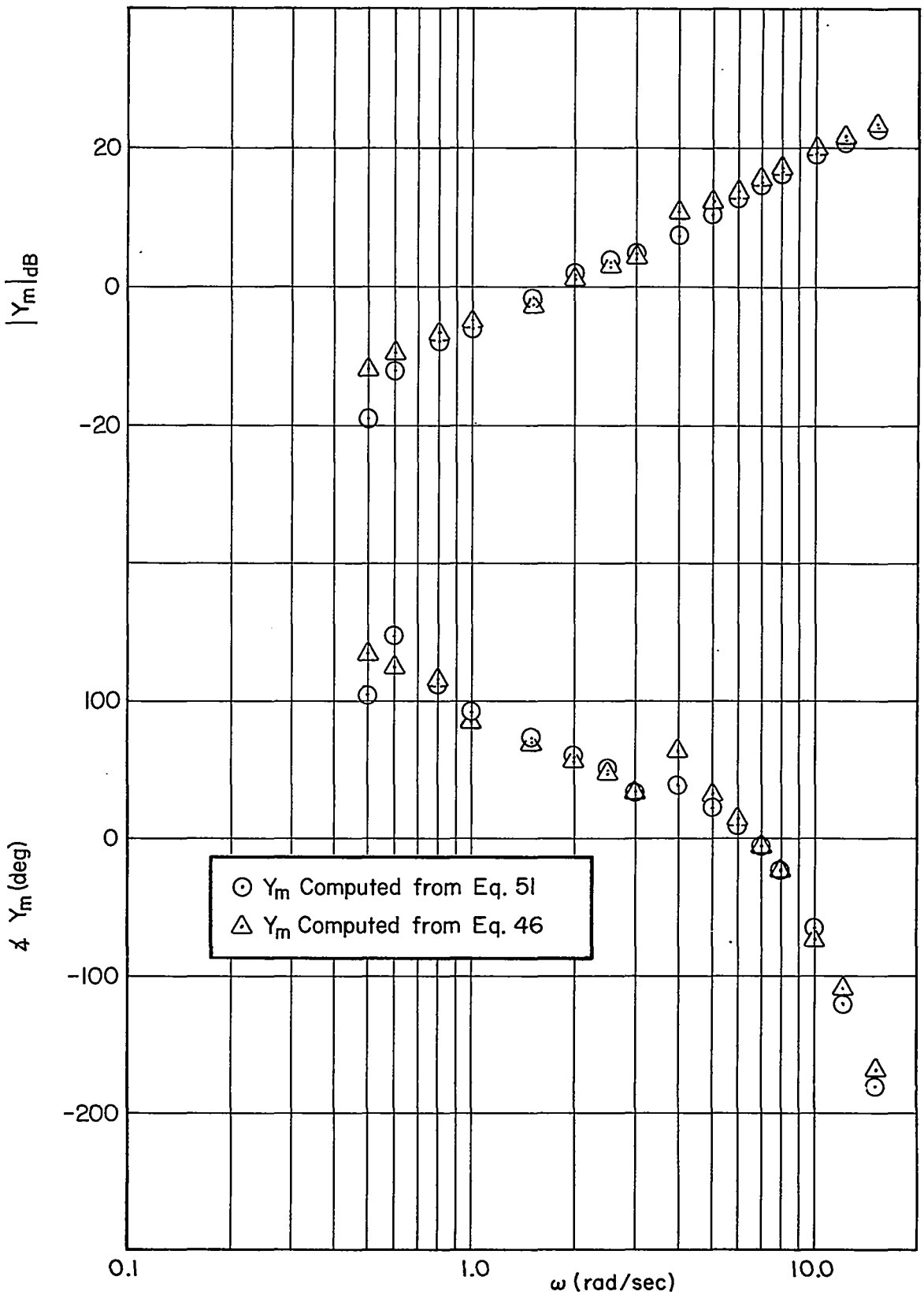

Figure 39. Example Y_m Data

REFERENCES

1. Peters, Richard A., Dynamics of the Vestibular System and Their Relation to Motion Perception, Spatial Disorientation, and Illusions, Systems Technology, Inc., Tech. Rept. 168-1, Feb. 1968 (forthcoming NASA CR-).

2. Meiry, Jacob L., The Vestibular System and Human Dynamic Space Orientation, MIT, Man-Vehicle Control Lab., Thesis No. T-65-1, June 1965.

3. Newell, F. D., Human Transfer Characteristics in Flight and Ground Simulation for the Roll Tracking Task, AFFDL-TR-67-30, Apr. 1968.

4. Shirley, Richard S., Motion Cues in Man-Vehicle Control, MIT, Man-Vehicle Lab., Thesis No. MVT-68-1, Jan. 1968.

5. Bullard, E. C., F. E. Oglebay, W. H. Munk, and G. R. Miller, A User's Guide to BOMM, Univ. of Calif. Institute of Geophysics and Planetary Physics, Jan. 1966.

6. Bendat, Julius S., and Allan G. Piersol, Measurement and Analysis of Random Data, John Wiley and Sons, Inc., New York, 1966.

7. McRuer, Duane, Dunstan Graham, Ezra Krendel, and William Reisener, Jr., Human Pilot Dynamics in Compensatory Systems; Theory, Models, and Experiments with Controlled Element and Forcing Function Variations, AFFDL-TR-65-15, July 1965.

8. McRuer, Duane T., and Ezra Krendel, Dynamic Response of Human Operators, WADC TR 56-524, Oct. 1957.

9. Elkind, J. E., Characteristics of Simple Manual Control Systems, MIT Lincoln Laboratory Tech. Rept. 111, Apr. 1956.

10. Seckel, Edward, Ian A. M. Hall, Duane T. McRuer, et al, Human Pilot Dynamic Response in Flight and Simulator, WADC TR 57-520, Aug. 1958.

11. Kuehnel, Helmut A., Human Pilots' Dynamic-Response Characteristics Measured in Flight and on a Nonmoving Simulator, NASA TN D-1229, Mar. 1962.

12. Smith, Harriet J., "Human Describing Functions Measured in Flight and on Simulators," Second Annual NASA-University Conference on Manual Control, NASA SP-128, Feb. 28-Mar. 2, 1966, pp. 279-290.

13. Kilpatrick, Philip S., Bending Mode Acceleration Influence on Pilot Control of Flexible Booster Dynamics, MIT, Man-Vehicle Control Lab., Thesis No. T-65-2, Sept. 1965.

14. Benjamin, Peter, Visual and Motion Cues in Helicopter Flight, MIT, Man-Vehicle Control Lab., Thesis No. T-66-1, Jan. 1966.

15. Sadoff, Melvin, Norman M. McFadden, and Donovan R. Heinle, A Study of Longitudinal Control Problems at Low and Negative Damping and Stability with Emphasis on Effects of Motion Cues, NASA TN D-348, Jan. 1961.

16. McRuer, Duane T., Dunstan Graham, and Ezra S. Krendel, "Manual Control of Single-Loop Systems: Parts I and II," J. Franklin Institute, Vol. 283, No. 1, Jan. 1967, and No. 2, Feb. 1967.

17. Young, L. R., and J. L. Meiry, "A Revised Dynamic Otolith Model," 3rd Symp. on Role of the Vestibular Organs in Space Exploration, Pensacola, Fla., Jan. 23-27, 1967.

18. Alex, F. R., Analysis of Two Manually Controlled Compensatory Systems with Inclusion of Motion Cues, Systems Technology, Inc., Working Paper 168-2, Feb. 1967.

19. McRuer, D. T., and H. R. Jex, "A Review of Quasi-Linear Pilot Models," IEEE Trans., Vol. HFE-8, No. 3, Sept. 1967, pp. 231-249.